**NTNU**
Norwegian University of
Science and Technology

# Nonlinear Mechanical Vibrations: The Effect of Gaps

## Anders Hillestad Hauglid

This page is intentionally left blank.

# NTNU

Date 02.02.2018

Faculty of Engineering
Department of Mechanical and Industrial Engineering

**MASTER'S THESIS SPRING 2018
FOR
STUD.TECHN. ANDERS HAUGLID**

## THE EFFECT OF NONLINEAR GAPS ON VIBRATIONS IN MECHANICAL ASSEMBLIES

**Effekten av ikke-lineære mellomrom under mekanisk vibrasjon**

Vibrations in mechanical assemblies are an important source of material fatigue, noise and discomfort. If allowed to act long enough, vibrations may very well cause mechanical failure. Many of these assemblies contain some form of joints or connections. The Norwegian Defence Research Establishment, herein FFI, conducts several experiments on behalf of the Norwegian Defence and others in regards to vibration. Experiments are often done on multi-body assemblies joined together in some fashion. When conducting a shaker-test on a prototype RIMFAX antenna in 2017, FFI observed an anomaly both in terms of simulated natural frequencies compared to experimental. The antenna's connections to the Mars rover is designed to be allowed for thermal expansion and thus have some deliberate play/gaps. It is believed that these gaps create nonlinearities that affect the vibrational properties of the assembly and is the source of the observed anomaly.

This master's thesis is the continuation of the author's project thesis written the fall of 2017. The project thesis constructed a first principles model and simulated it's response to a sine sweep input signal in both MATLAB and MSC software, and investigating the drift of natural frequencies when nonlinearities were included.

Note: The RIMFAX antenna is developed at the Norwegian Defence Research Establishment (FFI) and selected by NASA to be one of the science instruments on board the NASA rover to Mars in 2020. The radar has the ability to penetrate to more than 10 meters depth depending on ground conditions.

Tasks include:

1. Study available literature on experimental testing of nonlinear vibrations.
2. Propose and solve a first principles model using equations of motion and numerical solvers. Input from the literature study is considered natural.
3. Plan and conduct experiments on nonlinear vibrations. The experiments will be conducted at the Environmental Lab at FFI. One or several test jigs has to be drawn and produced.
4. Setup and run the same experiments with finite element analysis in MSC software. Investigate parameters and attempt to correlate simulation with physical experiments.
5. Correlate the new test and simulated results with the previous RIMFAX shaker test results in order to explain the original problem.

**Norges teknisk-naturvitenskapelige universitet**

If time permits:

6. Prepare a scientific paper.

<u>Contact</u>:

At the department (supervisor, co-supervisor): Terje Rølvåg, email: terje.rolvag@ntnu.no

From FFI:

Pål Martin Greni, phone; 6380 7577 email: <u>pmg@ffi.no</u>

Vedlegg: Kontraktsmal

# Abstract

In this report, the vibration properties of nonlinear mechanical joints have been explored. The nonlinearity is due to a clearance gap in the joint, which may arise intentionally in design or through wear and tear. How gap affects the response of the system has been investigated through numerical analysis, experimental tests and finally by means of commercial finite element software. The numerical model is based on solving the nonlinear second-order ordinary differential equation for the system. This is done with Runge-Kutta solvers in MATLAB. The problem is solved in the time domain and the result is transferred to the frequency domain by means of a Fourier transformation. Various relationships have been looked into, especially frequency response functions, Power spectrum density and the Coherence spectrum. The experimental work is based on coupon tests of structures with a bolted connection of different gap distance and different coupon material. The coupon is excited on a shaker table in the lab through harmonic, sine sweep and random vibration input signal. Post-processing is done by means similar to what is done in the numerical work. The work in finite element analysis proposes different formulations of the problem and looks into how gap may be represented efficiently.

The experimental work displays a chaotic behavior. Averaging techniques on data in the frequency domain show that the effective natural frequency - termed $\omega_e$ in this thesis, taken as the peak in power spectrum density, are reduced when clearance gaps is introduced to the system. There is, however, no conclusive trend in terms of the relationship between the amount of reduction in $\omega_e$ and gap distance, excitation amplitude or coupon geometry.
The numerical work in MATLAB and FEM display a good correlation with each other, both show the same tendency - $\omega_e$ is reduced by clearance. The work also shows that an increase in gap distance reduces $\omega_e$. The stiffness in the system has also been varied, the results indicate an increase in stiffness reduces the *relative* $\omega_e$. More work in the field of topic is recommended for a deeper understanding.

# Sammendrag

I denne rapporten har vibrasjonsegenskapene til ikke-lineære mekaniske forbindelser blitt undersøkt. Ikke-lineariteten kommer av klaring i forbindelsen, som kan komme fra intensjon i design eller gjennom slitasje. Hvordan klaring påvirker responsen har blitt undersøkt gjennom numerisk analyse, eksperimentelle forsøk og til slutt ved bruk av kommersiell finite element programvare. Den numeriske modellen baserer seg på å løse den ikke-lineære andre ordens ordinære differensialligningen for systemet. Dette gjøres ved hjelp av Runge-Kutta løsere i MATLAB. Problemet er løst i tidsplanet og resultatene er overført til frekvensplanet ved hjelp av Fourier transformasjon. Ulike sammenhenger er blitt sett på, særlig frekvens-respons spekter, Power spectrum density og koherens. Det eksperimentelle arbeidet baserer seg på kupongtesting av strukturer med en boltet forbindelse av ulik klaringsdistanse og med ulikt kupongmateriale. Kupongene er eksitert på et ristebord gjennom harmonisk, sinus sweep og random input signal. Post-prosessering er gjort på samme måte som i det numeriske arbeidet. Arbeidet i finite element metoden foreslår ulike formuleringer av problemet og ser på hvordan klaring kan bli representert på en effektiv måte.

Det eksperimentelle arbeidet viser en kaotisk oppførsel. Midlingsteknikker på data i frekvensplanet viser at den effektive egenfrekvensen - kalt $\omega_e$ i denne oppgaven, tatt fra toppen i power spectrum density, reduseres når klaring blir innført i systemet. Det er derimot ingen direkte trend som kommer frem fra målingene hva gjelder sammenheng mellom mengde reduksjon og klaringsdistanse, eksitasjonsamplitude eller kuponggeometri.
Det numeriske arbeidet i MATLAB og FEM har god korrelasjon seg i mellom, og viser begge den samme tendensen - den effektive egenfrekvensen går ned ved klaring. Arbeidet viser at ved å øke klaringsdistansen reduseres $\omega_e$. Stivhet i systemet har også blitt variert, og en øking av stivhet reduserer også den *relative* $\omega_e$.
Mer arbeidet på området er anbefalt for å få en dypere forståelse.

# Preface

This Master's thesis is the product of work done in spring 2018 as the final part of a five-year master degree program and counts for 30 credit points. The thesis is written at the Norwegian University of Science and Technology (NTNU) in Trondheim and at the Norwegian Defense Research Establishment (FFI) in Kjeller as part of the study program Applied Mechanics. The thesis is written for the Department of Mechanical and Industrial Engineering (NTNU) and the Department of Prototyping (FFI). The main supervision has been done by Professor Terje Rølvåg at NTNU and MSc Pål Martin Greni at FFI.

The project was chosen based on the interest to learn about the mechanics of vibrations and the interest for modeling, simulation and correlating this with experiments. The mechanics of vibration has been a vaguely covered topic during my time at NTNU prior to my project and master's thesis, so the potential learning outcome was a key driver. The project came about as the result of three years of summer interning at the Department of Prototyping, FFI and is supporting the RIMFAX-project at FFI which is supplying instruments for the NASA Mars 2020 mission.

Trondheim, June 2018

*Anders H. Hauglid*

Anders Hillestad Hauglid

**NTNU**
Norwegian University of
Science and Technology

**FFI** Forsvarets
forskningsinstitutt
Norwegian Defence Research Establishment

# Acknowledgments

# Contents

# List of Figures

# List of Tables

# Nomenclature

**Abbreviations**

DOF(s)  Degree(s) of freedom

EOM(s)  Equation(s) of motion

FFT  Fast Fourier Transform

FRF  Frequency Response Function

LFEA  Linear Finite Element Analysis

NASTRAN  NASA STRucture ANalysis

NLFEA  Non Linear Finite Element Analysis

POM C  Polyoxymethylene copolymer

PSD  Power Spectrum Density

**Symbols**

$\ddot{x}$        Acceleration (m/s$^2$)

$\dot{x}$        Velocity (m/s)

$\nu$        Poisson's ratio

$\omega$        Frequency of oscillation (rad/s)

$\rho$        Mass density (kg/m$^3$)

$\zeta$        Damping ratio

$a$        Gap distance (usually in mm or $10^{-3}$ m)

$c$        Damping coefficient (Ns/m)

$C_{xy}$        Coherence spectrum between signal $x$ and $y$

$E$        Young's modulus (MPa $10^6$ N/m$^2$)

$F$        General forcing term (N)

$f$        Linear frequency (Hz)

$f_s$        Sampling frequency (Hz)

$g$       Standard acceleration due to gravity, considered to be 9.81 m/s$^2$

$I_{ij}$       Mass moment of inertia in the $ij$-th direction (kg m$^2$)

$k$       Stiffness (N/m)

$m$       Mass (kg)

$q$       Generalized coordinate

$r$       Frequency ratio

$S_{xx}$       Power spectrum density of signal $x$

$S_{xy}$       Cross spectrum density of signal $x$ and $y$

$u_i$       Displacement in the $i$-th direction

$x$       Displacement (m)

# Chapter 1

# Introduction

The aim of this chapter is to introduce the background, objective and structure of this report.

## 1.1 Introduction

Vibrations in mechanical structures are an important source of material fatigue, noise and discomfort. If allowed to act long enough, vibrations may very well cause mechanical failure. In many practical applications, mechanical structures are joined together in some fashion and excited to vibrate. The theory of linear systems, systems where the joints are ideally joined together, i.e. no clearance is very well understood. The principle of superposition holds and one can calculate vibration properties such as eigenvalues and eigenvectors by means of known methods (such as solving the eigenvalue problem from the stiffness matrix $\mathbf{K}$). However, for real system, these joints often exhibit some clearance or looseness. For instance, it may be designed to allow for rotation or translation is one or several directions. Or it may be designed to allow for thermal expansion. As a consequence, real joints in mechanical structures that are designed to move about often become nonlinear. The theory of nonlinear vibrations as a consequence of clearance or looseness is less known and solutions techniques have to be chosen on a case-by-case basis.

Classical important applications of such problems are the automotive and marine industry and gears with deadband. Also, other areas such as the aerospace or other industries where special loadcases are more frequent. A fair amount of literature is found on the topic.
The aim of this project is to perform vibration testing on several types of joints with different clearances in order to map the joint behavior. Also, the same kind of clearance will be modeled with differential equations and finite elements. This aims to broaden the understanding on how clearance and gaps affect vibration.

## 1.2 Background
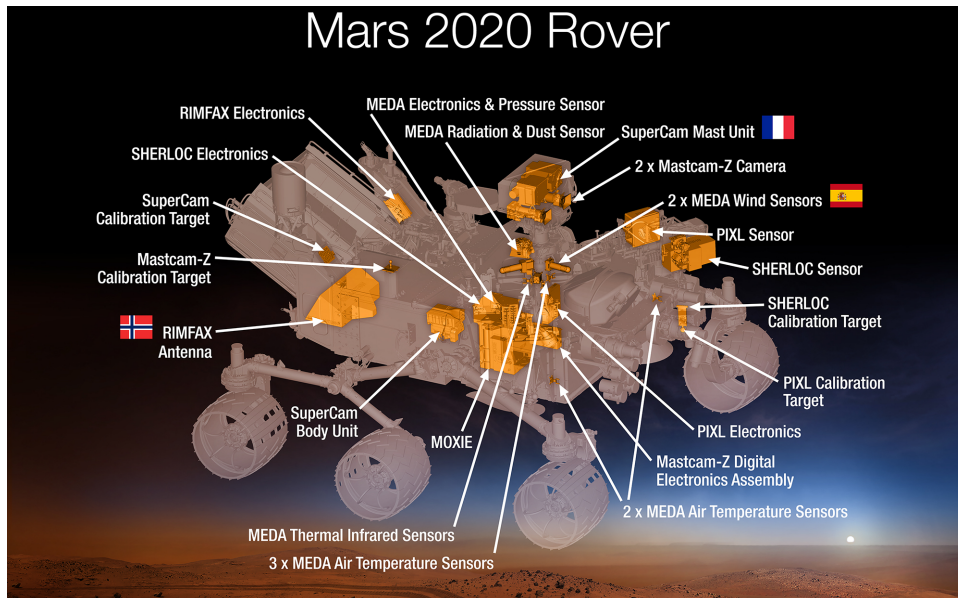


Figure 1.1: The various instruments on the Mars 2020-rover. RIMFAX on the aft-left.

The Norwegian Defense Research Establishment (herein FFI[1]) has been appointed a contract with the Jet Propulsion Laboratory (JPL) and NASA in conjunction with their Mars 2020-mission, designing, manufacturing and testing an antenna named RIMFAX. The Radar Imager for Mars' subsurFAce eXperiment (RIMFAX) is a ground-penetrating radar (GPR) instrument selected to fly on the 2020 Mars-rover and designed to produce from the surface of Mars, for the first time, high resolution stratigraphic information about the subsurface of the Red Planet. Specifically, RIMFAX supports and enhances the Mars 2020 investigation on the following, but not limited, ways: assess the depth and extent of regolith; detect different subsurface layers and their relationship to visible surface outcrops; characterize the stratigraphic section from which a cored-and-cached sample derives, including crosscutting relations and features indicative of past environments. The Department of Prototyping at FFI is responsible for the mechanical design and production of the antenna, herein mechanical testing.

---

[1]Norwegian acronym - Forsvarets forskningsinstitutt
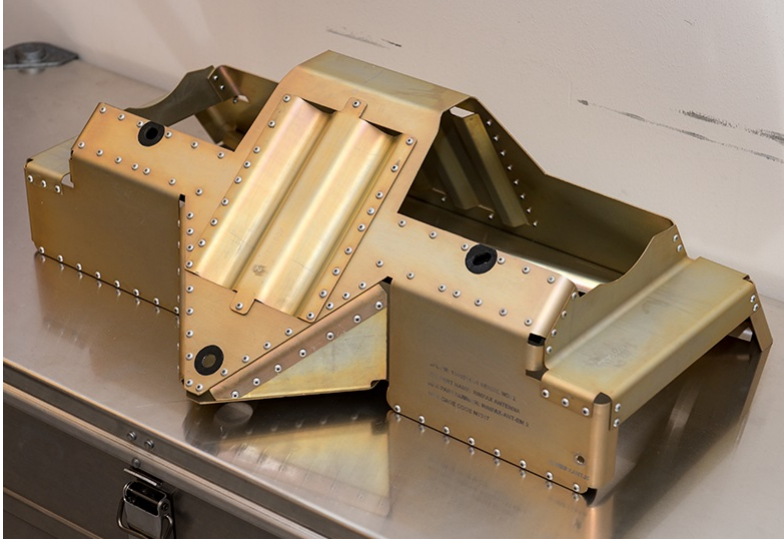
Figure 1.2: Manufactured prototype of the RIMFAX antenna.

NASA requires that the first natural frequency of the antenna is to be above 60 Hz. The design was simulated in MSC/Nastran and found to have a first natural frequency of 62 Hz. Then a prototype antenna was tested on a shaker table at FFI at which the experimental results yielded the first frequency to be 56 Hz. This was believed to be due to two reasons. 1) the assembly process of the sheet metal structure is done by riveting and some assembly error were thought to cause looseness in the rivets. 2) the whole RIMFAX structure is mounted to the Mars rover by three joints, so-called "kinematic joints". The kinematic joints allow for thermal expansion and contracting, considering that the antenna will be mounted to the rover at a temperature of 293K and that space is at 2.7K. Temperatures in operation on Mars may very from as much as 293K to 120K. Thus, temperature gradients and thermal strain are of importance. There is in total three joints connecting the RIMFAX to the rover, two of them having clearances to allow for contraction and expansion. One has a radial clearance, while the second has a slot clearance (one direction only).
The riveting assembly process became controllable and is no longer believed to cause the anomaly in natural frequency. The modeling of kinematic joints, however, are. They have for every simulation in Finite Element Analysis (FEA) been modeled as "glued" making the structure linear, when it, in reality, is not. It is mostly this erroneous assumption that this thesis will attempt to remedy.

The author made his project thesis work during the fall of 2017 [16]. Here a first principles SDOF model was built from the ground up and the equations of motion were solved numerical using a Runge-Kutta solver. The same model was built in MSC/Nastran and both methods were solved in the transient time domain before they were transformed into the frequency domain by FFT. The results yielded similar results for the two, and in conclusion, it was found that introducing a clearance nonlinearity *lowered* the effective natural frequency of the joint in comparison to a "glued" joint without clearance. This indicates that the anomaly observed at FFI ma, in fact, be due to a missing nonlinearity. To explore this conclusion further through a deeper understanding as well as real-life experimental testing will be the main goal of this project.

## 1.3 Problem and Scope

**Problem**

If we assume that we would have to solve for the nonlinear transient response in the time domain and then use a Fast Fourier Transform (FFT) to obtain the frequency domain for the structure, the whole RIMFAX structure and its geometry is extremely computationally expensive. The problem is broken down into two, and solved for those two separately.

**Scope**

Some limitations have been set in consultation with the involved parties to manage the project. The overall aim remains to test and model a replica of the two RIM-FAX kinematic joints and compare. The outcome will be used to asses the effect of clearances on structural joints in future projects with similar joint geometry. The experiments has been limited to testing the joints separately and in the in-plane and out-of-plane directions separately. This is to have more control and to make simulations feasible. The whole antenna structure will not be simulated as it is believed that including the whole geometry and three different joints will add so many degrees of freedom that accurate simulations as well as reliable experiments are not possible (or at least adding unnecessary complexity to the problem).

## 1.4 Structure of the Report

The main thesis is divided into 8 chapters: Chapter 1, 2 and 3 introduces the reader to the problem and subject as well as presents the necessary background, literature and theory to solve the problem. Chapter 4 presents the numerical approach. Chapter 5 presents the experimental approach. Chapter 6 presents the finite element approach. A general discussion of the various approaches and their contribution is made in chapter 7. Finally, in chapter 8 concluding remarks are presented and suggestions for further work is presented. Details and complete results are left in the appendix and referred to in the text.
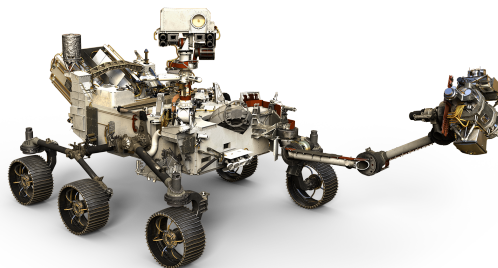


Figure 1.3: Render of the Mars 2020 rover.

# Chapter 2

# Literature

The topic of this thesis is covered by many terms in the literature. Vibro-impact dynamics, discontinuous dynamical systems, stick-slip motion, non-smooth mechanics and nonlinear oscillators are examples. Regardless of the label, much work has been conducted both in regards to mathematics, physics, dynamics and engineering. There is a rich dynamics to systems that inhabit the same properties as the RIMFAX joints. However, much of the work is theoretical and there is little to none work found applied to our specific problem.

Both old and recent research in the field of nonlinear vibrations has been reviewed. We do not wish to devote much space to reviewing and settle by mentioning the most important research to this thesis.

**Books**

- [18] is perhaps the single most relevant literature found on the topic. In this book the author presents topic ranging from Hertzian contact formulation, Grazing Bifurcations, and both one and two DOF as well as MDOF systems under vibro-impact.

- [9] provides a thorough presentation of non-smooth mechanics and gives a comprehensive reference list. The book is written from a control engineering point of view but has a good review of the underlying physics before control problems such as stability and feedback.

- [11] One of the classical works on mechanical vibrations. Includes two chapters on Self-Excited Vibrations and Systems With Variable or Non-Linear Characteristics. The problem of nonlinear springs is presented.

- [19] presents a thorough theoretical background on nonlinear ordinary differential equation. Stiffening springs (the later much cited *Duffing equation*) and methods to investigate these are presented.

### Mathematical work on simple systems

- [13] [14] is a two-series article establishing and simulating the SDOF system with clearance by splitting up and solving it as piecewise linear and for each discontinuity using the previous boundary conditions to start the next linear scheme. The second article in the series simulates the equation of motion and present the dynamic response. This work confirms much of the work done in the project thesis [16].

- [25] presents a rigorous mathematical background to solve the problem of a piecewise linear forced oscillator. Phenomena as bifurcation, Poincaré maps, period doubling, horseshoes and strange attractors are taken care of.

- [8] presents an overview of approaches for modeling the dynamics of mechanical joints in assembled structures. Friction models are covered, together with how to model joints in finite element analysis.

### Experimental work

- [7] provides an equivalent SDOF model as the project thesis. Solves the problem by harmonic balance method and uses the numerical Newton-Raphson method for solution. Validates the solution by means of a torsional model of a gear pair.

- [6] looks at impact response and the influence of friction. They use a two-sided impact stopper to limit the movement of a beam. An excellent reference list is provided.

- [10] investigates random vibration conditions for a beam with impacting stops.

# Chapter 3

# Theory

The objective of this chapter is to introduce the theory needed to understand the numerical model, the results and the engineering context.

## 3.1 The Fundamentals of Vibration

This section introduces the reader to the concepts and notation in general vibration analysis. Much of this is derived with respect to linear systems and stead-state response. A great deal of this is useful when we later explore nonlinear systems and transient response.

The simplest vibrating system is described by its equation of motion:

$$m\ddot{x} + c\dot{x} + kx = F(t) \tag{3.1}$$

or for a MDOF system we use matrix notation:

$$\mathbf{M}\,\ddot{\mathbf{x}} + \mathbf{C}\,\dot{\mathbf{x}} + \mathbf{K}\,\mathbf{x} = \mathbf{f} \tag{3.2}$$

where $x$ or $\mathbf{x}$ represents the generalized coordinate position and a dot represents differentiation with respect to time $t$. $m$ or $\mathbf{M}$ indicates mass, $c$ or $\mathbf{C}$ represents damping and $k$ or $\mathbf{K}$ represents the stiffness. Both equation 3.1 and 3.2 yields directly from Newton's 2. law of motion. For more complicated systems it might be tempting to use Lagrange's equation to derive the EOMs (see [20] for an excellent derivation of Lagrange's and Hamilton's equation).

Eq 3.1 has a solution on the form of two parts:

$$x(t) = x_h(t) + x_p(t) \tag{3.3}$$

where $x_h$ denotes the solution to the homogeneous equation (F(t) = 0) and $x_p$ denotes the particular solution. We introduce the following terms:

| | |
|---|---|
| $\omega_n = \sqrt{\frac{k}{m}}$ | natural frequency |
| $c_c = 2m\,\omega_n$ | critical damping coefficient |
| $\zeta = \frac{c}{c_c}$ | damping factor |
| $\omega_d = \omega_n\sqrt{1 - \zeta^2}$ | damped natural frequency |
| $\delta_{st} = \frac{F_0}{k}$ | static deflection |
| $r = \frac{\omega}{\omega_n}$ | frequency ratio |

Table 3.1: Fundamental terms of vibration.

By rearranging eq 3.1 we may write it as

$$\ddot{x} + 2\zeta\omega_n\dot{x} + \omega_n^2 x = \frac{F_0}{m}\sin\omega t \tag{3.4}$$

We assume that we are in the oscillatory underdamped regime, $\zeta < 1.0$. This is necessary as we otherwise would have no motion after one period. Friction is the main source of damping. Friction models is another topic of discussion, but in short we may withing reason assume that the equivalent viscous damping factor $\zeta_{eq} < 1.0$ for friction. The homogeneous solution is traditionally found by assuming $x_h = e^{st}$ and then substituting in and solving via the characteristic equation. Every book on vibration contains this derivation ([24], [11], [28]), and it is also found as the solution to a homogeneous second order differential equation in other literature. We skip the details and present the solution for $\zeta < 1$:

$$x_h(t) = e^{-\zeta\omega_n t}(C_1 \sin\omega_d t + C_2 \cos\omega_d t) \tag{3.5}$$
$$= X_h e^{-\zeta\omega_n t}\sin(\omega_d t + \phi_h) \tag{3.6}$$

where $C_1, C_2$ are found through initial conditions and subscript $h$ indicates homogeneous. $X_h, \phi_h$ is dependent on $C_1, C_2$ and is found through trigonometric identities

Given a excitation on the form $F(t) = F_0 \sin\omega t$. The particular solution is a steady-state oscillation of the same frequency $\omega$ as the excitation. Assuming that

$$x_p(t) = X \sin(\omega t - \phi) \tag{3.7}$$

$X$ being the amplitude of oscillation, $\phi$ the phase of the displacement w.r.p exciting force. By substituting eq 3.7 into the EOM eq 3.1 and using trigonometric relations we may arrive at (see [24, p. 271] for details)

$$X = \frac{F_0}{\sqrt{(k - m\omega^2)^2 + c^2\omega^2}} \tag{3.8}$$

and

$$\phi = \tan^{-1}\left(\frac{c\,\omega}{k - m\,\omega^2}\right) \tag{3.9}$$

Dividing both numerator and denominator of eq 3.8 by $k$ and making substitutions we obtain

$$\frac{X}{\delta_{st}} = \frac{1}{\sqrt{(1 - (\omega/\omega_n)^2)^2 + (2\zeta\omega/\omega_n)^2}} = \frac{1}{\sqrt{(1 - r^2)^2 + (2\zeta\, r)^2}} \tag{3.10}$$

and

$$\phi = \tan^{-1}\left(\frac{2\zeta\, r}{1 - r^2}\right) \tag{3.11}$$

And we may thus conclude with the total solution of the problem $x(t)$:

$$x(t) = \delta_{st}\underbrace{\frac{\sin(\omega\, t - \phi)}{\sqrt{(1 - r^2)^2 + (2\zeta\, r)^2}}}_{\text{particular}} + \underbrace{X_h e^{-\zeta\omega_n t}\sin(\omega_d\, t + \phi_h)}_{\text{homogeneous}} \tag{3.12}$$
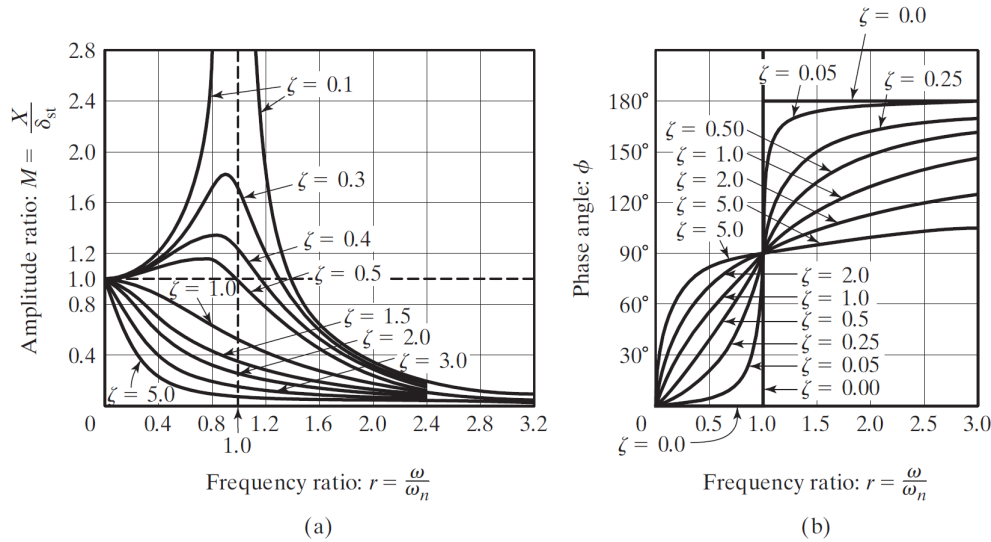


Figure 3.1: Plot of eq 3.10 for various damping and frequency ratios in terms of amplitude (a) and in terms of phase angle (b).[1]

Fig 3.1 (a) is very useful for understanding the steady-state amplitude ratio $M$ as a function of how close to the natural frequency $r$ the system of interest is. There are several interesting general properties of vibration that can be found from 3.1. The most prominent perhaps being the dramatic spike in response when $r$ is close to 1. This is phenomena is termed *resonance*. Secondly, we observe that at a driving frequency of approximately 0, the amplitude ratio is 1, meaning that the observed amplitude is equal to the static deflection $\delta_{st}$. This makes sense as there is nothing to drive the system, hence it behaves statically. Thirdly, we may observe that for $r \gg 1$ the amplitude ratio actually tends to zero. Physically this means that for relatively high frequencies, the system response will be very small. One last interesting observation is that damping, $\zeta$, will lower the system response in the regime $0 < r < \sqrt{2}$ while for $r > \sqrt{2}$ the response is increasing by increasing damping (see [28, p. 65] for more.

---

[1]Image courtesy of [24, p. 296].

**What *is* resonance?**

Mathematically it is easy to explain resonance as "when the forcing frequency acting on an oscillating system equals the natural frequency of the very same system". However, this does not really give us much in terms of understanding the concept of resonance. Resonance may be thought of more conceptually like the following: a swing with a child on it swings back and forth. The potential and kinetic energy take turns in being the largest source of energy: kinetic on the bottom of the swing and potential on the top of each side. In order to swing the child higher, in other words, to put more energy into the system, we need to push the child at specific time intervals - we have to push with the same oscillating frequency as the swing has. If we push at the wrong time, we would not really change the height of the swing or we may even slow it down (pushing in the opposite direction and acting effectively as a damper). This is hopefully a more everyday-approach to the concepts explained mathematically above.

## 3.2 Nonlinear Vibrations

A great deal of the concepts and relations provided in the previous section (3.1) serves to explain much of the behavior of oscillatory systems. However, in the real world a number of oscillatory phenomena may not be predicted by means of linear theory. Linear systems have a linear relation: if we double the load, the response is doubled. For nonlinear systems this is no longer the case. It will later be presented some force-displacement relations useful for clearance-type vibration. We shall not reveal this yet, but common sense tells us that if we have a clearance there shall be little or no force in that area whereas when it is in contact the force should be large. I.e. a doubling of the displacement making us switch regime from the clearance no-force to contact large-force is a nonlinear behavior.

The differential equation describing a nonlinear oscillatory system can have the general form of [28, p.436]:

$$\ddot{x} + f(\dot{x}, x, t) = 0 \tag{3.13}$$

In our case the forcing term $f(\dot{x}, x, t)$ is dependent on displacement $x$ through the following $f = k(x)x + c(x)\dot{x}$. It is $k(x)$, $c(x)$ which makes the system nonlinear.

Few nonlinear differential equations have an analytical solution ready, and to obtain one the treatment is often difficult and require extensive mathematical study. A large part of the solutions are based on numerical approximations, such as from the Runge-Kutta method. However, much can be learned from studying the state space and the motion presented in the phase plane [19].

## 3.3 Vibro-Impact Systems

As stated by [18] vibro-impact systems have been known to human long before they were considered in the scientific community. Throwing a skipping stone on water or a woodpecker toy are common examples. "Generally, vibro-impact systems involve multiple impact interactions (...). In most cases, there is energy loss due to impacts (...). The time scale involved during impact is much smaller than the time scale of the natural frequency of the oscillator. The motion of vibro-impact systems in the presence or absence of friction, is usually described by strongly nonlinear non-smooth differential equations." [18, p. 1]. It is the sudden change in velocity prior to and after impact that is the origin for the nonlinearity and thus resulting in what is nown as *non-smooth dynamics* [18, p. 7]. According to [18] there exist three different techniques to transform non-smooth models into smooth models. These include power-law phenomenological modeling, the Zhuravlev and Ivanov non-smooth coordinate transformations and the Hertzian contact law.

The previous section presents the response of a forced, damped mass-spring system, let us look into vibro-impact systems. The author's project thesis [16] derived the EOMs for the simplest vibro-impact system. We shall repeat the results here as an initial foundation to the problem.
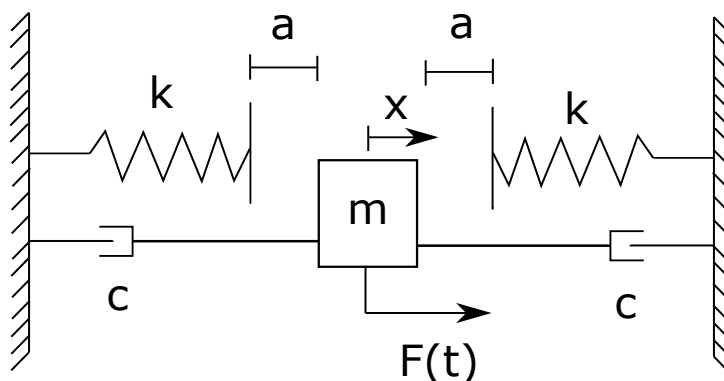


Figure 3.2: Mass-spring damper with clearance.

The problem is reduced as seen on fig 3.2. The mass is oscillating between to springs with stiffness $k$ and with a gap $a$. This makes the problem vibro-impact in nature. $k$ is formulated as eq 3.14. The damping term $c$ may also be discontinuous and nonlinear, but for this purpose we will keep it linear. One practical application of having the presence of damping is for instance friction.

$$k(x) = \begin{cases} 0 & -a < x < a \\ k & \text{else} \end{cases} \tag{3.14}$$
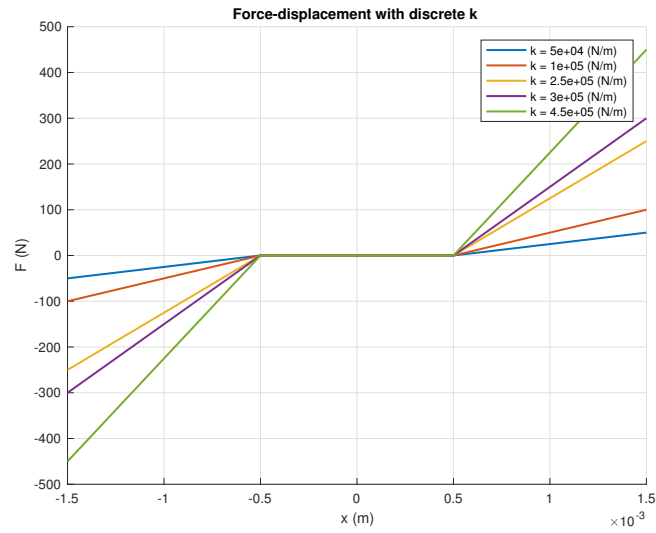
Figure 3.3: Force-displacement curve for a discrete $k$-formulation. $a = 0.5$ mm.
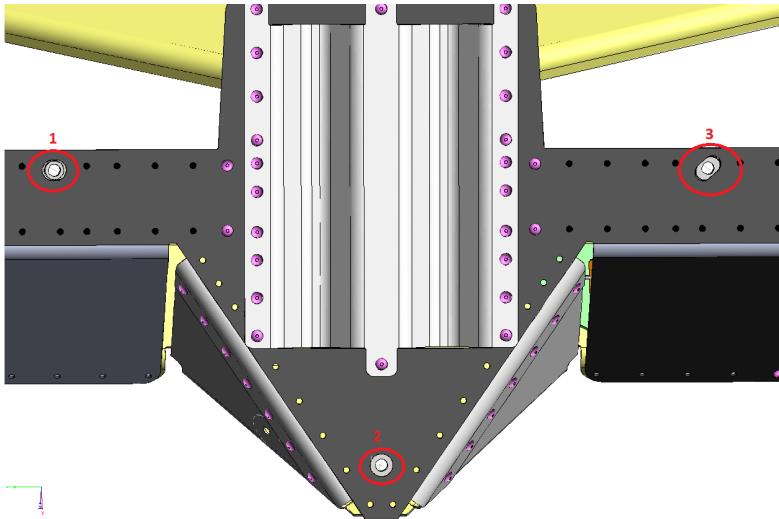


Figure 3.4: CAD revealing the kinematic joints on RIMFAX. 1) radial: allows radial expansion, 2) rigid joint, 3) slot: allows translation in one direction.

## 3.4 Power-Law Phenomenological Modeling

This is one of several ways of modeling the phenomena observed in fig 3.2. It models the spring force on a power-law based formulation. Consider a particle with mass $m$ moving between two walls positioned at $x = \pm a$. If we assume rigid impact the constraint becomes $x \leq |a|$, $x$ being the particle displacement. We want to express the spring force as being very weak (in fact close to zero) in between the walls, and fast growing in the proximity of $x = \pm a$. We represent this as:

$$F_s = \kappa \left(\frac{x}{a}\right)^{2n-1} \tag{3.15}$$

where $\kappa$ is a positive constant, usually based on experiments, and $n >> 1$ is an integer. This formulation is inspired by [18, p. 8]. Figure 3.6 shows the spring force as a function of the dimensionless coordinate $x/a$ for different values of $n$. We observe that as $n \to \infty$ we get the case of completely rigid impact. By adjusting $n$ we can adjust the nonlinearity of the problem, high $n$ giving a strongly nonlinear formulation of the problem.
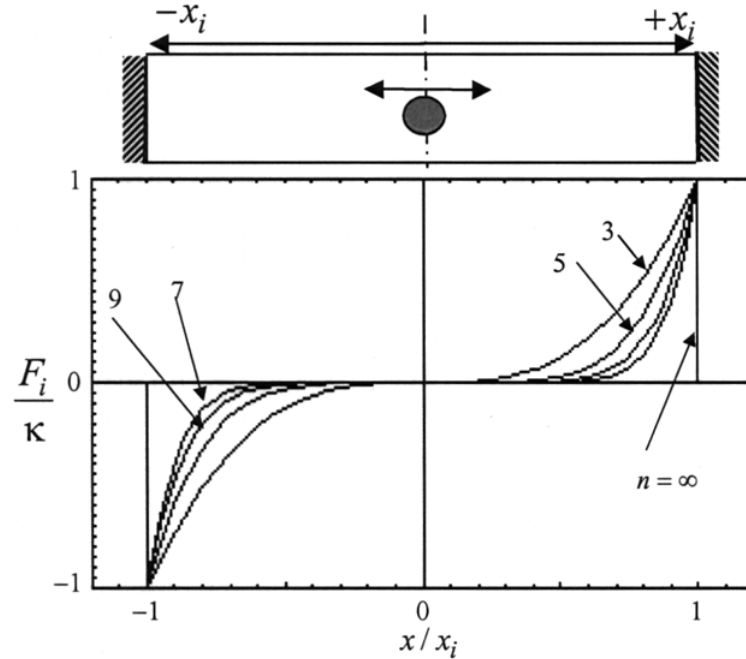


(a)

Figure 3.5: Plot of eq 3.15 in dimensionless form. [18, p. 8]

The damping term may be formulated in a similar way:

$$F_d = c \left(\frac{x}{a}\right)^{2p} \dot{x} \tag{3.16}$$

$c$ being the constant coefficient also determined experimentally as $\kappa$, and $p >> 1$ an integer. The equations of motion will thus take the form

$$m\ddot{x} + \kappa \left(\frac{x}{a}\right)^{2n-1} + c \left(\frac{x}{a}\right)^{2p} \dot{x} = F(t) \tag{3.17}$$

The solution of eq 3.17 may be solved numerically according to [16] by reducing it to a set of first order differential equations. Given a set of initial conditions it is possible to solve the problem by use of for instance Runge-Kutta methods. `ode15s` is a function which implements RK-methods for *stiff* [2] differential equations in MAT-LAB.
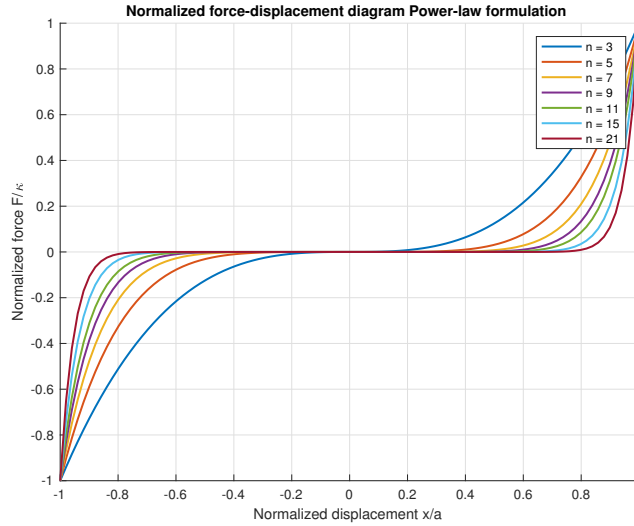


Figure 3.6: Normalized Power-law formulation.
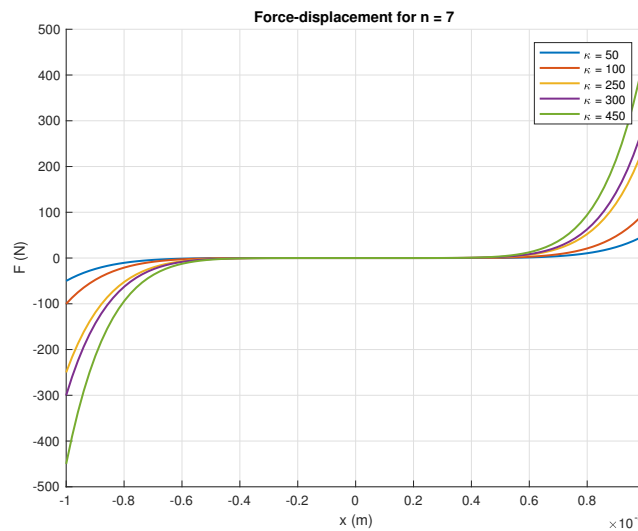


Figure 3.7: Force-displacement curve for Power-law formulation

---

[2]Stiff differential equations are classified by that a small change in time step gives rise to a large change in forces/acceleration. In this particular case, the differential equations are stiff in the proximity of the walls - a small change in time and the acceleration changes from zero to a high value.

## 3.5   Friction and Contact Models

Friction models are important in the sense that they describe the state of stick / slip and determine whether we have micro or macroslip. The literature typically classify friction models into phenomenological and constitutive. The former representing the friction force as a function of the relative displacement and the latter being based on interface physics in the contact area [15].

### Why spend time on friction models?

The following pages will spend some time on presenting a few different friction models. These models are important in a sense that they provide the current state of work on the topic and that they may be used later. In our later analysis (Section 3 and onward) we have not been so advanced in that we have implemented the following models. The reason for this being that we are assuming a full macroslip-regime. However, if we later want to examine the transition from stiction to slip we might want to look further into some of the later models hereby presented.

### Phenomenological friction models

A friction interface in a joint connection is considered. The friction force acts as an internal force in the tangential direction of the contacting surfaces. Below a critical value, the force is causing no relative motion between the surfaces. At a critical value, the force obeys a constitutive equation such as Coulomb's law and act in opposite direction to the relative velocity. The required force to keep the joint moving depends on relative velocity and many other factors. [15] also separates between static and dynamic friction models. The Signum-Friction or Coulomb's law is an example

$$F = F_c \operatorname{sgn}(v) = \mu F_N \operatorname{sgn}(v) \tag{3.18}$$

$F_N$ being the normal load ($mg$) and $\mu$ the friction coefficient and $v$ the velocity.

$$\operatorname{sgn}(v) = \begin{cases} -1 & v < 0 \\ 0 & v = 0 \\ +1 & v < 0 \end{cases} \tag{3.19}$$

[15] also includes dynamic friction models in their study. (3.18) is a *static* friction model. A drawback of classical, static models are their inability to describe the elastic deformation in the joint surfaces before slip occurs. Recognizing that friction is a dynamic problem remedies this. The LuGre model being one of two dynamic models, it is based on the force generated by solid-to-solid contact. At the microscopic level, surfaces are irregular and make contact at a number of asperities which can be considered contact between bristles. The bristles deflect like springs and create the friction force when a tangential force is applied. The model is based on the average behavior of bristles, since the contact surfaces have high irregularities. The model was designed reproduce all observed friction phenomena over a wide range of operating conditions. We leave the interested reader to dive into the literature (i.e. [15]) as this is not considered the scope of this report.

## Constitutive contact models

Constitutive models establish a relationship between stress and displacement fields. Continuum mechanics is used as the framework for this. There are several ways to describe this relationship. [15, p. 96] bases laws of normal and tangential contact on the basis of a statistical surface model. The surface being rough and only having contact at asperities. As both [15, p. 96] and [8, p. 2805] mentions, the Hertz contact theory can be used to describe normal contact of such asperities on a micro scale. Constitutive contact models are for instance used in resolving the contact of two surfaces. The `CGAP` element in NASTRAN is an example of such a formulation. As this project work focus more towards nonlinear springs than contact per se, we will limit the topic of discussion here - albeit the field of constitutive contact is wast it is not considered *as* relevant here.

## Energy dissipation

Damping is present in all oscillatory systems. Its effect is to remove energy from the system. Energy in a vibrating system is either dissipated into heat or radiated away. For instances, to surfaces sliding against each other get warm and an object given a sharp blow radiates sound ([28]). Energy dissipation is the conversion of mechanical energy into heat. If non-conservative forces are acting on a system and excerting work, they are a source of energy dissipation. When kinetic energy is reduced due to friction through heat generation, we call friction a energy dissipator.

## Friction solved by equivalent viscous damping

One of the early, classical works on mechanical vibration is the work of den Hartog [11]. The last chapter in this book is devoted to nonlinear systems. Here, a model for forced vibration with nonlinear damping is proposed. This is very relevant as it serves a the simplest case for our problem. [24, p. 149 and 250] derives this in detail. We skip the most basic free-body derivation of the equations of motion and continue to the case of forced vibration with Coulomb damping for a single degree of freedom (SDOF) system:

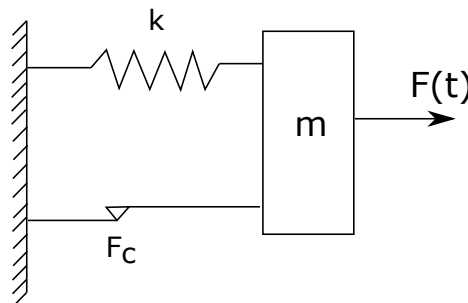$$m\ddot{x} + kx + F_c \operatorname{sgn}(\dot{x}) = F_0 \sin \omega t \tag{3.20}$$



Figure 3.8: Forced vibration of SDOF system with Coulomb damping.

The $\operatorname{sgn}(\dot{x})$ indicating that when the motion is positive, $F_c$ acts in the negative direction and vise versa.

An exact solution of (3.20) is fairly extensive. Assuming that $F_c$ is large compared to $F_0$, the displacement of mass will be discontinuous. That implies that for small dry friction damping - small $F_c$ - the steady state solution is expected to be nearly harmonic. The most general method replaces the friction damping term ($F_c \operatorname{sgn} \dot{x}$) with an equivalent viscous viscous damping ratio, $c_{eq}$. These assumption simplify the derivation and clarify the first principles. We find this ratio by acknowledging that the work done by $c_{eq}$ has to be equal that of dry friction. Let the motion be assumed to be $x = X \sin \omega t$. For a general damping force $f(\dot{x})$ the work dissipated per cycle $T$ is:

$$\Delta W = \int f(\dot{x}) \, dx = \int_0^T f(\dot{x})\dot{x} \, dt = x_0 \int_0^{2\pi} f(\dot{x}) \cos \omega t \, d(\omega t) \tag{3.21}$$

In our case $f(\dot{x}) = \pm F_c$. Also, recognizing that we can split the integral in quarter and multiply we get

$$\Delta W = 4X \int_0^{\pi/2} F_c \cos \omega t \, d(\omega t) = 4F_c X \tag{3.22}$$

The energy dissipated by a general viscous force $F_d = c\dot{x}$ is

$$\Delta W = \int_0^{2\pi/\omega} c\dot{x} \, dt = \int_0^{2\pi} cX^2 \omega \cos^2 \omega t \, d(\omega t) = \pi c \omega X^2 \tag{3.23}$$

Equating (3.22) and (3.23) we get

$$c_{eq} = \frac{4F_c}{\pi \omega X} = \frac{4\mu m g}{\pi \omega X} \tag{3.24}$$

And following the familiar definition of damping ratio $\zeta$:

$$\zeta_{eq} = \frac{c_{eq}}{c_{crit}} = \frac{4\mu m g/\pi \omega X}{2m\omega_n} = \frac{2\mu g}{\pi \omega \omega_n X} \tag{3.25}$$

This general procedure may be applied to any type of damping, even if its law is given merely in curve form, where the integral 3.22 must be evaluated graphically. We use the $c_{eq}$ in the familiar EOM for a forced viscously damped mass-spring system and eq 3.20 becomes:

$$m\ddot{x} + kx + c_{eq}\dot{x} = F_0 \sin \omega t \tag{3.26}$$

Eq 3.26 has readily steady state- and transient solutions. From textbooks on mechanical vibrations ([28, p. 30], [24, p. 143], [11, p. 45] we know that damped systems has the *damped* natural frequency

$$\omega_d = \omega_n \sqrt{1 - \zeta^2} \tag{3.27}$$

For most practical situations however, the damped natural frequency *is* the natural freqency, $\omega_d \approx \omega_n$ as a realistic damping ratio is in the vicinity of $\zeta < 0.1$ and so (for $\zeta = 0.1$) $\omega_d = 0.995\omega_n$.

## 3.6 Duffing Equation

We may approximate this thesis' problem by use of the *Duffing equation*. Presented by German Georg Duffing (1861-1944), the equation represents mass on a cubic spring.

$$m\ddot{x} + c\dot{x} + kx + \mu x^3 = F\cos\omega t \qquad (3.28)$$

This is in fact very close to the power-law formulation we saw in eq 3.15. Duffing presents $F_s = kx + \mu x^3$ while power-law formulation yields $F_s = \kappa(x/a)^{2n-1}$. If we let the Duffing equation be to the power of $(2n-1)$ (any odd integer, not just 3) and we term $k$ a "relaxation stiffness" $k = k_r$ and $k_r \ll 1$. We need also alter the power-law formulation somewhat. The term $(x/a)$ is in reality just a variable we may choose however we like. $x/a$ is a neat, clear formulation as $\pm 1$ indicates the "walls", but we may as well choose to use $x \in [-a, a]$. Finally we equate $\mu = \kappa$ and end up with $F_{s\text{ powerlaw}} \approx F_{s\text{ duffing}}$. Thus we may conclude that with the correct valued parameters, the Duffing equation describes the motion of our system. This is highly useful as much work as research is already conducted on the Duffing equation.

We now wish to explore to different solution techniques that may be used to solve the Duffing equation. We initially simplify and then add terms and complexity as we go on.

**Perturbation method**
This method is used when a small parameter $\mu$ is associated with the nonlinearity, such as in our case with the Duffing equation. The solution is a series development in the neighborhood of the solution, based in terms of $\mu$. We assume that if the solution of the linearized problem is periodic and $\mu$ small, then the perturbed solution is also periodic. We wish to show that the period is a function of the amplitude of vibration. This derivation is based on the works of [28, p. 445-451] [19, p. 149-180]. First, consider the free oscillation of an undamped spring:

$$\ddot{x} + \omega_n^2 x + \mu x^3 = 0 \qquad (3.29)$$

with initial conditions $x(0) = A$ and $\dot{x}(0) = 0$. For $\mu = 0$ we get the well known linear spring and the frequency of oscillation is that of the linear system $\omega_n = \sqrt{k/m}$. Wee seek a solution in on the form

$$x = x_0(t) + \mu x_1(t) + \mu^2 x_2(t) + \ldots \qquad (3.30)$$

As we have assumed that frequency of nonlinear oscillation $\omega$ is dependent on amplitude we may write this in series of $\mu$:

$$\omega^2 = \omega_n^2 + \mu\alpha_1 + \mu^2\alpha_2 + \ldots \qquad (3.31)$$

$\alpha_i$ is a yet undefined function of amplitude and $\omega$ is the frequency of nonlinear oscillation. For the familiar linear case of free oscillations, we know that $\omega = \omega_n$. For the nonlinear case, we keep these apart, $\omega_n$ still denotes the natural frequency of the linear system.
Consider only the first two terms of the previous two equations and substitute into eq 3.29 to obtain:

$$\ddot{x}_0 + \mu\ddot{x}_1 + (\omega^2 - \mu\alpha_1)(x_0 + \mu x_1) + \mu(x_0^3 + 3\mu x_0^2 x_1 + \dots) = 0 \tag{3.32}$$

As the perturbation parameter $\mu$ may be chosen arbitrarily, the coefficients of the various powers of $\mu$ must equal to zero. This leads to:

$$\ddot{x}_0 + \omega^2 x_0 = 0 \tag{3.33}$$
$$\ddot{x}_1 + \omega^2 x_1 = \alpha_1 x_0 - x_0^3 \tag{3.34}$$

The solution to the first equation, considering the initial conditions is $x_0 = A \cos \omega t$. This is in the literature termed the *generating solution*. Substituting this into the right hand side of the second equation we get

$$\ddot{x}_1 + \omega^2 x_1 = \alpha_1 A \cos \omega t - A^3 \cos^3 \omega t \tag{3.35}$$

$$= \left(\alpha_1 - \frac{3}{4}A^2\right) A \cos \omega t - \frac{A^3}{4} \cos 3\omega t \tag{3.36}$$

Here the identity $\cos^3 \omega t = \left(\frac{3}{4} \cos \omega t + \frac{1}{4} \cos 3\omega t\right)$ is used. Note that the term $\cos \omega t$ would lead to $t \cos \omega t$ in the solution of $x_1$. This will become a condition of resonance which violates the initial assumption of periodic motion. Hence, the following condition is imposed:

$$\alpha_1 - \frac{3}{4}A^2 = 0$$

thus

$$\alpha_1 = \frac{3}{4}A^2 \tag{3.37}$$

is the relation we stated above that $\alpha$ is a function of $A$. With the term $\cos \omega t$ eliminated, the solution for $x_1$ is

$$x_1 = C_1 \sin \omega t + C_2 \cos \omega t + \frac{A^3}{32\omega^2} \cos 3\omega t \tag{3.38}$$

$$\omega^2 = \omega_n^2 + \frac{3}{4}\mu A^2 \tag{3.39}$$

Imposing $x_1(0) = \dot{x}_1(0) = 0$ we get $C_1, C_2$:

$$C_1 = 0 \qquad C_2 = -\frac{A^3}{32\omega}$$

which yields

$$x_1 = \frac{A^3}{32\omega^2}\left(\cos 3\omega t - \cos \omega t\right) \tag{3.40}$$

and the total solution $x = x_0 + \mu x_1$ is

$$x = A \cos \omega t + \frac{A^3}{32\omega^2}\left(\cos 3\omega t - \cos \omega t\right) \tag{3.41}$$

$$\omega = \omega_n \sqrt{1 + \frac{3\,\mu A^2}{4\,\omega_n^2}} \tag{3.42}$$

The solution is found to be periodic and the fundemental frequency $\omega$ is increasing with amplitude $A$.

**Method of Iteration**

Method of iteration is a process of successive approximation, where an assumed solution is substituted into the differential equation, this is then integrated to obtain a solution with higher accuracy. The procedure may be repeated several times to achieve the desired accuracy. It differs from the preceding perturbation method in that we assume a solution and then iterate on that until we are satisfied with the accuracy. The perturbation method is linearizing the problem by a series development with the use of $\mu$. For illustration, let us first consider the case *without* damping, such that eq 3.28 becomes:

$$\ddot{x} + \omega_n^2 x + \mu x^3 = F \cos \omega t \tag{3.43}$$

We seek a solution to eq 3.43 and uses the technique of [28, p. 448]. The solution we seek is steady-state harmonic, and we use the method of iteration.

Let us assume the first solution to on the well known form of:

$$x_0 = A \cos \omega t \tag{3.44}$$

and substitute this into the differential equation 3.43:

$$\ddot{x} = \omega_n^2 A \cos \omega t - \mu A^3 \left( \frac{3}{4} \cos \omega t + \frac{1}{4} \cos 3\omega t \right) + F \cos \omega t$$

$$= \left( -\omega_n^2 A - \frac{3}{4} \mu A^3 + F \right) \cos \omega t - \frac{1}{4} \mu A^3 \cos 3\omega t$$

We integrate this. Setting the integration constants to zero to obtain a harmonic solution with period $\tau = 2\pi/\omega$. The improved solution is then

$$x_1 = \frac{1}{\omega^2} \left( \omega_n^2 A + \frac{3}{4} \mu A^3 - F \right) \cos \omega t - \cdots \tag{3.45}$$

and higher order harmonic terms are neglected.

We may proceed if wanted, but Duffing reasoned that if the first and second approximations are reasonable the coefficients of $\cos \omega t$ must not differ greatly. In other words:

$$A = \frac{1}{\omega^2} \left( \omega_n^2 A + \frac{3}{4} \mu A^3 - F \right) \tag{3.46}$$

which may be solved for $\omega^2$:

$$\omega^2 = \omega_n^2 + \frac{3}{4} \mu A^2 - \frac{F}{A} \tag{3.47}$$

As a check of consistency we observe that if the nonlinear parameter $\mu = 0$ we end up with:

$$A = \frac{F}{\omega_n^2 - \omega^2} \tag{3.48}$$

which is the exact linear system solution we previously observed in eq 3.8 (let $c = 0$). For $\mu \neq 0$ $\omega$ is a function of $\mu, F, A$. For $F = 0$ we get:

$$\frac{\omega^2}{\omega_n^2} = 1 + \frac{3\mu A^2}{4\omega_n^2} \tag{3.49}$$

We observe that frequency $\omega$ increases with amplitude. One important notice here is that $\omega_n$ is the *linear natural frequency* $\sqrt{k/m}$ while $\omega$ is the frequency of oscillation. For the case of no forcing term $F = 0$, $\omega$ will thus be the *nonlinear natural frequency*. We will keep calling this for $\omega$. The result above is the same as we previously obtained from the perturbation method. This proves that the two techniques solve the problem.

We can map the amplitude-frequency response diagram for the Duffing equation.
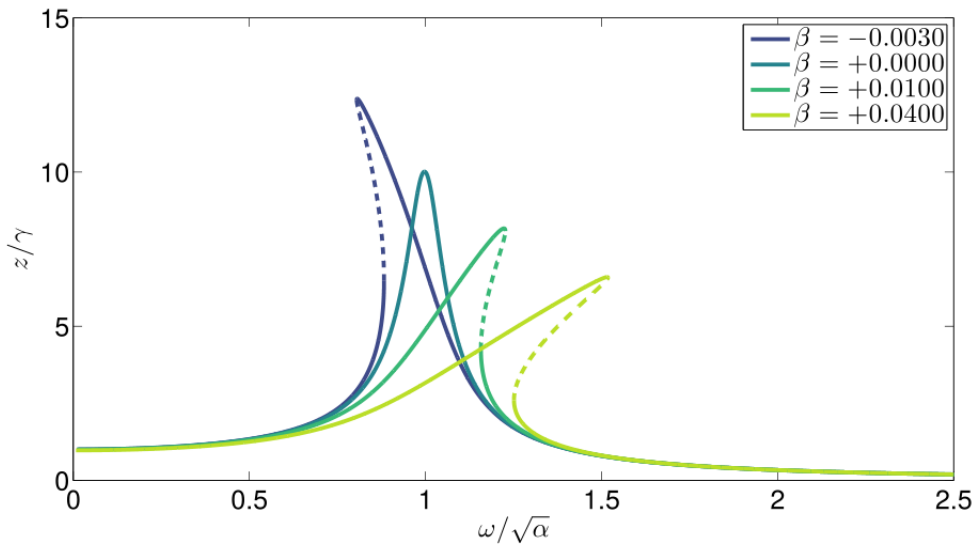


Figure 3.9: Frequency response of the Duffing equation. Here the steady-state response is $x(t) = z\cos(\omega t - \phi) + \ldots$, $\alpha = \omega_n^2 = 1$, $\gamma = F = 1$ and $\beta = \mu$. Image courtesy of [3].

There are several interesting elements from fig 3.9. Most prominently is perhaps the fact that the nonlinear natural frequency is *amplitude dependent*. A higher amplitude, the more we will move up the force-displacement diagram and the higher natural frequency. See trend line in fig 3.10.

---

[3]Image courtesy of [1].
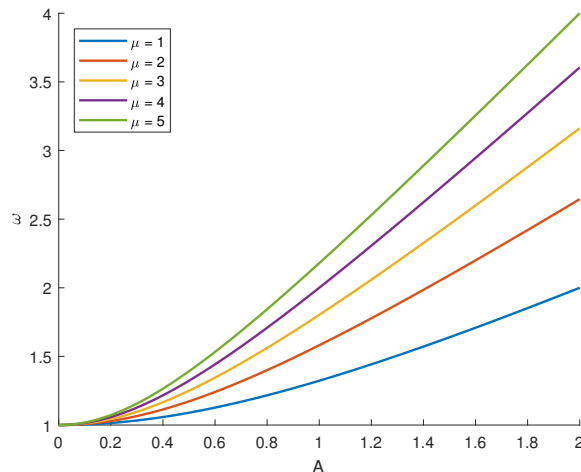
Figure 3.10: Frequency $\omega$ in the Duffing relation as a function of amplitude $A$ from eq 3.49.

## 3.7 Mapping of Bifurcations

Bifurcation theory investigates the effect an alteration of a differential equation has on the equilibrium points of that differential equation. A way of visualizing this effect is through a *bifurcation diagram* which will plot the equilibrium points along the $y$-axis and the bifurcation parameter being altered along the $x$-axis. This will for many dynamic systems reveal when the system go from one to several equilibrium points and in some cases (e.g. nonlinear differential equations). Bifurcation occurs when a small change to a parameter causes a qualitative change in the way the solution looks like (e.g. number of equilibrium points change).

**Grazing bifurcations and C-bifurcations**
"The bifurcation associated with zero velocity just at the barrier is referred to as grazing bifurcation. Of particular interest of grazing impact bifurcation is its mapping. This chapter presents the basic concept of grazing bifurcation and the discontinuity mappings. It also addresses another type in which the fixed point or a periodic orbit may cross or collide one of the boundaries and this type is referred to as border-collision or C-bifurcation" [18, p. 31].

**Poincaré map**
A *Poincaré map* or *Poincaré section* is a method of visualizing the chaotic behavior of nonlinear systems. The method is based upon investigating the state-space representation of the system. For oscillatory system this is typically done by use of the phase portrait, where displacement ($x$-axis) is plotted against velocity ($y$-axis). This reveals the trajectories of the dynamical system. Imagine the systems trajectory being an orbital path. It is orbiting in the state-space. We extract a subsection (Poincaré section) of the data everytime the orbit crosses for instance $\theta = 0$. Every time the systems orbital crosses $\theta = 0$ we sample a point of $x, \dot{x}$. For chaotic systems, the orbit will not cross $\theta = 0$ with the same $x, \dot{x}$ which makes it possible to generate rather interesting plots, or Poincaré maps. It is possible to not only let time $t$ be a variable (this gives rise to the numerous passings of $\theta = 0$) but we can also vary $\theta$, going around the orbit. Based on this it is possible to make a range of

Poincaré maps into an animation to study the system.

**Period doubling**

Period doubling is a phenomena where a slight change in a parameter causes the system to behave in a manner with twice the period of the original system. In relation to the current topic, a slight change in forcing amplitude may cause the system to oscillate at twice the original frequency.

## 3.8    Nonlinear Finite Element Analysis

A brief background on the topic of dynamic problems under nonlinear conditions with transient response will be given for the reader to posses the essential understanding.

The first thing to notice is that the problem is *dynamic*, it changes over time. The bushing is moving back and forth in the given play inside the joint. Secondly, the stiffness $k$ is *nonlinear* as previously seen. As one term in the EOM is nonlinear, the whole problem becomes nonlinear. Thus, the principle of superposition is not applicable and we need to solve the problem with different methods. Thirdly, in order to replicate the response from the experiment, we will be using a time-varying input force $F(t)$. This will not yield a steady-state solution, and we must calculate the *transient* response of the structure. Combining all of this and using finite element analysis to solve the problem, we are dealing with *nonlinear transient dynamic finite element analysis*.

There are two conceptually different solution methods to choose from: *explicit* or *implicit*. The most profound difference is that explicit methods obtains its solution in terms of known quantities while implicit methods obtains the solution in terms of unknown quantities. What we mean by this is that for explicit methods the displacement at time $t_{n+1}$, $\boldsymbol{D}_{n+1}$ is obtained from the equilibrium conditions at one or more preceding time steps without solving an equation system. The displacement values are obtained from information already known to us. For implicit methods $\boldsymbol{D}_{n+1}$ is obtained from the equilibrium conditions *at* time $t_{n+1}$ - equation solving is required. One very popular explicit method is the central differences method. It requires little computational effort during each step since equation solving is not necessary.

| Explicit | Implicit |
| --- | --- |
| + Equation solving is not necessary. Computationally inexpensive time steps | + Method is unconditionally stable. Time increment size is not limited and fewer increments required to complete |
| + Equilibrium iterations not necessary. Convergence is not an issue | + Ideal for problems where response period is long and/or where nonlinearites are smooth (such as plasticity) |
| + Ideal for high-speed dynamic simulations where small time increments are required | - Algebraic equations must be solved at each time step. Each increment is computationally expensive. |
| + Usually reliable for problems with discontinuous nonlinearites such as contact, buckling and material failure. | - Equilibrium iterations are necessary, convergence must be obtained for each increment |
| - Conditionally stable. Requires very small time steps | |

Table 3.2: Explicit vs implicit solution method

The case of this thesis requires solving the response in the time domain for a period of several tens of seconds (a sine sweep in the lab takes anywhere from 1 to 6 minutes depending on the frequency range and the ramp speed in octaves/min). Taking into consideration the fact that we need to avoid aliasing, the Nyquist frequency rule $f_s = 2f$ where $f_s$ is the sampling frequency and $f$ is the frequency we are interested in sampling. So for instance if we wish to look at response of our structure up to 1000 Hz, we must sample at 2000 Hz in order to represent the signal sufficiently. And so if we sweep from 0-1 kHz at $f_s = 2$ kHz over a time period of 60s we would need 120,000 data points. And so it reasonable to request to have a) varying time steps and b) possibly large time steps. The *implicit* method may be the most applicable here.

One widely used numerical time-stepping scheme for solving implicitly is the predictor-multicorrector form of the *Newmark family* of methods for the integration of equations which govern nonlinear transient dynamic problems [17, p. 285]. It may be summarized as follows:

1. Predict velocities and displacement using the "explicit" (we know at time $t_n$) approximation[4]

$$\ddot{\tilde{d}}_{n+1} = \mathbf{0}$$
$$\dot{\tilde{d}}_{n+1} = \dot{d}_n + (1-\gamma)\Delta t\, \ddot{d}_n$$
$$\tilde{d}_{n+1} = d_n + \Delta t\, \dot{d}_n + (1/2 - \beta)\Delta t^2 \ddot{d}_n$$

2. obtain correction to displacement from the linearised equilibrium equation written at time $t_{n+1}$:

$$\Delta d_{n+1} = K^{-1} r(d_{n+1}) \tag{3.50}$$

where the effective stiffness matrix is given as

$$\hat{K} = K + \frac{\gamma}{\beta\Delta t}C + \frac{1}{\beta\Delta t^2}M$$

3. increment displacement, velocity and acceleration:

$$d_{n+1} = \tilde{d}_{n+1} + \Delta d_{n+1}$$
$$\dot{d}_{n+1} = \dot{\tilde{d}}_{n+1} + \frac{\gamma}{\beta\Delta t}\Delta d_{n+1}$$
$$\ddot{d}_{n+1} = \frac{1}{\beta\Delta t^2}\Delta d_{n+1}$$

4. increment time $n = n + 1$, $t = t + \Delta t$ and go back to step 1.

---

[4]$\beta$ and $\gamma$ are free parameters. Average acceleration: $\beta = 1/4, \gamma = 1/2$ w/ unconditional stability. Linear acceleration: $\beta = 1/6, \gamma = 1/2$ w/ conditional stability

### 3.8.1 Time Step Selection

For both explicit and implicit time integration schemes, the time step has to be selected appropriately. The critical time step for making the Newmark method conditionally stable is

$$\Delta t_{cr} \leq \frac{\Omega_{cr}}{\omega_{max}} \tag{3.51}$$

where $\omega_{max}$ corresponds to the highest natural frequency of the corresponding eigenvalue problem. The critical sampling frequency $\Omega_{cr}$ is given as

$$\Omega_{cr} = \frac{\zeta\left(\gamma - \frac{1}{2}\right) + \sqrt{\frac{\gamma}{2} - \beta + \zeta^2\left(\gamma - \frac{1}{2}\right)^2}}{\frac{\gamma}{2} - \beta} \tag{3.52}$$

where $\zeta = c/c_{cr}$. A conservative value for $\Omega_{cr}$ is obtained by setting $\zeta = 0$:

$$\Omega_{cr} = (\gamma/2 - \beta)^{-1/2} \tag{3.53}$$

For explicit analysis with undamped material the critical time step becomes

$$\Delta t_{cr} \leq \frac{2}{\omega_{max}} \tag{3.54}$$

Where $\omega_{max}$ is said to be the highest frequency of the FE mesh, i.e. the highest mode of interest. For nonlinear problems, all modes might not be known a priori. In that case a reasonable $\omega_{max}$ in the frequency area of interest may be chosen. In general, for all types of integration schemes, $\Delta t$ must be small enough that information does not propagate more than the distance between adjacent nodes during a single time step. See among others [23] for more information.

## 3.9 Fast Fourier Transform

Fourier transforms are widely used in this thesis. The problem at hand is as stated earlier nonlinear and cannot be solved by modal techniques in MSC/NASTRAN (SOL 103, 111) and thus we must use direct techniques. This implies solving in the time domain. However, in order to analyze the data we would very much like to operate in the *frequency domain*. The time domain shows how amplitude varies over time whereas the frequency domain shows how much of the amplitude (displacement, velocity or acceleration in our case) lies within each given frequency band. The input signal we are applying to the jig through the shaker table consist of sine waves of many different frequencies and so will the response as well. These frequencies are however not easily perceived in the time domain. The solution to this is well known and widely used in science engineering and mathematics for a vast range of problem, and consists of applying a fast Fourier transform (FFT) on the data set when we post-process it.

A fast Fourier transform is an algorithm that samples a signal over a period of time and divides it into its frequencies components [2]. Many different algorithms exist, this thesis uses the built in function `fft` in MATLAB .
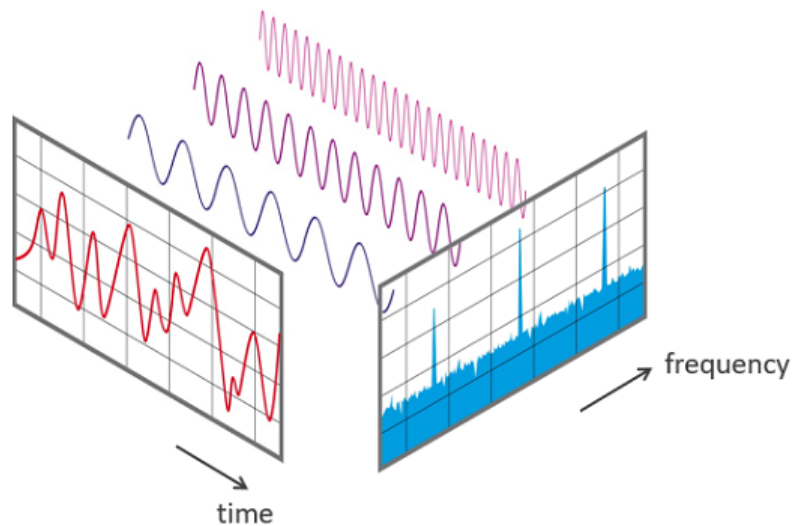


Figure 3.11: Illustration of how data in the time domain (red) is transformed into the frequency domain (blue) by splitting up the quantity of each frequency[5].

A signal in the time domain $f(t)$ may be transformed into the frequency domain $\mathcal{F}(\omega)$ by the following:

$$\mathcal{F}(\omega) = \frac{1}{\sqrt{2\pi}} \int_{-\infty}^{\infty} f(t) e^{-i\omega t} \, \mathrm{d}t \tag{3.55}$$

and the inverse transformation:

$$f(t) = \frac{1}{\sqrt{2\pi}} \int_{-\infty}^{\infty} \mathcal{F}(\omega) e^{i\omega t} \, \mathrm{d}t \tag{3.56}$$

---

[5]Image courtesy of [3].

A FFT computes the discrete Fourier transform of a signal. The discrete FT approximates an infinite series with infinite values into a definite series:

$$Y_k = \frac{1}{N} \sum_{n=0}^{N-1} y_n e^{-i\frac{2\pi}{N}kn} \tag{3.57}$$

where $y_n$ are the values in the time domain ranging from $n = 0, 1, \ldots, N-1$. $Y_k$ are the computed values in the frequency domain with $k = 0, 1, \ldots, N-1$ [27].

For vibration analysis FFT is important as it easily displays the amount of response at any sampled frequency. A frequency which displays a significant peak in amplitude may be assigned to be a natural frequency of the system as the system experience resonance and thus a large response in measured amplitude.

## 3.10 Descriptive Statistics

Descriptive statistics gives an overview of data that has been contained from repeated measurements. The simplest, standard deviation and variance, are calculated to give an overview of the distribution of data. . Consider a finite sequence of data $x_{n_{n=1}^N}$. Its mean value is given as

$$\bar{x} = \frac{1}{N} \sum_{i=1}^{N} x_i \tag{3.58}$$

Standard deviation $\sigma = \sqrt{\sigma^2}$ is a measure of deviation from the mean

Variance $\sigma^2$ is the expectation of the squared deviation in a distribution. It is given by

$$\sigma^2 = \frac{1}{N} \sum_{i=1}^{N} \overline{(x_i - \bar{x})^2} = \overline{x^2} - \overline{x}^2 \tag{3.59}$$

Max-min values are sometimes interesting to evaluate extreme events. Max($x_i$) or min($x_i$) are calculated.

# Chapter 4

# Numerical Approach

This chapter presents the numerical models used to solve the thesis problem. The overall aim is to model the problem as accurate as necessary yet as computationally inexpensive as possible.
MATLAB is an efficient tool for solving differential equations, doing post-processing and other general computing tasks. A study of the nonlinear equations of motion has been conducted in MATLAB and serves as an idealized introduction to the solution.

The structure of this chapter is:

- Present the numerical method in MATLAB. This includes reduction of order in the equations of motion (EOMs), the structure of the script and other relevant aspects in MATLAB

- Present the results from solving the EOMs

- Discuss the validity of the numerical method and results

## 4.1 Method

The author's project thesis built a set of MATLAB scripts and functions to solve the EOMs. This has been elaborated in this thesis through Power-law modeling in chapter 3.4 and Duffing equation in chapter 3.6. This extension of the previously developed scripts has been simulated.

MATLAB is utilized with its implemented Runge-Kutta solvers in order to find solutions of the differential equations of motion. Care must be taken in order to solve the equations properly. The nature of our problem is that when the mass comes in contact with the hard spring, a small time/displacement step results in a large force/acceleration difference. In other words, a small input difference leads to large output difference, hence the difference equation is *stiff*. In order to resolve this correctly, a very small step size has to be performed in the area of contact/no contact. MATLAB provides two useful ODE-solvers for stiff differential equations `ode15s, ode23s` [12]. In order to use these we have to reduce our EOM to a set of first order differential equations. Duffing eq 3.28 rearranged and taking into account nonlinear $k, c$ looks like

$$\ddot{x} = \frac{1}{m}\big(F(t) - k_r x - \mu x^3 - c\dot{x}\big) \qquad (4.1)$$

From this we may wish to experiment with different types of EOM. The author knows from the project thesis that if we wish to compare identically with MSC/Nastran we must include a relaxation stiffness $k_r$ as Nastran does not allow for complete zero force at the deadband. This is easily solved by letting the relaxation stiffness approach zero. For most of the MATLAB simulations $k_r$ =1E-05. $k_r$ operates for all $x$. By writing it as two first order differential equations we get:

$$f_1 = \dot{x} \qquad (4.2)$$

$$f_2 = \dot{f}_1 = \ddot{x} = \frac{1}{m}\big(F(t) - k_r\,x - \mu x^3 - c\dot{x}\big) \qquad (4.3)$$

this being the core of the work in MATLAB, it is implemented as a function in the following way:

```
function f = duffing_func(t, x)
global m c a krelax kappa n A w
%DUFFING FUNCTION Mass-spring damper excited at mass by force
f = zeros(2,1);
f(1) = x(2);
f(2) = (1/m)*(A*sin(w*t) - krelax*x(1) - kappa*(x(1)/a)^(3) - c*x(2));
end
```

We could obviously add or subtract from this, adding for instance friction laws, base excitation formulations and more. A function that uses an array as the forcing term allows for non-harmonic input. This opens up for sine sweep, random excitation or even copying the input on the experimental shaker by using the output from the control accelerometers.

A main script, named `duffing_solver.m`, deals with setting the parameters such as $a$, $k$, $m$ and others. It also calls on the function above and export the results. A third MATLAB script deals with the post-processing. It imports the results from `duffing_solver.m` and executes an FFT on the data set, plot the Power Spectrum Density and Frequency Response Function as well as phase-plane and time history plots. The numerical approach is illustrated in fig 4.1:
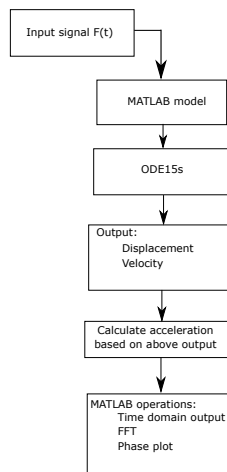


Figure 4.1: Flowchart of numerical analysis.

## 4.2 Results

This section presents the key results from the numerical simulation work.

**Summary of results from project thesis**

The author's project thesis [16] made an extensive study of the discrete formulation of $k$ (i.e. a deadband for $x < a < a$ and a linear stiffness $k$ else). Damping was included for all values of $x$. The system was excited at the mass by a sine sweep input. The gap distance $a$, the stiffness $k$ and the damping $\zeta$ was varied. The results was post-processed in the same manner as described above. The peak in in the PSD and FRF plot was considered to be the new "effective natural frequency" and termed $\omega_e$. Then the effect of $a$, $k$ and $\zeta$ on $\omega_e$ was studied. The following plots also show the results for $a = 0$ i.e. the linear system as well as the MSC/Nastran results.
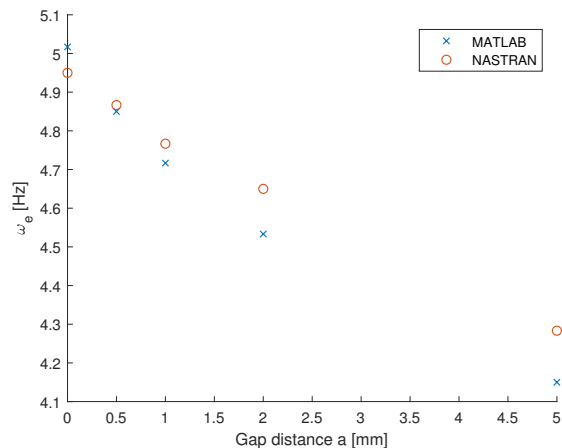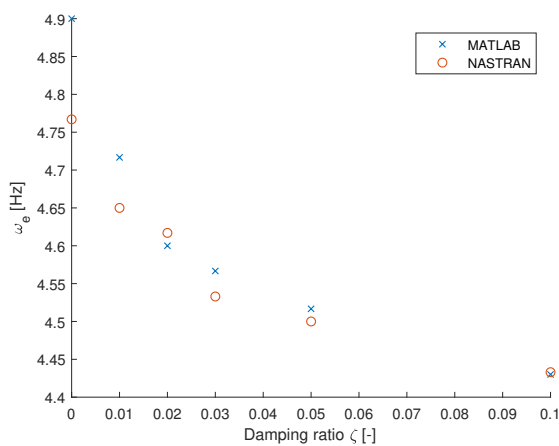


Figure 4.2: Results from varying gap distance $a$



Figure 4.3: Results from varying damping $\zeta$

Figure 6.12 shows that increasing $a$ decreases the effective natural frequency. Figure 4.3 shows that increasing damping $\zeta$ decreases the effective natural frequency $\omega_e$.
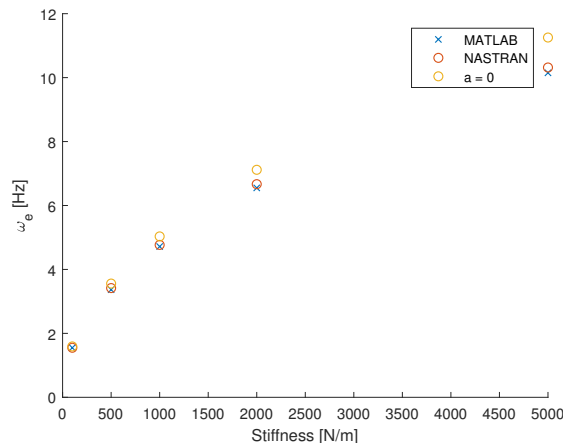
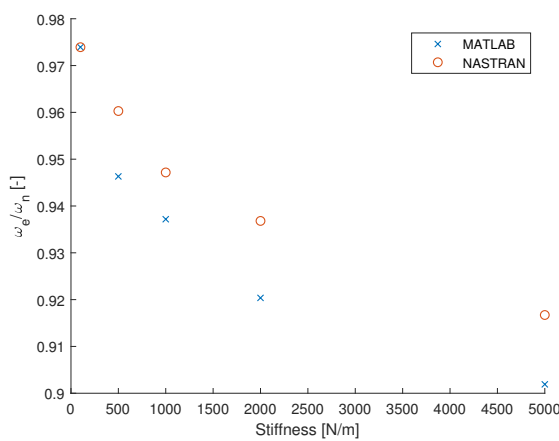

Figure 4.4: Results from varying stiffness $k$



Figure 4.5: Results from varying stiffness $k$ considering the relative frequency

33

Figure 6.13 shows that increasing $k$ increases the effective natural frequency. This result is however not that interesting as the natural frequency *should* increase with $k$. If we plot the relative difference $\omega_e/\omega$ we will however see the behavior relative to $\omega$. This is illustrated in fig 6.14 and shows that increasing $k$ will give a relatively lower $\omega_e$.

The main conclusion in the project thesis was that the nonlinearities introduced in the EOMs through a discrete $k$ gives rise to an overall decrease in the effective natural frequency. It was also concluded that this is supporting the behavior the Department of Prototyping at FFI observed with the shaker test of RIMFAX, as it too lowered its natural frequency when nonlinear gaps were introduced.

### Free oscillation of Duffing equation and effect of power law

Perhaps the simplest type of vibration is the case of free oscillation. We impose the following initial conditions on the system and solve the equations of motion in MATLAB.

$$x(0) = a \qquad \dot{x}(0) = 0 \tag{4.4}$$

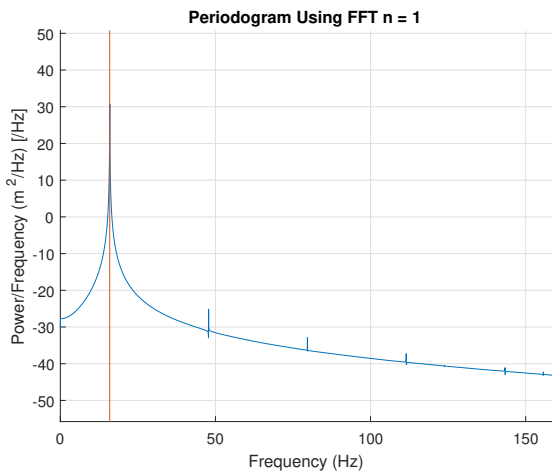We alter the nonlinearity of our system by means of $n$ in eq 3.17.
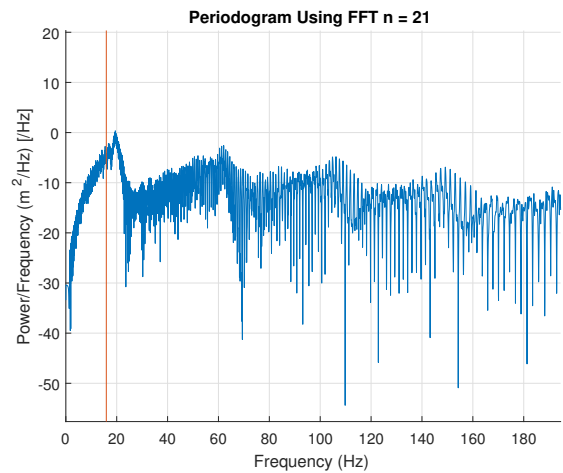


Figure 4.6: PSD of $n = 1$.



Figure 4.7: PSD of $n = 21$.

Several plots for $n$ have been excluded here for the purpose of clarity. The trend in the PSD plots is that the peak is split into several peaks from $n = 1$ to $n = 3$ (see fig 4.6 and then from there and upwards to $n = 21$ the PSD peaks are "smoothed" out as we can see on fig 4.7 where there is starting to become difficult to point out a single eigenvalue. It is therefor useful to separate between the *fundamental* frequency (the first natural frequency, or the first peak in the PSD plot) and the natural frequenci*s*. A 1DOF system should only have one natural frequency but as we saw in chapter 3.6 nonlinear system does not obey this.
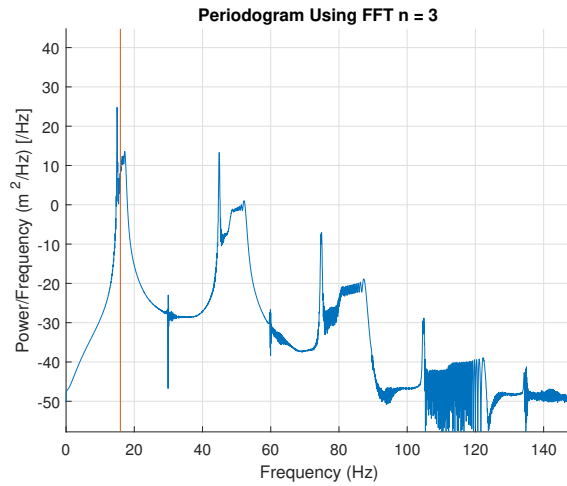
Figure 4.8: Free oscillation $n = 3$

The first peak on the PSD plot is extracted at termed the "new effective natural frequency" $\omega_e$. This is plotted against all $n$-values in fig 4.9. A clear trend is that increasing the nonlinearity increases $\omega_e$. It is also interesting to see that introducing nonlinearity to the system (i.e. $n > 1$ for $n$ odd) gives rise to subharmonics or *several* natural frequencies which is in line with what we saw from the theory on the Duffing equation.
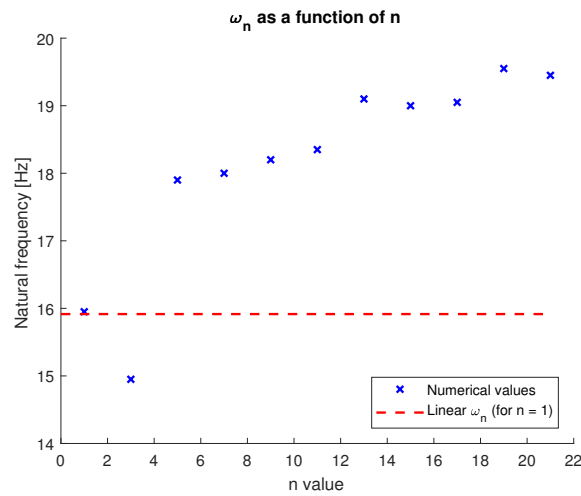


Figure 4.9: $\omega_n$ as function of $n$.

35

**Effect of gap size $a$**

The case of free oscillation for the Duffing equation was studied further by varying the gap size $a$. It is clear that larger gaps are less noisy and the peaks of the PSD plot are more distinct. See fig 4.10 4.11. All simulations are with $n = 3$, $\kappa = 10$.
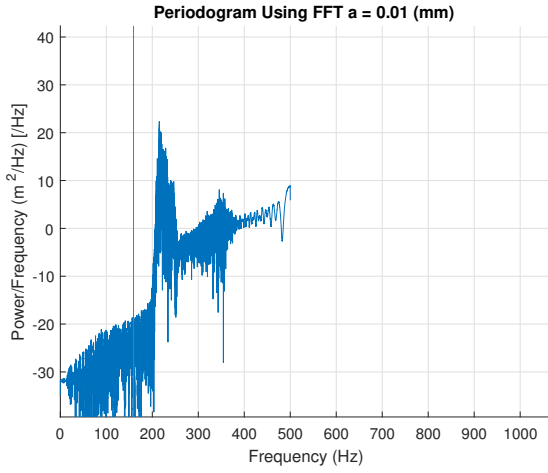


Figure 4.10: PSD of $a = 0.01$ mm.
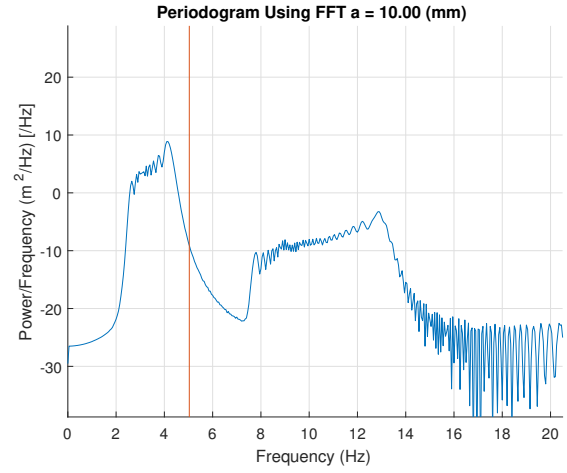


Figure 4.11: PSD of $a = 10$ mm.
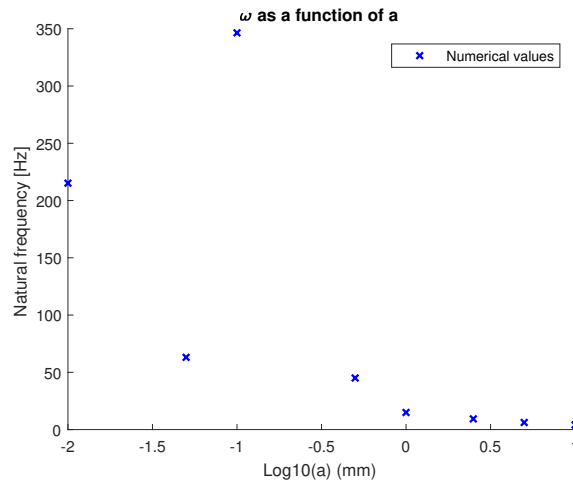


Figure 4.12: $\omega_n$ as function of $a$.

As we see from figure 4.12, introducing a gap $a$ to the system lowers $\omega_e$, and increasing $a$ lowers $\omega_e$ further.

**Effect of forcing amplitude $A$**

We investigate the case of forced oscillations. The equations of motion are written as

$$m\ddot{x} + c\dot{x} + kx + \kappa x^n = A \sin \omega t \tag{4.5}$$

and we vary the forcing term parameters $A$ and $\omega$. The initial conditions are

$$x(0) = 0 \qquad \dot{x}(0) = 0.1 \tag{4.6}$$

We begin with a forcing frequency of $\omega = 0.5\,\omega_n$ where $\omega_n$ is taken as the linear natural frequency of the system, calculated $\omega_n = \sqrt{\kappa/a\,m}$. We vary $A$ bringing us further up the force-displacement curve as seen in fig 4.13.
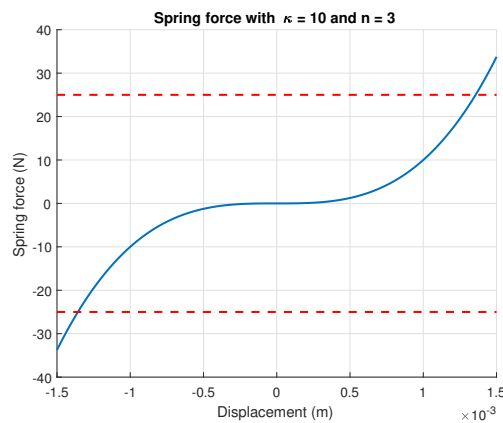


Figure 4.13: Force-displacement curve for Duffing equation. Forcing amplitude depcited as red dotted lines, $A = 25$ N.
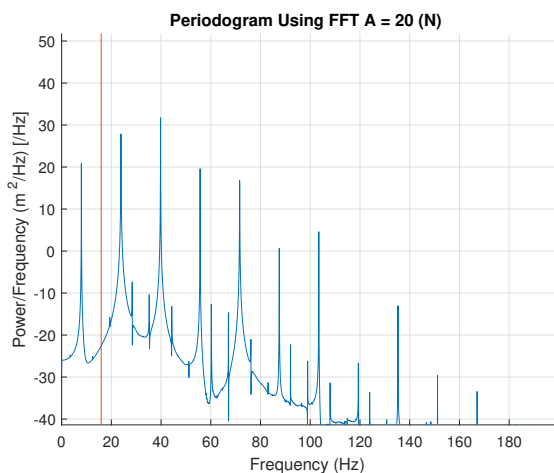


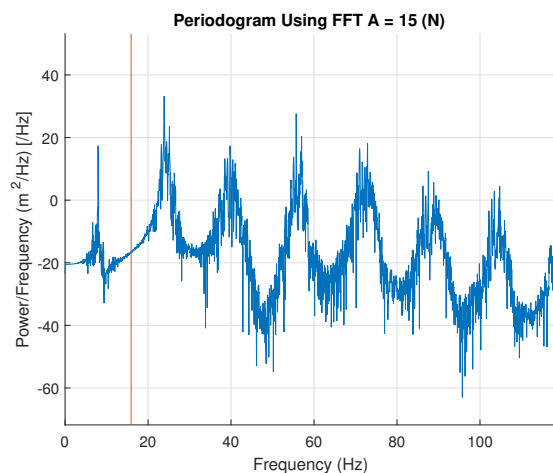Figure 4.14: PSD of forced oscillation $A = 20$ N.

Figure 4.15: PSD of forced oscillation $A = 15$ N.
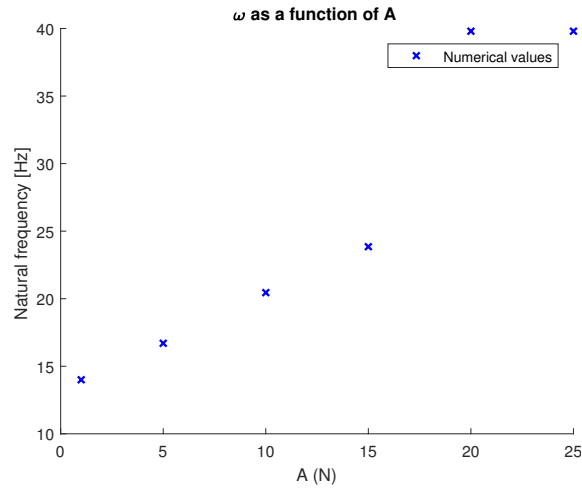
Figure 4.16: $\omega_n$ as function of forced amplitude $A$.

It is clear from fig 4.16 that the problem of nonlinear vibration is amplitude dependent. This is in-line with theory previously presented.

**Effect of forcing frequency $\omega$**

We now let $A = 15\text{N}$ be constant and vary the forcing frequency $\omega$ by means of the frequency ratio $r = \omega/\omega_n$ where $\omega_n$ is estimated as before. $\omega_e$ is now not really the natural frequency. It is more the frequency at the system responds with the most energy in the PSD plot[1]. The results display as follows:



Figure 4.17: PSD of forced oscillation $r = 1$.



Figure 4.18: PSD of forced oscillation $r = 0.1$.

---

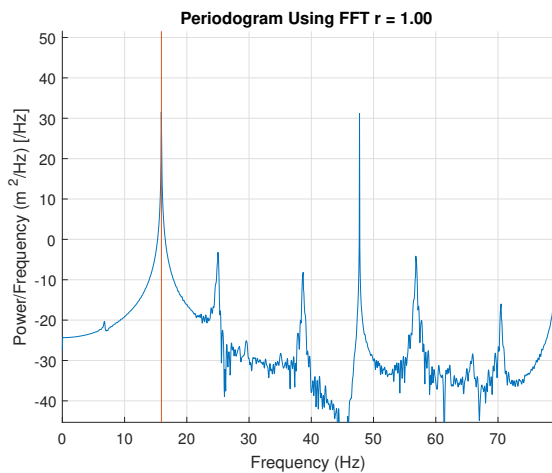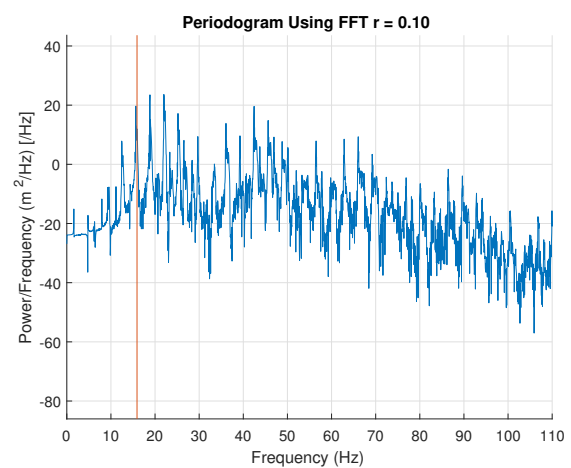[1]One way of looking at PSD plots is as the amount of energy in the system at a given frequency. Classically, we have the most energy at resonance and thus we may extract the natural frequency from the PSD plot.
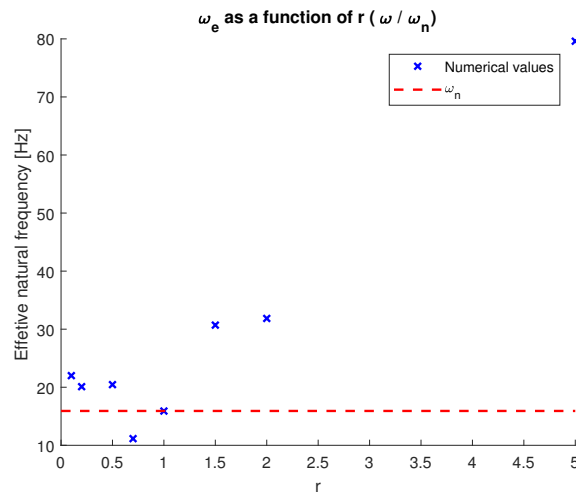
Figure 4.19: $\omega_n$ as function of forced amplitude $r$.

## 4.3 Discussion

Discussion of numerical approach.

**Free oscillation of Duffing equation and effect of power law**

Even this simple case proved to be sensitive to especially a) damping and b) solver. For "soft" nonlinearities, such as $n = 3, 5, 7$ the `ode15s` proved significant different results than the standard `ode45`. This is in line with numerical simulations done by the author in the fall of 2017 with different numerical solvers in MATLAB used to characterize the difference between them. We also see that the damping value $c$ has a fairly large effect. As the spring constant is really given as $\kappa/a^n$ we see that as $n$ increases the effective $k$ increases drastically as well. This effects the damping value $c$ as this is given as $c = \zeta c_{cr}$ where $c_{cr}$ is a function of $k$. This was overcome by using $\kappa$ (which is invariant of $n$) to calculate $c_{cr}$.

# Chapter 5

# Experimental Approach

This chapter presents the experimental method used to solve the thesis problem. The overall aim is to design an experiment representative for the RIMFAX problem but simplified where possible.

This thesis conducts two different of experiments to validate the physical nature of the joint. First, the joint is assembled and its stiffness is characterized through a tensile test. This gives the Force-Displacement relation needed in the numerical simulation. Secondly, the joint is mounted on a shaker table to characterize its vibration properties. The results from the shaker test are to be post-processed and then compared with numerical simulations.

## 5.1 Method

### 5.1.1 Reductions and Assumptions

The experiment is designed with the numerical simulation in mind, as it is highly time-consuming (nonlinear, transient). The basic concept has been to design an experiment which is easily meshed, symmetric, no large multi-part assembly, easy to produce and last but not least - controllable in the sense that we test only the parameters we want to. In doing this, we distance ourselves slightly from the RIMFAX problem. This is thought to be necessary in order to solve the problem. It is also believed that by using the identical joint geometry, we may still be on par with RIM-FAX in order to solve the initial problem. Full scale testing on the whole RIMFAX antenna structure is discarded. This is due to several reasons. The main one being that the structure is superfluous to the joint clearance behavior. It is beneficial to have a model both in finite element software and experimentally which is as simple as possible yet represents the problem. Therefore we discard the antenna structure and focus on the joints. This alters the stiffness and mass of structure being investigated.

Another alteration is the material used. The RIMFAX antenna and its joints are made of expensive materials such as titanium grade 5 and a material prone to galling[1] - aluminium 6082. In RIMFAX, to remedy galling around the bushing/joint area, the area is anodized. We use a more reliable choice: a standard steel alloy (SS355). This is both cheaper (compared to titanium) and is not prone to galling (compared

---

[1]Galling - a form of wear caused by adhesion between sliding surfaces

to aluminium). It is also easier to produce as we exclude the anodizing procedure. The material of choice is not irrelevant, but we allows ourselves to do this as we have already distanced ourselves slightly from RIMFAX. The cost benefit is regarded to be significant. For reasons we will later see, the thermoplastic POM C (polyoxymethylene copolymer) has also been used as coupon material

The solution is as follows: two types of circular coupons machined for either radial clearance or slot clearance. The circular design allows for symmetry, making it easy to mount accelerometers to the coupons. The coupons have the following features:

- Production: easy to machine, only specified tolerances where need be. Lathing and 3-axis milling.

- Assembly: one-part solution

- Symmetrical: making it independent of mounting direction and in some sense geometrical invariant. This is wanted as the problem at hand is the joint clearance, not so much the structure around.

- Cost: relatively inexpensive (compared to full RIMFAX antenna)

- Design allows for testing of the two principal directions out-of-plane and in-plane on the same coupon.

## 5.1.2 Characterizing Stiffness

From Chapter 3.2 it was established that the joint stiffness $k$ is nonlinear in nature. Several ways of representing $k$ was presented. In order to compare experiments with numerical simulations, we need to quantify $k$ for later input in the numerical software. One very effective way of obtaining the stiffness / force-displacement relation is to put the joint in a tensile test jig and pull it while measuring force and displacement. This will directly yield results we may use in the numerical software later.

The following components are made in conjunction with the tensile test and represents the tensile test jig assembly:

- Tensile jig fork (2 pcs)

- Tensile base

In addition two clamps from the tensile machine manufacturer is used to clamp the pieces in the machine.

The tensile test consist of the following:

1. Zwick BZ2.5 TN1S at a load rate of 10 N/s.

2. Coupon assembled with bushing and tensile jig
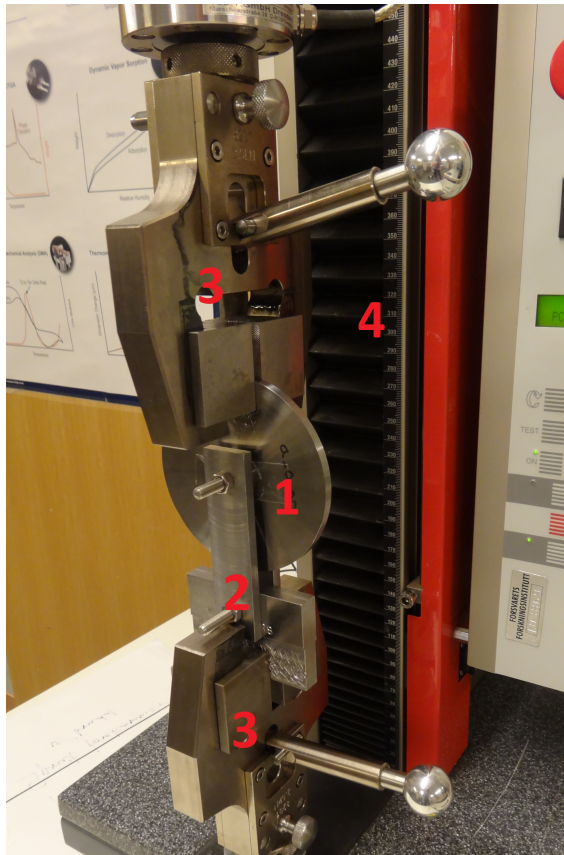
3. Nuts, bolts and washers

Figure 5.1: Setup of tensile test. 1) Coupon speciment 2) Test jig fork and base connected by bolts 3) Upper and lower clamps 4) Zwick BZ2.5 tensile machine.

Each coupon type - slot and radial - is tested 5 times for a representative sample size. The coupons are pulled, released and repeated 5 times. The steel S355 coupons were loaded to 500 N while POM C coupons were loaded to 200 N. This was done based on estimates on the load case for the shaker test, as well as considering the yield strength of the materials. We obviously need to avoid any plastic deformation in the tensile tests as the specimens are to be used in shaker tests later. Only loading to 200 - 500 N has especially one weakness. Such a small load value allows for small movements and spurious movements in the test jig / tensile machine may affect the results to a larger extent compared to loading at higher values. This was a trade off. The results may be found in section 5.2.1.

As the results from the experimental test where not to be trusted (see section 5.3.1 for elaboration) a series of numerical simulations where ran in order to give a better estimate as well. We present the method in the section for FE Approach. The linear static FEA became an ad hoc solution to the tensile test for characterizing stiffness.

### 5.1.3  Shaker Experiment Design

The shaker table experiment's objective is the following:

- Measure the accelerometer response of in-plane vibration of both the radial and slot-type clearance. This is done by mounting the coupons vertically to a jig. The jig is then mounted to the shaker table which is translating in the vertical direction. This yields an in-plane vibration of the coupon.

- Measure the accelerometer response of out-of-plane vibration of both the radial and slot-type clearance. This is done by mounting the coupons horizontally to a jig. The jig is then mounted to the shaker table which is translating in the vertical direction. This yields an out-of-plane vibration of the coupon.

The experiment consist of the following parts:

1. Shaker table

2. Jig fixture

3. Coupon with specified machined clearance

4. Two-part bushing, identical to RIMFAX

5. Three accelerometers per coupon

6. Accelerometer on jig fixture to control the input signal
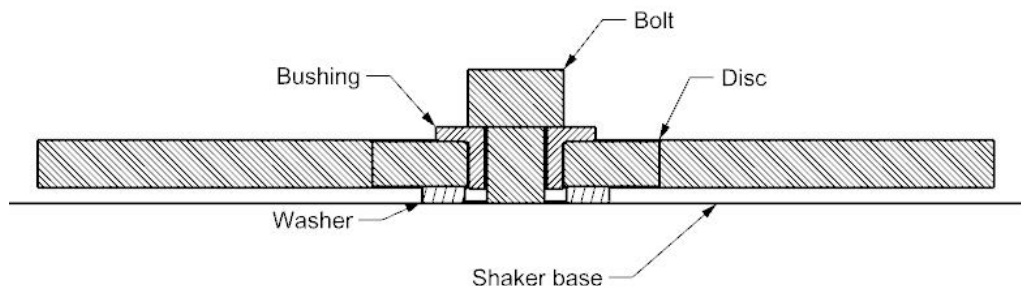


Figure 5.2: Experimental setup on shaker table. Image courtesy of [2].

---

[2]Image courtesy of Petter Østby, Rainpower AS which used the thesis' setup in conjunction with a report in the course UNIK4910 at the University of Oslo.
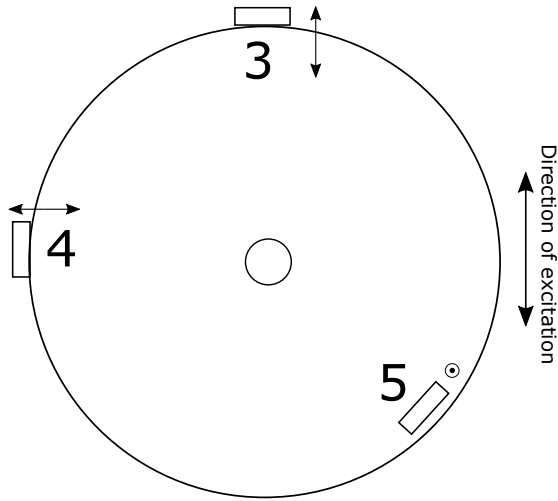
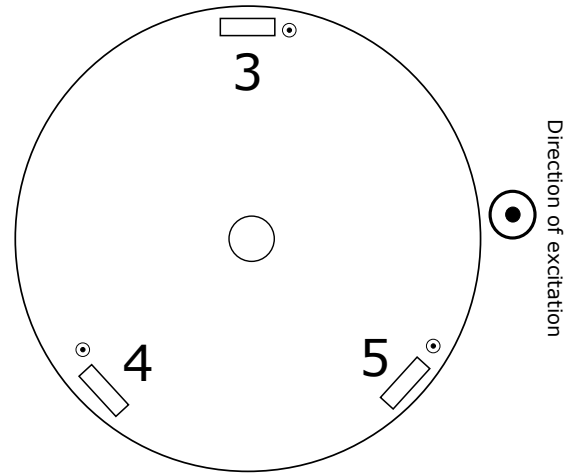Figure 5.3: Location of accelerometers in-plane orientation



Figure 5.4: Location of accelerometers out of plane orientation. Excites in and out of paper.

Figure 5.3 and 5.4 show the location of the accelerometers for the two different shaker orientations. Dotted circle marks translation in and out of the paper plane.

### 5.1.4 Test Pieces and Tolerances

**Steel S355**

To mimic the material in the RIMFAX joint, 6 different gap sizes $a$ were machined for both the radial and slot-type coupon in steel S355.

**POM C**

After initial tests with coupons in S355 were done and found to be too stiff as well as generating too much noise in regards to the steel-to-steel contact (clash sound) it was decided to make the three smallest gap sizes 0.00, 0.05 and 0.10 mm in POM C for the slot and radial type (an elaborate discussion on this follows).

All the parts were machined in-house at the Department of Prototyping, FFI. The coupons and bushings were measured in the Measurement Lab at the Department of Prototyping (FFI) using inside and outside micrometers, gauge pins and a precision measuring table. The following tables (table D.3, D.5, D.4 and D.6) show the results of the various parts. The tables show a base value which is the specified value on the machine drawing. The difference measure shows how far of the measured distance is from the base value. All parts are within specified tolerances (see machine drawings in Appendix E for more details). The given values are the values which are driving for the clearance in-plane and out-of-plane for the problem.

We also have a small variation in the manufacturing of the cylindrical and slot bushings. This makes it possible to somewhat adapt the measurements to different parts to obtain the desired clearance size. The measurements from table D.3 and D.4 are matched to get desired size, and measurements from table D.5 and D.6 are matched.

| Property | S355 | POM C | Unit |
|---|---|---|---|
| Young's modulus, $E$ | 210,000 | 2,800 | MPa |
| Yield strength, $\sigma_y$ | 355 | 67 | MPa |
| Poisson's ratio, $\nu$ | 0.3 | 0.44 | – |
| Density, $\rho$ | 7850 | 1410 | kg/m$^3$ |

Table 5.1: Properties of steel S355 and POM C.

### 5.1.5   Equipment and Experiment Procedure

**Equipment**

All of the following equipment was used from the Environmental Testing Lab at FFI:

1. Shaker table, type LDS V830 with shaker control software "ShakerControl"

2. Jig fixture, appendix E for drawing

3. Coupon with specified machined clearance, appendix E for drawings

4. Two-part bushing, identical to RIMFAX

5. Three accelerometers per coupon, PCB 352C23

6. Two accelerometers on jig fixture to control the input signal, PCB XX

7. Computer with log system National Instruments Signal Express 2015

8. Link box National Instruments cDAQ-9172 with 2 modules

9. Battery power supply

10. Cables for accelerometers

**Procedure**

The shaker test procedure is as follows:

1. Mount jig to head-expander on shaker table

2. Mount two control accelerometers on opposing sides of head expander

3. Mount coupon on jig by means of one M6 hex bolt

4. Mount three accelerometers on specified locations on coupon. For in-plane test accelerometers are mounted on the edge, for out-of-plane they are mounted on the flat facing side. Beeswax is used as adhesive.

5. Connect accelerometers to link box

6. Connect link box to external log computer

7. Turn power supply, air supply and control systems on

8. Start logging via NI SignalExpress on external log computer

9. Commence test on control systems computer with specified input (sine sweep or random, g-value, ramp speed in octaves / min and sensitivity of control and measurement accelerometers)

10. Stop logging NI SignalExpress when test finishes.

11. Save auto-generated spectrum-plot from control systems software

12. Save logged .tdms-file from NI Signal Express
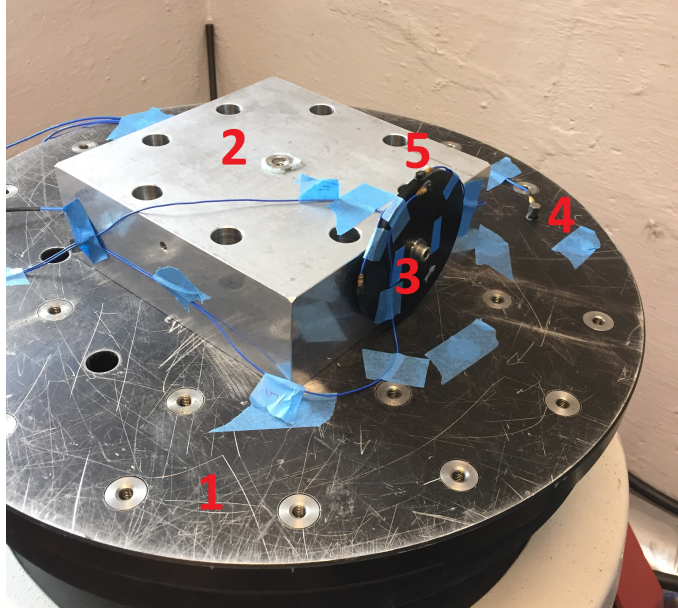
13. Begin new test

Figure 5.5: Experimental setup on shaker table. 1) Shaker table 2) Jig cube for different mounting orientations 3) Coupon-bushing assembly 4) Control accelerometer 1 out of 2 5) Log accelerometers 2 out of 3.
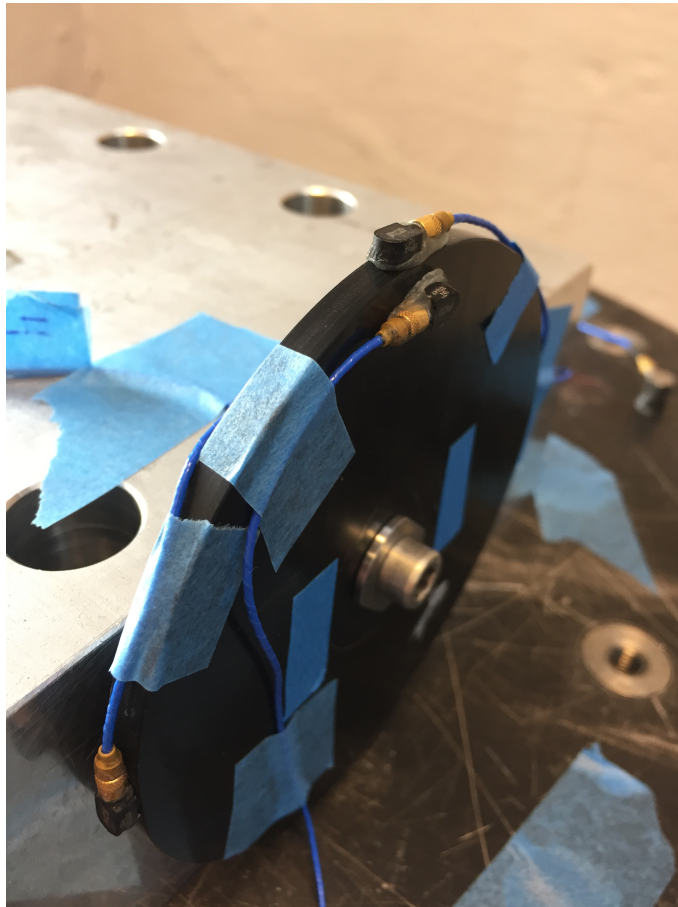


Figure 5.6: Detail of POM C coupon.

### 5.1.6 Input Signal

The shaker control software allows for a range of different input signals on the shaker head. This thesis have utilized the following three forms of input signal:

**Sine sweep**

The sine sweep signal is an input where the acceleration is given as

$$a(t) = a_0 \cos \omega(t) t \qquad (5.1)$$

where $\omega(t)$ is a linearly increasing function that yields the "sweeping" aspect. For instance we may wish to sweep from 1-60 Hz at a constant acceleration amplitude $a_0 = 1g = 9.81\mathrm{m/s^2}$. Fig 5.7 shows how this specific sine sweep is generated in MAT-LAB using the `chirp` function. The Bruel and Kjær controller software generates this for us in the experiment. We only need to specify start and end frequency, rate of change in octaves / minute (generally chosen to be 1 oct/min) and the amplitude in $g$.
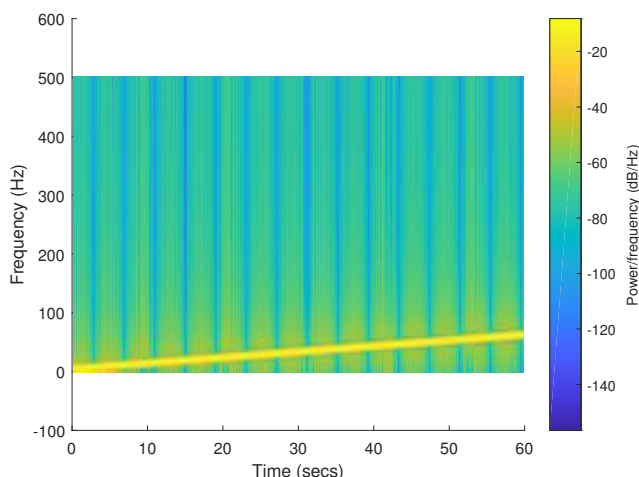


Figure 5.7: Spectogram of the linearly increasing sine sweep input signal. From 1 Hz to 60 Hz over 60s. Sampling frequency of 1000 Hz.

A sine sweep signal has the advantage that a range of frequencies are swept over and one measures the response for every frequency continuously. It is therefore efficient for determining frequencies of interest in one run. One disadvantage is that the sweep has to have a controlled feedback for every frequency in order to complete the sweep. If there exist frequencies that make the system unstable (i.e. the feedback controllers on the shaker software are struggling to achieve the desired input) this may compromise that run. One remedy of this is to first sweep up to the problem frequency and then sweep downwards from the highest desired frequency down to the problem frequency. This will require to stitch the data sets afterwards.

Another sine sweep method is the step-sine sweep which is similar but for excitation at each frequency is considerably longer period so that full amplification of each frequency in the response can be seen. It is more accurate, but also more time-consuming.

**Random white signal**
Specifically, band-limited multisine excitation. Consists of the sinusoidal waves for all frequencies in the frequency band of excitation at any time. Random vibration is widely used in the industry as it is well suited for product qualification tests and characterizing a structure's dynamics. As it excites all frequency at the same time it will also excite all the natural frequencies at the same time. This causes a more "harsh" test on the test object compared to sine sweep which for most cases excites one natural frequency at a time. Particularly for validation or destructive testing, random vibration is a better input form than sine sweep. In this thesis random vibration is used to complement the other experiments.

**Harmonic input**
A standard harmonic forcing term on the form

$$F = a_0 \sin \omega t \tag{5.2}$$

has also been used in the experiments. It is specified through its amplitude $a_0$ and frequency $\omega$. The harmonic input is useful when isolation of one frequency is interesting. In this thesis it is used to investigate what other frequencies than the forcing frequency are excited and we discuss why these frequencies occur and what they may be attributed to. Signal noise and chaos in the system were early hypothesis' that is believed to be important to have an understanding of.

### 5.1.7 Post-Processing

The post-processing consists of handling the `.tdms` data files that are the output from NI Signal Express. FFI has supplied a MATLAB-script for reading the files into MATLAB. The rest of the work uses scripts written by the author in MATLAB. In general, as much as the workflow as possible has been automated. The general procedure is as follows:

1. Run master_tdms.m. This script takes in the tdms-file, sorts out the columns of interest, locates where the test started and stopped and crops the data thereafter. It plots the time series so the user may check if the crop is reasonable and finally export the data in MATLAB .mat format for further processing.

2. post_processing_tdms.m. This script handles all the advanced post-processing. In general it loops through the data series from master_tdms.m and calculates the PSD, FRF and Coherence spectrum with Welch averaging. Finally it prints the figures in the correct folder and export the post-processed data.

Both scripts may be found in the Appendix.

**Power Spectral Density and Welch's Method**

The power spectral density (PSD) is defined as the square Fourier transformation of the time signal per unit time

$$S_{xx}(\omega) = |\mathcal{F}\{x\}|^2 \tag{5.3}$$

We may interpret the value of $S_{xx}$ as the energy density of the signal at each frequency. If the signal $x$ is read from an accelerometer, the dimension of the PSD is givens as $\mathrm{g}^2/\mathrm{Hz}$. The estimation of the PSD in this thesis is based on averaging methods from Welch. Basics on signal processing, with references to Welch may be seen in chapter 13 in [28] and chapter 6 in [27]. Welch's overlapped segment averaging (WOSA) is very useful when the signal has noise and high resolution in frequency is not needed. If we average the PSD over $N$ consecutive and equally sized frequency intervals it will reduce the variance of the PSD by a factor of $1/\sqrt{N}$ within each frequency. The PSD calculated by Welch's method is less noisy and easier to interpret. We use a $\log_{10}$ scale along the $y$-axis and a linear scale along the $x$-axis for the PSD plot. The $\log_{10}$ is to densify the peaks of the PSD somewhat. A linear scale along the $y$-axis would make the peaks especially large. We do not choose a $\log_{10}$ scale on the $x$-axis (although this is common in vibration analysis) because this densifies details for high $x$-values too much in the author's opinion. A lin-scale provides the same detail for all $x$-values (frequency values).

**Coherence Spectrum**

The coherence between to signals $x, y$ is given by

$$C_{xy} = \frac{|S_{xy}|^2}{S_{xx}S_{yy}} \tag{5.4}$$

where $S_{xy}$ is the cross spectral density between signals $x, y$. It has a maxima at frequencies where the two signals have high correlation. The coherence spectrum $C_{xy}$ gives a value between 0 and 1 and expresses the relation between $x, y$. A value close to zero indicates no relation while close to 1 indicates that the signals follow each other. We would like to examine the coherence spectrum between the control accelerometers (input) and the various measurement accelerometers (output). A value between 0 and 1 indicates that the assumption of linearity between $x, y$ is wrong or that there are noise sources which affect the system or measurements. So, in our case a value between 0 and 1 may indicate nonlinear behavior or poor measurements. The first is wanted, the second is not. A weakness in this procedure is that we do not know what causes the value.

It is worth noticing that calculating coherence without averaging gives $C_{xy} = 1$ which is trivial.

## 5.2 Results

This section presents the key results from the experimental work. The structure of this chapter is as follows:

- Present the results from the tensile test characterizing the stiffness $k$

- Present the results from the shaker table experiments, including initial runs, high acceleration load runs, S355 coupons and POM C coupons.

- As there exists a fair amount of data to be discussed, it has been decided to execute the discussion of the results directly below the relevant table or plot. This is to reduce the need for the reader to browse back and forth pages far apart.

- In the end, an executive discussion of the most important results is presented.

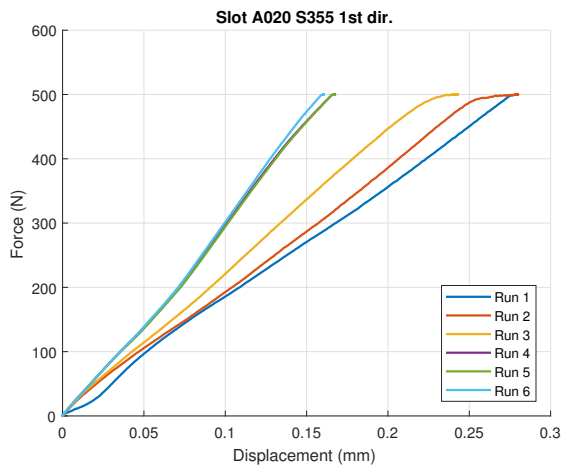## 5.2.1 Static Experiment: Tensile Test



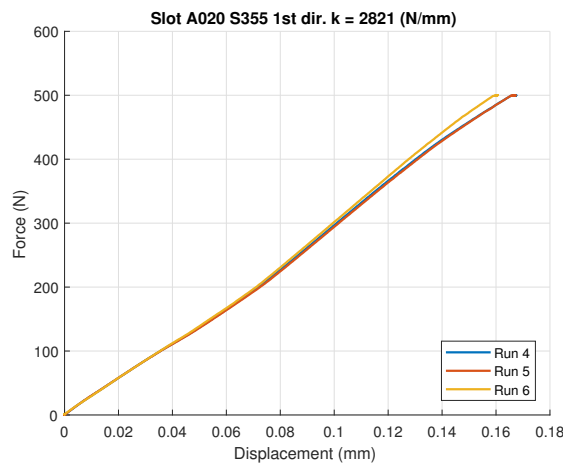Figure 5.8: All 6 specimens from slot-type $a_{020}$ coupon.

Figure 5.9: The last three specimens which showed consistency.

| Coupon and load case | Material | F (N) | $k_e$ (N/mm) |
|---|---|---|---|
| Slot 1st principal | POM C | 200 | 2670 |
| Slot 2nd principal | POM C | 200 | 2772 |
| Slot 1st principal | S355 | 500 | 2821 |

Table 5.2: Estimates of $k$ based on the last three stable runs.

Figure 5.8 shows the complete 6 runs. Figure 5.9 shows only the last three, which is the basis of the average value seen in table 5.2. Notice of the POM C and S355 yields almost the same numerical value, indicating that we are measuring the test setup stiffness, rather than the joint stiffness. A complete discussion of this follows in chap 5.3.1.

### 5.2.2 Dynamic Experiment I: Initial Shaker Tests

**Fundamental mode from zero clearance**

In order to quantify the modes of the coupon as well as verify the FE analysis (see chapter 6) the Radial $a = 0$ coupon was used together with a standard washer which ensured no clearance in any direction (out-of-plane or in-plane). The structure was excited with a sine sweep sequence.
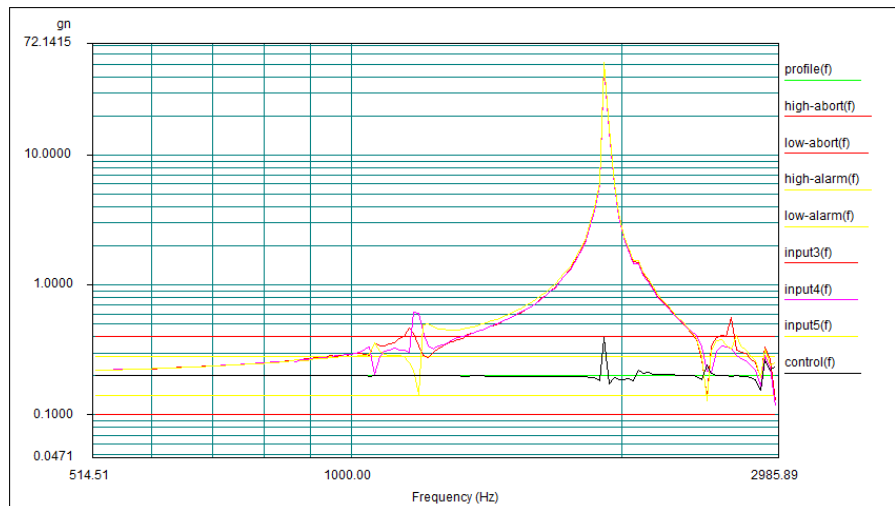


Figure 5.10: Sine sweep of fixed coupon radial $a = 0$. Fundamental mode is seen at 1900 Hz.

**Initial runs**

A set of initial runs with the S355 coupons were done in order to characterize areas of interest. This showed no conclusive trend. Experimentation with different frequency ranges, acceleration amplitudes (and thus displacement amplitude), sine sweep rate of changes (octaves/minute), coupon orientations and both joint types were conducted.
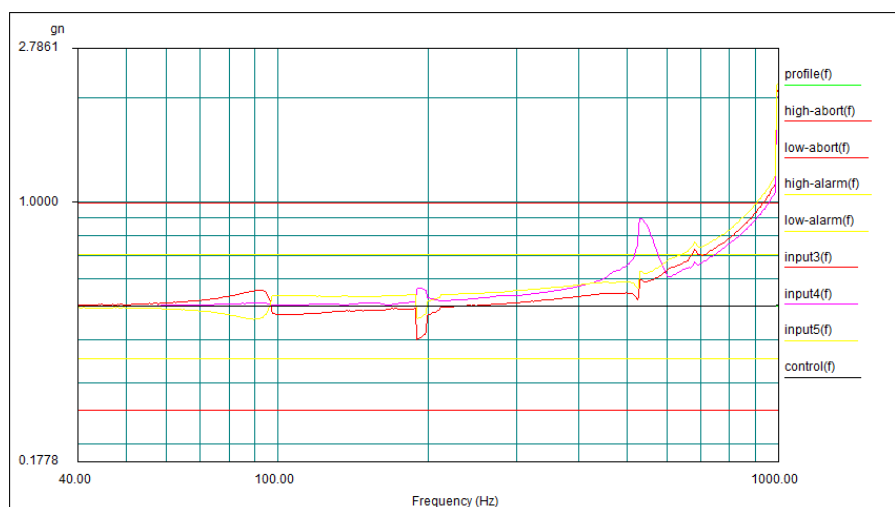


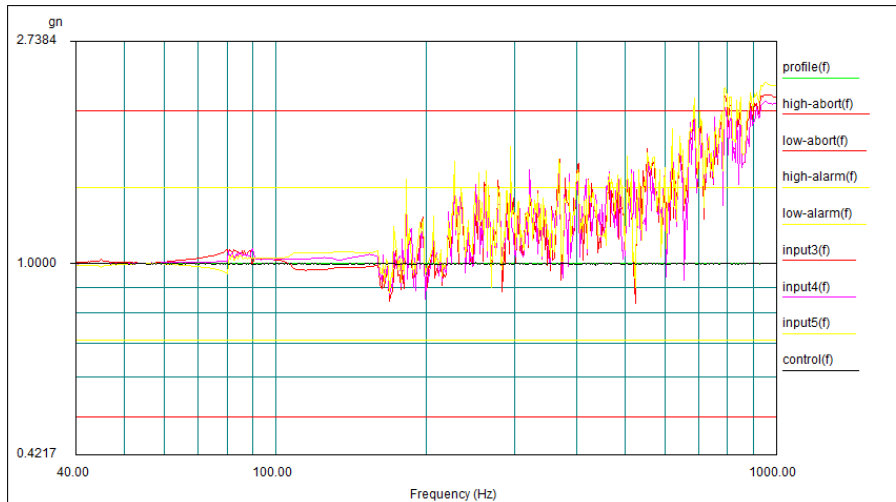Figure 5.11: Radial $a = 0$. Out of plane. 0.5 g.

Figure 5.12: Radial $a = 0$. Out of plane. 1.0 g.

Figure 5.11 and 5.12 show how the g-load displays to different behavior regimes. The 0.5g load seen in fig 5.11 is not enough to displace the bushing sufficiently to impact the joint on both sides. It is therefore resting on one side of the joint and following the joint's motion. We do observe events at 100, 200 and 550 Hz. This is believed to be rocking motions of the coupon (as it has both in-plane and out of plane clearance it is free to tilt or rock about). When increasing the acceleration amplitude to 1.0 g as seen in fig 5.12 we see a much more chaotic behavior especially at $f > 200$ Hz.
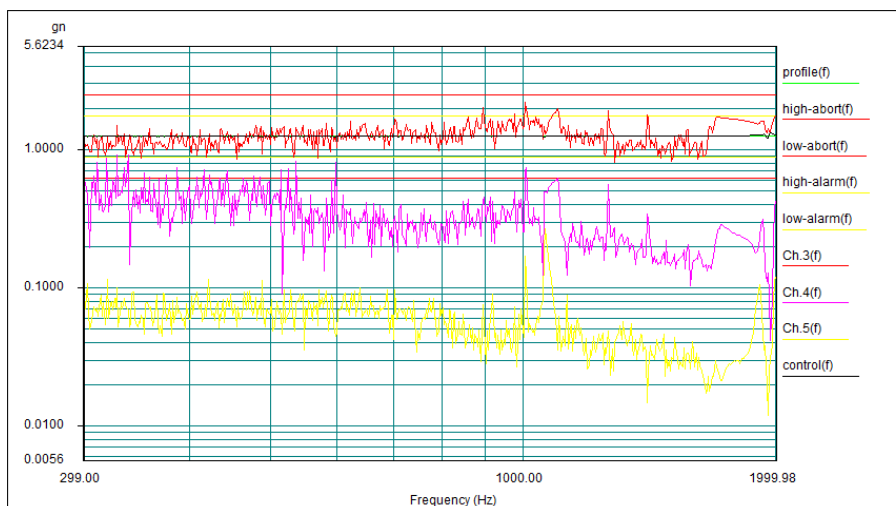


Figure 5.13: Slot $a = 0.40$ mm. In-plane 1.25 g.

Figure 5.13 shows seemingly complete chaos in the frequency response results.

57

**High acceleration load**

The sine sweep generated in the Bruel & Kjær Shaker control systems software is a signal that keeps the amplitude of acceleration constant. In order to do this, the displacement and velocity has to be varied. Given that

$$a(t) = a_0 \cos \omega t$$

is the form of the input signal on the shaker. $a_0$ is given as the amplitude, in number of g. $a_0 = n\,g = n \times 9.81\mathrm{m/s}^2$ for $n > 0$. The displacement $x(t)$ on the shaker may be found by integrating twice

$$x(t) = \frac{a_0}{4\pi f^2} \cos \omega t$$

Here we have used that $\omega = 2\pi f$. The amplitude of displacement $A$ as a function of the increasing frequency f is thus

$$A = \frac{a_0}{4\pi^2 f^2} \tag{5.5}$$

It is easily seen from this that when we sweep upward and increase $f$ the displacement amplitude $A$ is lowered. The interesting aspect of this is that our given clearance $a$ is constant. And so we may start out with an $A$ large enough to cover our clearance range and impact the joint in both directions. However, as the frequency is increased $A$ will at some point become smaller than $a$. Thus, the vibrating bushing will not impact in both direction and will oscillate "for itself" inside the joint without acting any force on the coupon structure.
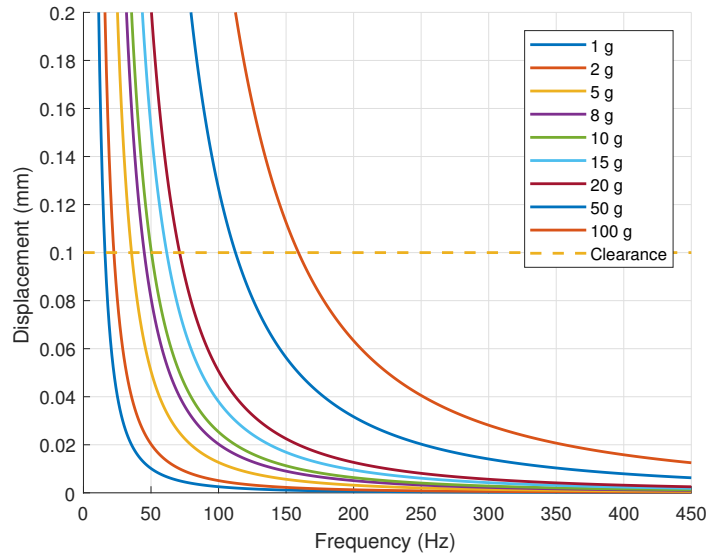


Figure 5.14: Displacement as a function of excitation frequency for different g. A clearance of $a = 0.10$ mm is chosen for illustration.

Figure 5.14 shows how narrow the permissible area above the dashed line is in order to ensure full impact on every oscillation. As we see, lowering the clearance will significantly increase the permissible area as well as make the driven $g$-load useful for a broader frequency range.

This was confirmed by using the Slot a_0_20 coupon. A range from $a_0 = 0.2g$ to $a_0 = 20g$ was tested as well as a variety of sine sweep ranges. Based on audible feedback from the experiment one could hear when there was "full double impact" between bushing and coupon and when it was not. The behavior was similar for every test: a clear rattling sound was produced up to a certain frequency where the sound of rattling was more random indicating that full impact occurred for some time interval, for then to go back to oscillate inside the clearance-deadband $x \in < -a, a >$. For even higher forcing frequencies the random rattling stopped, indicating that the displacement amplitude $A$ was so small that there is no possibility of impacting both sides. As the test environment includes gravity it is likely that the coupon is "resting" on the bushing at these frequencies and oscillating just slightly. For instance, at 400 Hz and $a_0 = 1g$ the shaker is oscillating at $A = 0.00155$mm which is clearly not even close to initiate contact in the slot joint ($a = 0.2$mm, or 0.1 mm on each side of the bushing). Increasing $a_0$ confirms this. The distinct sound of rattling is now audible to a higher frequency, indicating that the shaker is able to oscillate at higher $A$ and exert full impact on the joint for a wider frequency range.

**S355 Coupon runs**

As the S355 coupons yielded too much rattle noise, they were not continued. Below is an example of post-processed results with the following properties

| Property | Value |
|---|---|
| Joint type | S355 Slot |
| Clearance $a$ | 0.20 mm |
| Orientation | In plane |
| Frequency sweep | 40-3000 Hz |
| Acceleration amplitude | 1.0 g |
| Sampling frequency | 5688.9 Hz |
| Welch window | 1024 |
| Welch overlap | 512 |

Table 5.3: Shaker test of S355 with post-processing properties
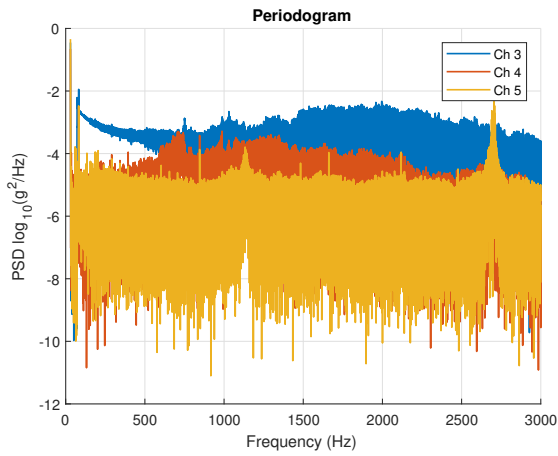
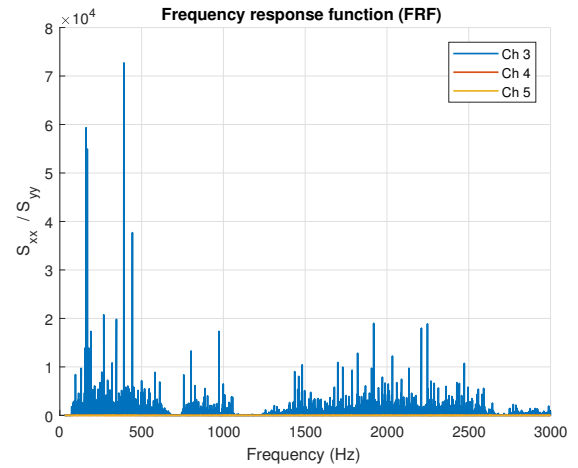Figure 5.15: PSD without Welch averaging



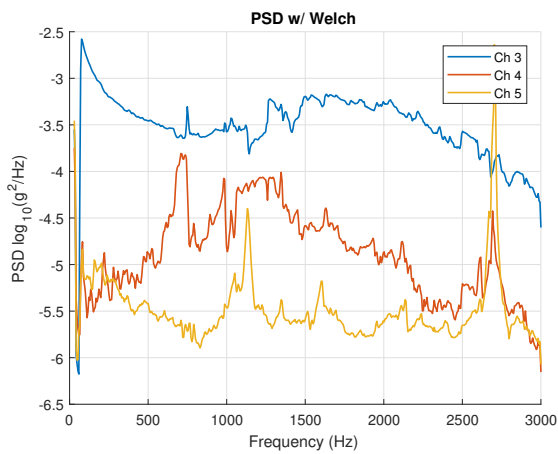Figure 5.16: FRF without Welch averaging
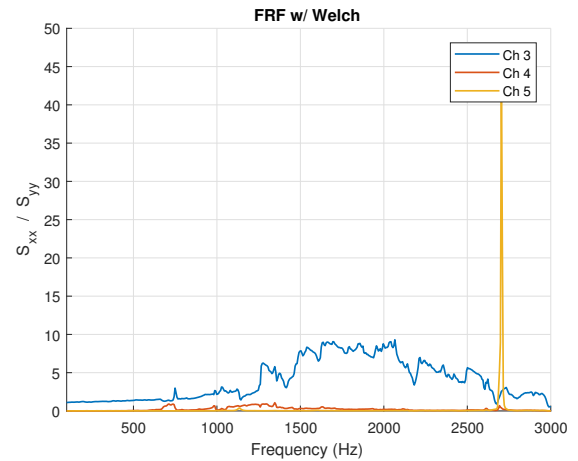


Figure 5.17: PSD with Welch averaging



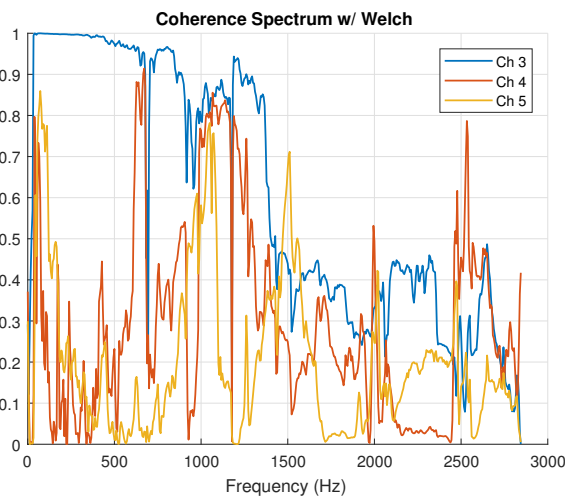Figure 5.18: FRF with Welch averaging



Figure 5.19: Coherence plot

From the preceding figures it is clear that the averaging methods provided by Welch

are working properly, but no conclusive trend is shown. When this was realized, the thesis work focused more on POM C coupons.

### 5.2.3 Dynamic Experiment II: POM C Shaker Tests

An initial test with POM C slot a_0_20 was conducted. The signals were significantly less noisy compared to S355. As the first modes of the structure was still high (about 580-590 Hz theoretical from Nastran) the thickness was reduced.

The thickness was reduced to nominal $t = 2.60$ mm. This yields the three first modes theoretically to be 314, 364 and 411 Hz. See table 6.5. This was confirmed experimentally by the same means as earlier with S355, see fig 5.20, 5.22. Power spectrum density (PSD), coherence spectrum and frequency response function (FRF) have been used to post-process the results. Unless otherwise specified the following post-processing parameters were used:

| Property | Value |
|---|---|
| Sampling frequency | 5688.9 Hz |
| Welch window | 1024 |
| Welch overlap | 512 |

Table 5.4: Post-processing parameters.

In total, 92 shaker tests of various excitation methods, orientations and clearances have been conducted. The following sections present the results from these. The complete list of plots may be found in Appendix F. A complete table of the tests with the corresponding load and frequency range is specified in Appendix F, table F.1. The positioning of the accelerometers (channel 3, 4, 5) for the two different orientations is seen in figure 5.3 and 5.4. The positioning is consistent for the 92 tests.

**Sine sweep**

A total of 72 sine sweep tests have been conducted. The latest POM C coupon ($t = 2.60$ mm) were swept in the following six manners:

| $g$ (m/s$^2$) | Sweep (Hz) | Octave rate (oct/min) |
|---|---|---|
| 0.5 | 5-500 | 1.0 |
| 1.0 | 15-500 | 1.0 |
| 2.0 | 15-500 | 1.0 |
| 5.0 | 25-500 | 1.0 |
| 10.0 | 50-500 | 1.0 |
| 15.0 | 50-500 | 1.0 |

Table 5.5: Sweep routines.

Every coupon was swept in both in-plane and out-of-plane directions. Both the radial and the slot joint was tested with 3 different clearances ($a = 0.00, 0.05, 0.10$ mm). This makes in total 72 tests. The variation in sweep ranges compensate for the displacement limits on the shaker (higher $g$-loads have higher displacement amplitude at lower frequencies, topic previously discussed - see fig 5.14).

*Fundamental mode from zero clearance*
As a benchmark, the new POM C coupon was fixed by the same means as in sec 5.2.2. Both sine sweep (5-500 Hz, 0.5 *g*) and random vibration (5-1000 Hz) was run. The results are consistent with the theoretical modal analysis. Fig 5.20 show a small peak at 316 Hz and a distinct peak at 367 Hz. It is believed that the first two modes (314) are more difficult to excite than the third (364), hence the difference in magnitude response.
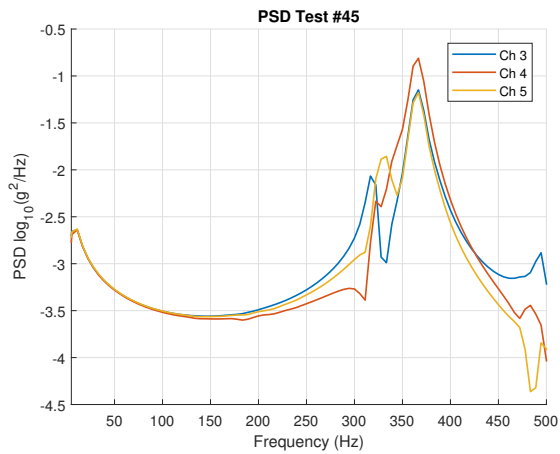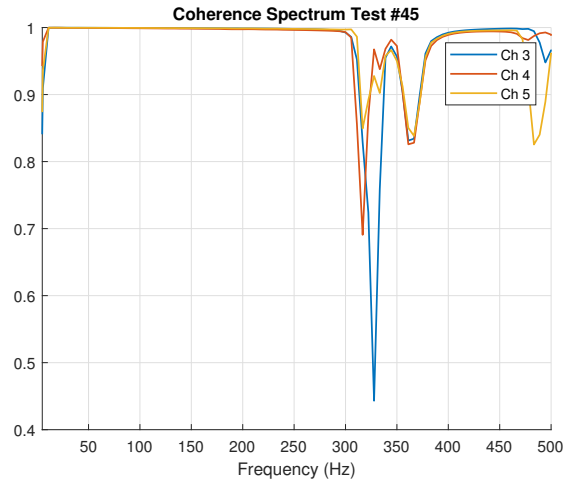


Figure 5.20: PSD of sine sweep test #45.



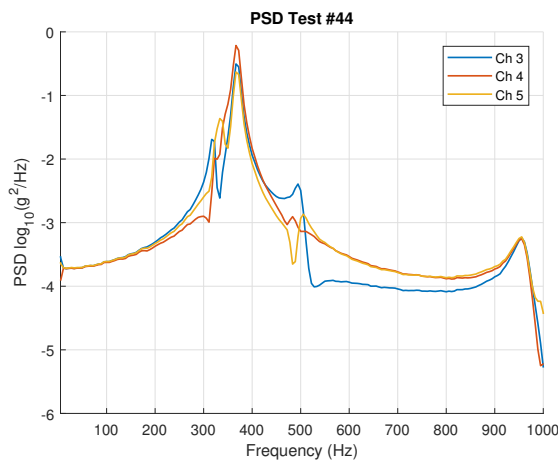Figure 5.21: Coherence of sine sweep test #45



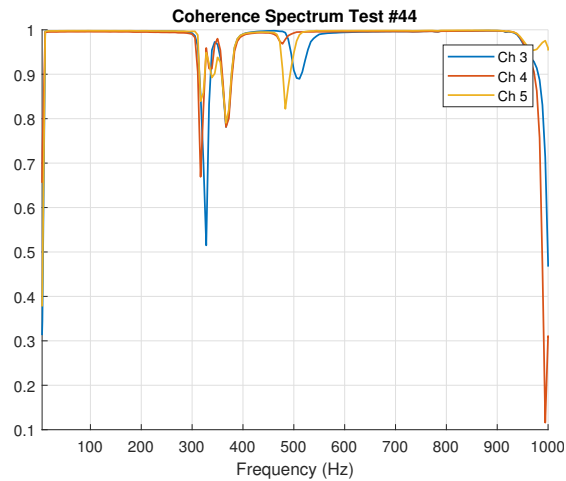Figure 5.22: PSD of random test #44.



Figure 5.23: Coherence of random test #44.

We observe consistency between the random and sine sweep vibration. It should therefore be possible to use both sine and random in post-processing. The random has the advantage of ranging to 1000 Hz without being time consuming. The results in fig 5.20 - 5.23 serves as a benchmark for comparison for the rest of the analysis.

*Sine sweep tests with clearance*
The sine sweep results separate into two different regimes. The first regime is where the coupon is excited out of plane. This orientation excites the first modes of the system, giving rise to distinct peaks in the PSD and FRF plots (as would be expected in a linear system excited the same orientation). The coupons excited in-plane do not manage to excite these modes and thus does not display the same behavior in the PSD and FRF plots. This is the second regime. This difference generates two different approaches to post-processing the results. For the coupons out of plane, it is interesting to see how the natural frequency shifts as we vary clearance. Especially the value of the first 3 modes. For the coupons in-plane, a peak in PSD / FRF would indicate the joint frequency in itself. The fact that the joint has a natural impact frequency of its own was the main hypothesis to begin with.
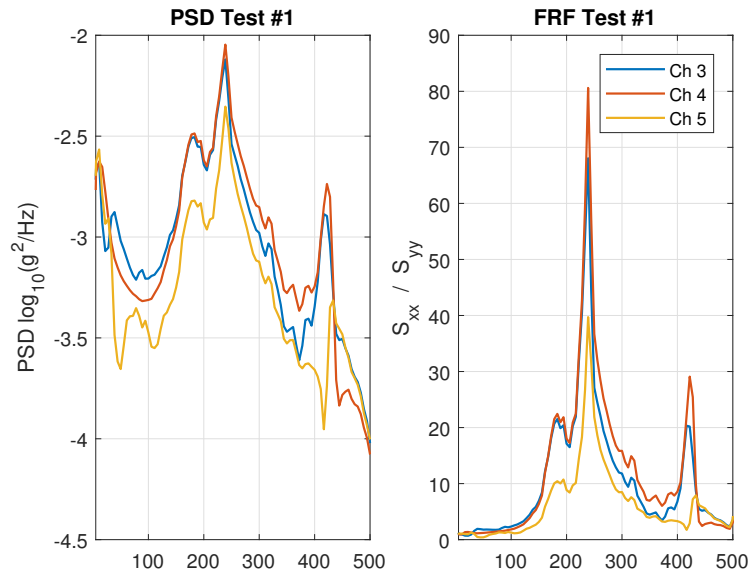


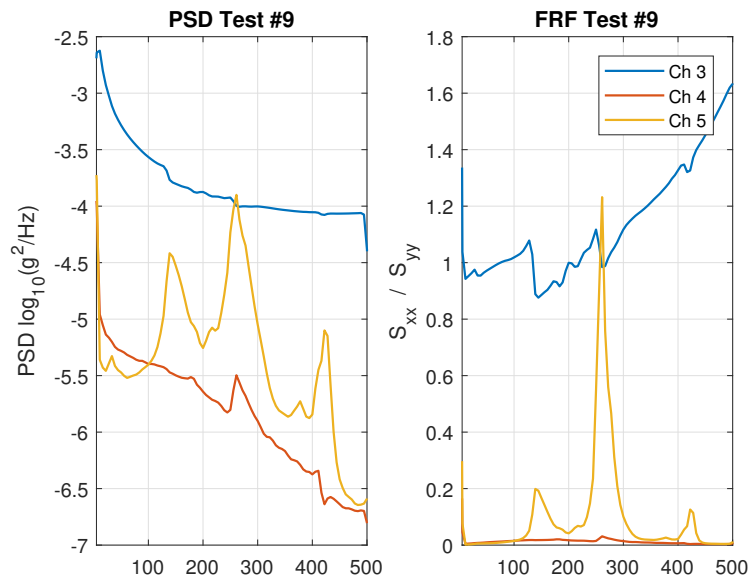Figure 5.24: PSD and FRF of test #1: in-plane.



Figure 5.25: PSD and FRF of test #9: out of plane.

The two different regimes are clearly seen in fig 5.24 and 5.25 which are both radial $a = 0.00$mm, 0.5 $g$ but out of plane and in-plane, respectively. Notice the difference in magnitude, for example for the FRFs. This makes sense as the system is much more flexible in the out of plane direction than in-plane. It is in general difficult to say anything clear from the in-plane results. The "joint frequency" as previously referred to and the hypothesis is not visible from the results in these experiments.
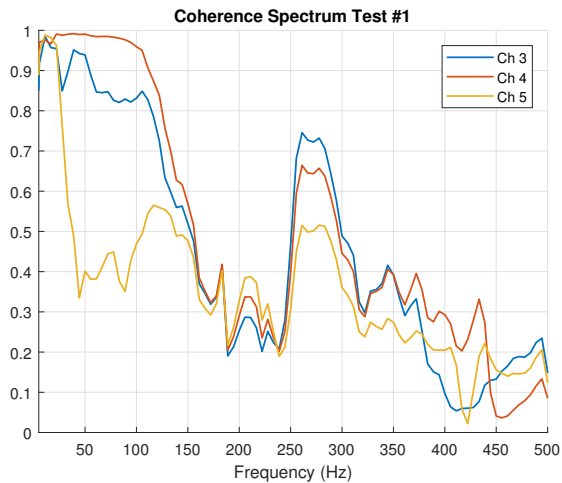


Figure 5.26: Coherence of test #1.
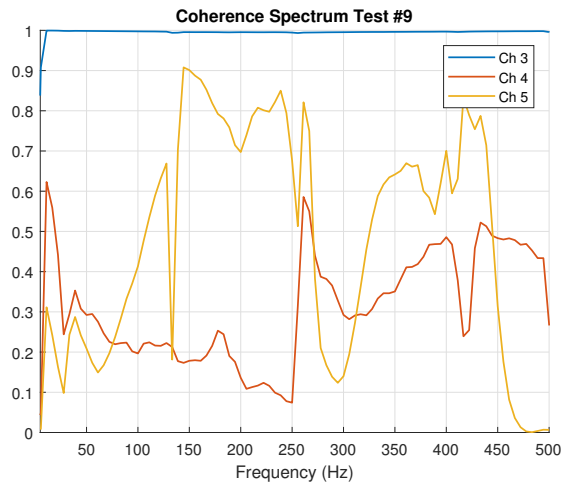


Figure 5.27: Coherence of test #9.

Figure 5.27 shows how channel 3 has a perfect coherence with the input signal. This makes sense as there is no clearance and since the system is fairly stiff in the in-plane direction, accelerometer 3 should follow the input. Comparing test #9 with test #42 (maximum clearance $a = 0.10$, maximum load $g = 15.0$.) we get



Figure 5.28: PSD of test #42.
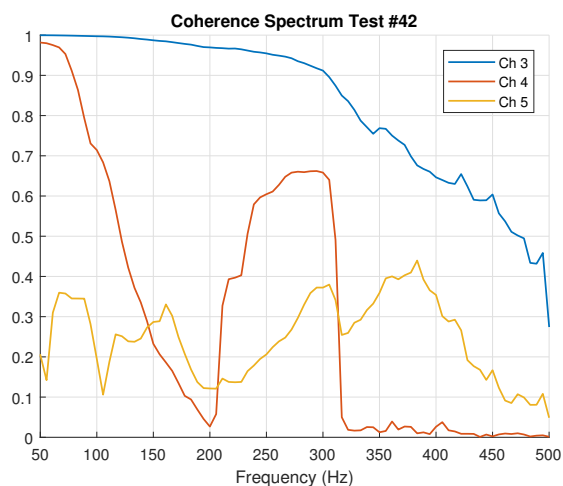


Figure 5.29: Coherence of test #42.

Observing in fig 5.29 that the coherence is dropping with increasing frequency, significantly after the third mode, $f = 366$ Hz. Comparing this to out of plane excitation with the same setup we observe a quite different behavior.
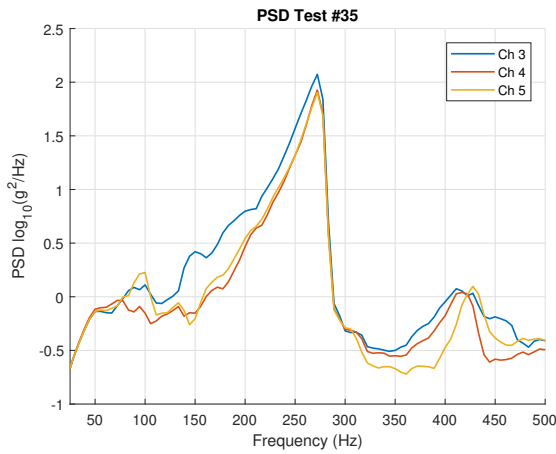
Figure 5.30: PSD test #35. 15g.
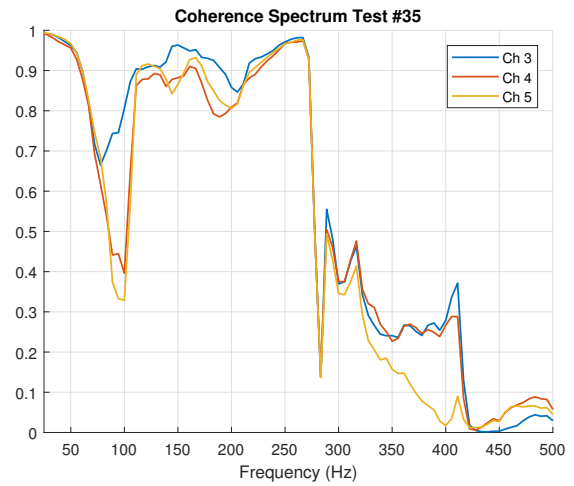


Figure 5.31: Coherence test #35.
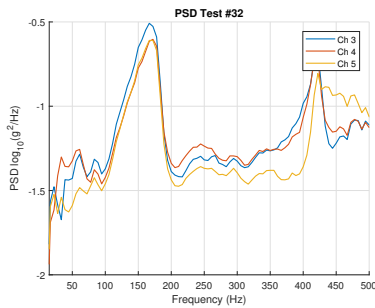


Figure 5.32: 2g



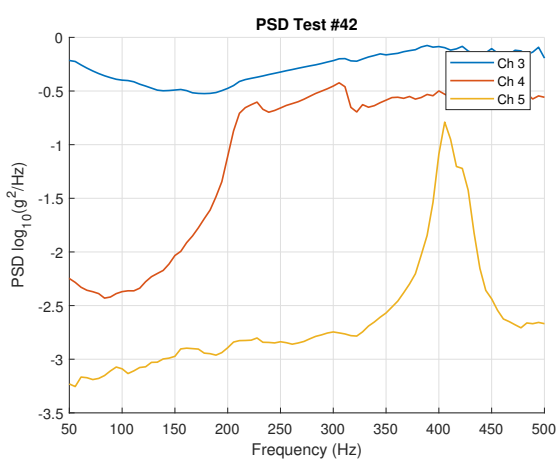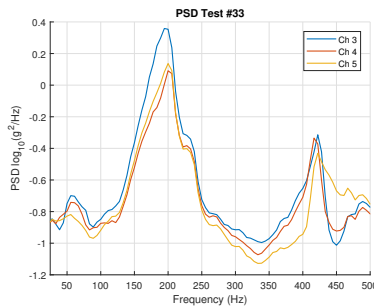Figure 5.33: 5g
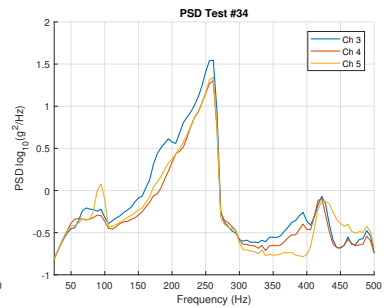


Figure 5.34: 10g

Figures 5.32-5.34 and 5.30 show an interesting phenomenon. As the g-load increases, the shaker manages to have full impact on both sides of the clearance for a higher frequency. This is why we see the sudden drop in the PSD-plot. This is completely in line with the displacement amplitude versus frequency we previously discussed in fig 5.14. The phenomena were clearly audible during the experiments. The peak shifts from 170 Hz at 2g to 270 at 15g.

**Random vibration**

All the 6 coupons were in both directions also excited by random vibration. This makes up 12 tests. Parameters in the shaker control software for random vibration allows specification of the load in $gn^2$/Hz and from there it is able to read off the g-load. A load of 0.0002 $gn^2$/Hz was read to be 0.4464 g. The random vibration had the following test properties:

| Load | Freq range (Hz) |
|------|-----------------|
| 0.0002 $gn^2$/Hz | 5-1000 |

Table 5.6: Random vibration parameters.
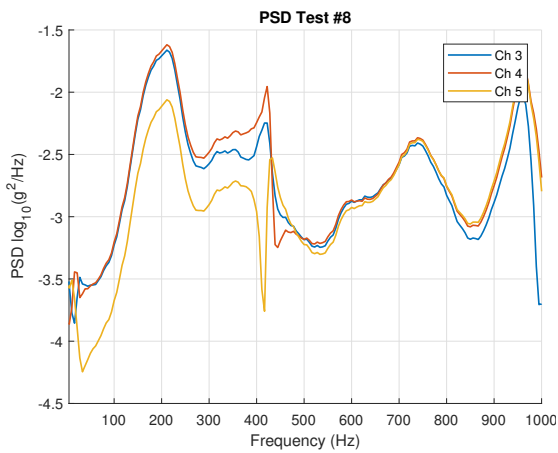


Figure 5.35: PSD of random test #8. Radial out of plane, $a = 0.00$.
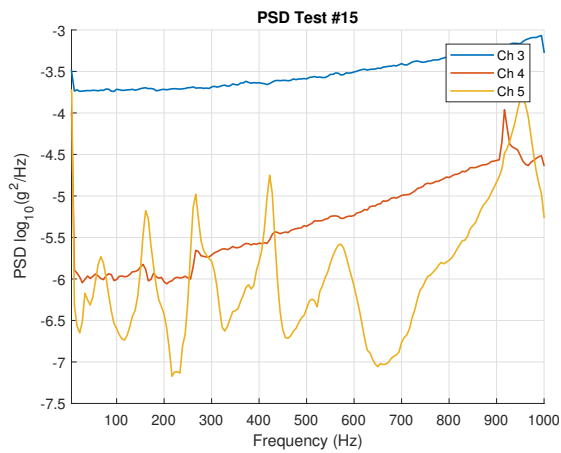


Figure 5.36: PSD of random test #15. Radial in-plane, $a = 0.00$.
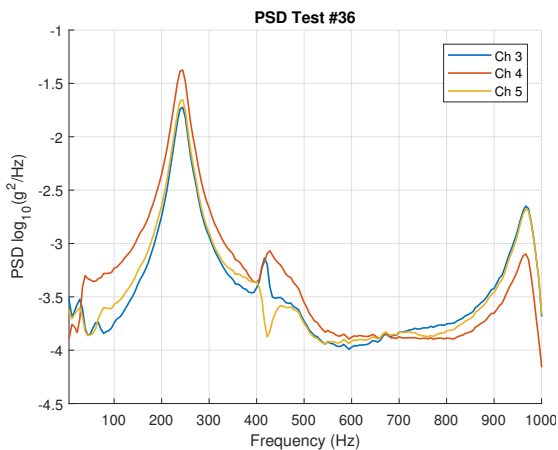


Figure 5.37: PSD of random test #36. Radial out of plane, $a = 0.10$.
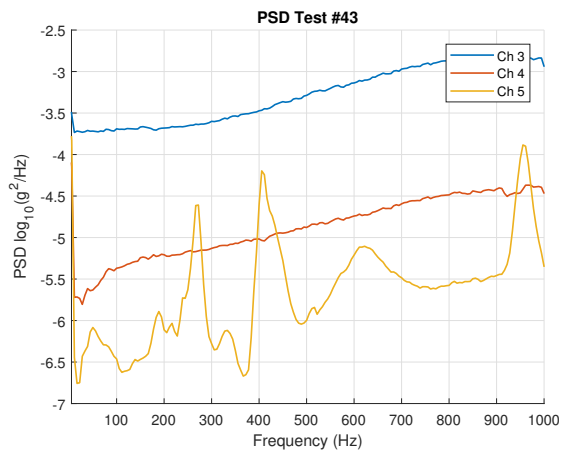


Figure 5.38: PSD of random test #43. Radial in-plane, $a = 0.10$.
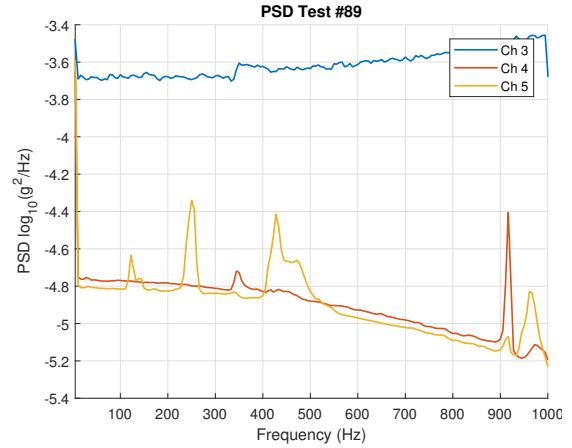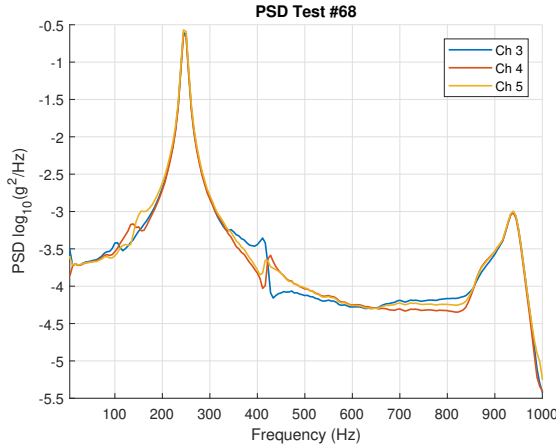
Figure 5.39: PSD of random test #68. Slot out of plane, $a = 0.10$.



Figure 5.40: PSD of random test #89. Slot in-plane, $a = 0.10$.

Again, we observe that there is a distinct difference in the response of the different orientations (notice that ch 3 is the accelerometer measuring in the excitation direction). As the results are very similar for the in-plane excitation, we do not report every run here. The interested reader is referenced to the Appendix F.

For the out of plane orientation the peak is approximately at the same frequency for all runs, at $f = 250$ Hz. It is interesting that the peak in PSD drops 126 Hz by introducing a clearance in the system. There is also some behavior at 400 Hz worth noticing. It is noteworthy that the PSD-peak at 250 Hz is common regardless of joint type or clearance.

**Harmonic input and notch filtering**

A total of 8 tests were run with harmonic input (single frequency excitation). The objective of the harmonic input is to understand 1) the potential noise in the experimental setup and 2) the chaos generated by the nonlinear gap. The radial a_0_10 coupon was chosen as it turns out to be the coupon-bushing combination with the most clearance. It was excited at 50 (low frequency), 250 (peak in PSD from test), 315 (1. natural frequency from Nastran) and 366 Hz (2. natural frequency from Nastran). The coupon was tested at 1.0 and 10.0 g, representing low and high amplitudes from the previous sine sweep testing. For the 1.0 g we have previously experienced little rattling chaos while for 10.0 g the tests have overall yielded chaos. The Welch averaging parameters were changed to increase resolution.

| Property | Value |
|---|---|
| Sampling frequency | 5688.9 Hz |
| Welch window | 2048 |
| Welch overlap | 1024 |

Table 5.7: Post-processing parameters for harmonic input.
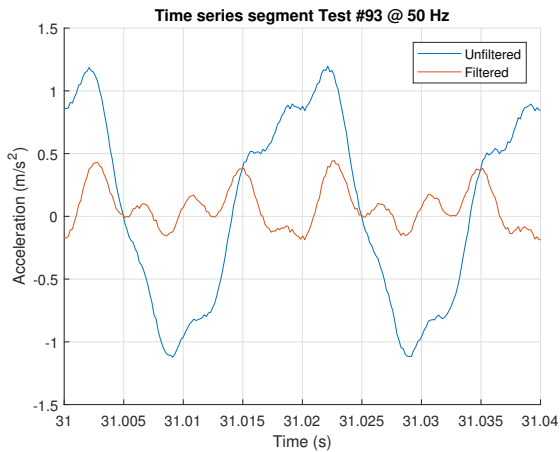
Figure 5.41: Time series segment #93. 0.5g.
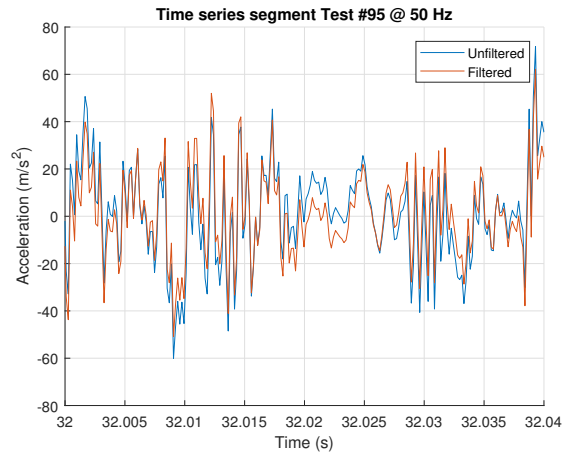
Figure 5.42: Time series segment test #95. 10g.

Figure 5.41 and 5.42 show a representative time series segment that spans over two periods of the excitation frequency (in this case $f_e = 50$ Hz and so $T = 1/50 = 0.04$s). The time series data has been notch filtered or attenuated, at the excitation frequency. This is clearly visible at fig 5.41 where the coupon is excited at 1 $g$. However, for the 10 $g$ load we see the resulting time series segment is by far more chaotic than at 1$g$ and has seemingly no periodic motion at 50 Hz as the filtered and unfiltered signals are almost the same. This result follows the general notion that a certain $g$-load is necessary in order to have full impact on both sides of the joint under excitation. The results also show that at 10$g$ the behavior is highly chaotic and even a low excitation frequency excites much higher response frequencies in the system.
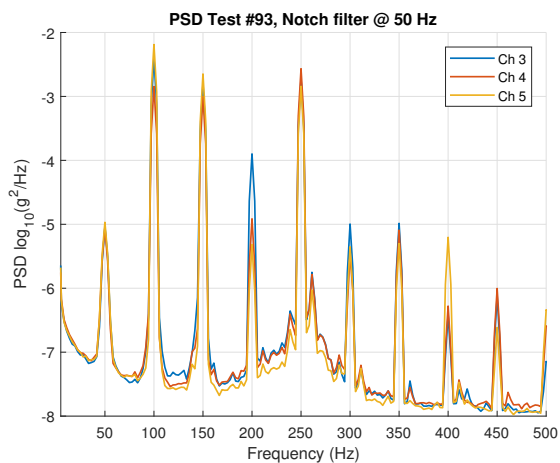


Figure 5.43: PSD #93. 0.5g.
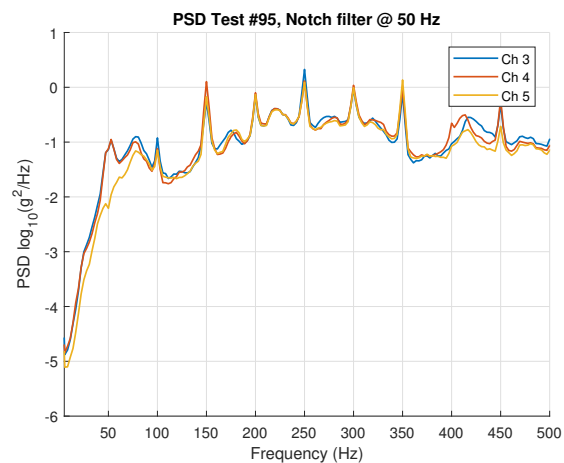
Figure 5.44: PSD test #95. 10g.

The observation of one excitation frequency manifesting itself in the response through several higher and lower frequencies, or period doubling, is seen in fig 5.43 and 5.44.

The idea behind the harmonic input is to also have a quantified opinion on noise in the system. Here, *noise* in the sense that chaos is introduced through the nonlinearities of impact vibration. For instance, the response displayed in fig 5.43 may be considered noise if we want to follow our previous logic. As the system in test 93

is believed to be linear as the *g*-load is too low to initiate full double impact, the resulting response after we have notch-filtered the excitation frequency *should* be noise. However, it is difficult to be absolutely certain the system behaves linearly even under 1g. Regardless, the magnitude of the response in the PSD plot of test 93 is very low, indicating that noise might very well not play a large role at these loads anyway.

**Using peaks to find trends**

Although it is interesting to look at the complete PSD or FRF plots, it is in essence the frequency at peak value that indicates the natural frequency. Using the built-in function `findpeaks` in MATLAB we can easily find the numerical value of peaks in different data sets. Three scripts have been written to accommodate for automation of this process. This makes it easy to process through a number of tests, finding the peak value and the corresponding frequency and then lastly plotting the values against each other in order to investigate any trends. We call the peak in the PSD plot for the *effective natural frequency* $\omega_e$. Then we explore how $\omega_e$ varies as we vary different parameters.

- $\omega_e$ vs $a$ in random excitation (fig 5.45)

- $\omega_e$ vs g-load in different coupons (fig 5.46, 5.47)

- $\omega_e$ vs a in all the radial joint tests combined. Similarly for the slot joint (fig 5.48, 5.49)

By varying the gap distance and looking at the random excitation results we find:
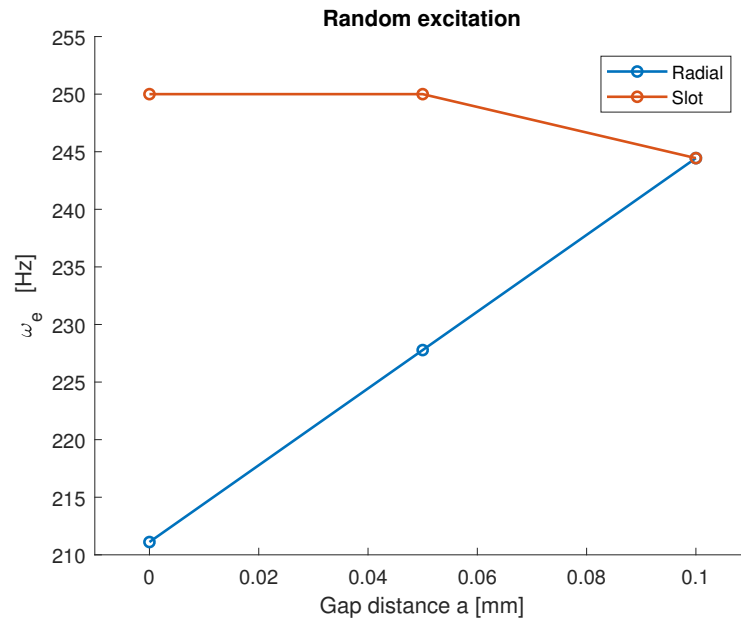


Figure 5.45: $\omega_e$ as a function of $a$ in random excitation. Both radial and slot type joint.
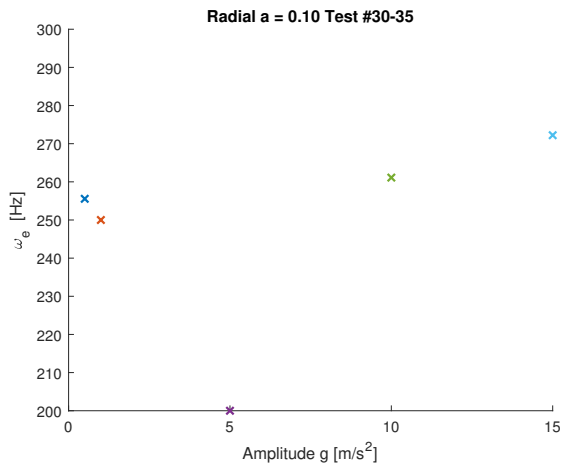
Figure 5.46: $\omega_e$ as a function of g-load in slot $a = 0.10$.
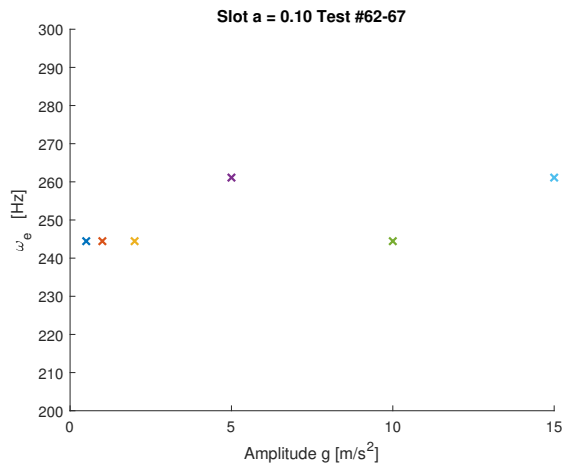
Figure 5.47: $\omega_e$ as a function of g-load in radial $a = 0.10$.

Figure 5.46 and 5.47 show little or no conclusive trend on $\omega_e$.
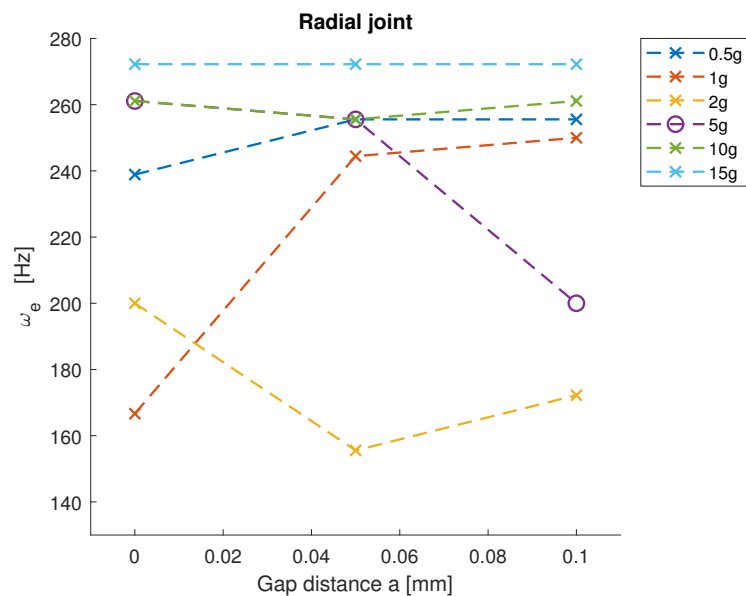


Figure 5.48: $\omega_e$ as a function of $a$ in every radial out of plane test.

71
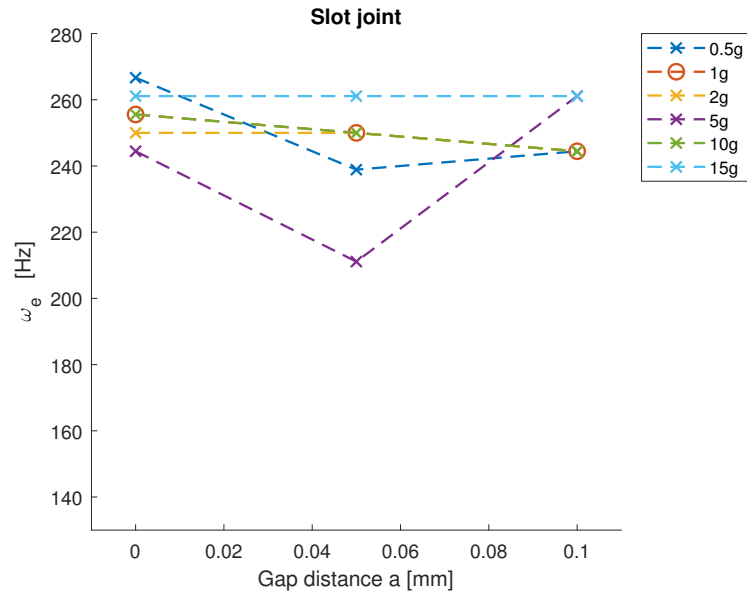
Figure 5.49: $\omega_e$ as a function of $a$ in every slot out of plane test.

Figure 5.48 together with 5.49 is perhaps the most elaborate plots of them all from the shaker tests. They each display 18 tests in one single plot, giving the essence of the results from the radial and slot joint tests, respectively. There is however difficult to claim any conclusive trend from the data.

Although we can not clearly give any correlation between $\omega_e$ and the test parameters, there is clear that the peak in PSD has been reduced for every out of plane test when nonlinearity was introduced. We wish to be careful in making claims based on such inconclusive data, but this fact might indicate that clearance lowers the natural frequency - which was the behavior the Department of Prototyping, FFI experienced with the RIMFAX in the first place.

## 5.3 Discussion

The objective is to summarize and discuss the most important aspects of the results from the experimental work.

### 5.3.1 Characterizing Stiffness

The S355 steel parts turned out to have a hardness and surface finish such that it could not be clamped properly. Thus the surface is partly knurled in order to increase grip. This process turned out to be an inexpensive remedy of the problem, but we observe that the different runs are getting increasingly stiffer. This is believed to be due to the grips "come into place" more and more during the runs. This is way run 1-3 is discarded and we only consider run 4,5 and 6 for the estimate on stiffness. After testing for several times and with different joint types (slot, radial) we observed the following:

- The results converge by stiffening. The first two runs typically have a large displacement. 2-3 additional runs are needed to have converged and consistent runs. It is reasonable to believe that this is due to poor jig-design and that the jig needs some amount of force to "set". When this is done one may start to record real results.

- The results for every coupon, slot and material yields the same $k_e$. This is believed to be due to the slipping of the specimen in the grips. Thus what we really measure is the "slipping stiffness" in the grips and not at all the joint contact stiffness. This renders the results practically useless.

- The test does not yield the same results for $k$ for the same specimen when it is remounted in the tensile jig. We were not able to reproduce the same results

- When loading the specimen to more than the target load of 500N, we observed more of the "grips come into place"-behavior. This indicates that the grips have not in fact "come into place" for loads under 500N. Thus, the specimen is still slipping.

These observations question the integrity of the tensile test completely.

The tests were run and the results can be found in fig 5.9. If we compare the results (tab 5.2) to the linear static finite element results (tab 6.4) we observe a difference in the order of $10^3$. Consequently, the results from the stiffness test are only reported - not used any further.

### 5.3.2 Dynamic Experiment I: Initial Shaker Tests

**Initial Runs**

The sine sweep tests of the steel S355 coupons were in the beginning hard to analyze. The problem is, as we are aware of, amplitude-dependent. This is confirmed through sine sweeps of varying the acceleration amplitude value $g$ in the values of $[0.2, 0.25, 0.5, 0.75, 1.0, 1.1, 1.4, 2.0, 3]$. They all yield different results. The most prominent observation from the amplitude variation is that for $g > 1.1$ the coupon starts to translate in the joint. For $g < 1.1$ the coupon is moving along with the jig, providing a much "cleaner" plot - although not giving us the physical joint behavior we are seeking. A lot of time was spent investigating by trial and error how the coupon behaved.

The stiffness of the S355 coupon is assumed to be too high for use in practical experiments. This is supported by the normal modes analysis in chap. 6.2.2. The first eigenvalue is 1953 Hz. This makes the analysis more difficult than necessary mainly because of:

- The shaker is operational from 5-3000 Hz. Having eigenvalues so close to the max operational frequency implies that we have less room to experiment with.

- When exciting at high frequencies, the Nyquist frequency increases. This corresponds to larger data sets. This in itself is no real concern as both the computers available and the post processing software MATLAB is capable of large data sets. However, when we want to compare our results with MSC/-Nastran, the case becomes drastically more computational expensive if we have to sample at 4 kHz instead of for instance 1 kHz or so. The step size decreases and thus the problem becomes more computationally expensive.

- Considering the amplitude-frequency relation seen in fig 5.14 we see that exciting at frequencies above 400 Hz or so makes it necessary to have extremely tight tolerances to enable the double impact behavior we seek. Exciting only at frequencies below e.g. 400 Hz makes the task much more manageable.

**Fundamental mode from zero clearance**

The classical experimental modal testing for finding the linear natural frequency was done on both S355 and POM C and they show both excellent correlation with the finite element analysis.

### 5.3.3 Dynamic Experiment II: POM C Shaker Tests

The POM C shaker tests yielded much more clear results, mainly because of the following:

- The ringing noise experienced with the metal-to-metal contact in S355 coupons is eliminated in POM C.

- The natural frequency was drastically reduced, down to 314 Hz. This is a much easier frequency area to operate in, as reasons mention above indicate.

- The S355 coupon tests served as a good indication of what worked and what did not. Subsequently, the POM C tests were more targeted and efficient as the author already had previous experience.

The highlights from the POM C shaker tests results as previously discussed are:

- There is a significant difference in response comparing out of plane and in-plane excitation. The system is too stiff in-plane to display any noticeable effect of clearance. The response is flat.

- The out of plane excitation shows that the peak in Power spectrum density drops from 367 to approximately 250 Hz by introducing clearance. This drop is similar for all clearances and joint types.

- Variation of the g-load confirms the belief that there is a clear correlation between the shaker displacement amplitude and whether or not the system has double impact or not. The displacement is inversely proportional to frequency, so the bushing does after a certain frequency not displace the gap completely. Hence, impact is not achieved and the system is much less chaotic. Higher g-loads have a higher displacement at the same frequency and manages to keep the full impact behavior for a longer frequency range.

- Harmonic input and notch filtering of the excitation frequency displays interesting results when it comes to chaos and noise in the system.

# Chapter 6

# Finite Element Approach

This chapter presents the numerical models used to solve the thesis problem. The overall aim is to model the problem as accurate as necessary yet as computationally inexpensive as possible.

FFI use the software package from MSC Software containing of MSC/Patran (herein Patran) and MSC/NASTRAN (herein NASTRAN or Nastran). Part of the thesis work is to solve the problem *for* FFI *in* this software package.

The structure of this chapter is thus:

- Present some general prerequisites and provide the underlying assumptions for consistency.

- Present the approach used in MSC/NASTRAN for the static and various dynamic analysis. This includes evaluation of alterations or simplifications required, different numerical schemes, element types and post-processing techniques.

- Present the results of the said analysis.

- Discuss the said results.

## 6.1 Method

### 6.1.1 Finite Element Prerequisites

**Units**

As with other comparable finite element software packages, Nastran employs the user to be consistent in their use of units. In this thesis the following units are chosen:

| Property | Unit |
|---|---|
| Length | m |
| Mass | kg |
| Mass density | $kg/m^3$ |
| Force | N |
| Elastic modulus | Pa ($N/m^2$) |

| Output | |
|---|---|
| Displacement | m |
| Acceleration | $m/sec^2$ |
| Stress | Pa |

Table 6.1: FEA unit consistency.

**Damping**

Damping may come from several sources such as viscous effects (dashpot, shock absorber), internal friction (i.e. hysteresis), external friction (slippage in structural joints) and/or structural nonlinearities (plasticity). Nastran cosideres two different damping types: viscous and structural [26, p. 9.3-4]. Viscous damping use discrete elements such as CVISC or CDAMPi. They are mainly used to model actual damping components in a structure, such as hydraulic damper and other viscous interfaces. Structural damping is a global damping proportional to the stiffness. A realistic value is between 0.5% and 4%. According to [26, p. 9.3-5] the relation between viscous and structural damping is

$$c = g\,\omega_n m = \frac{g}{\omega_n}k \tag{6.1}$$

or

$$g = \frac{c\,\omega}{k} = 2\zeta\frac{\omega}{\omega_n} \tag{6.2}$$

which at resonance is equivalent to

$$g = 2\zeta \tag{6.3}$$

**Notes on SOL400**

The project thesis used SOL129 Nonlinear transient response. As this is a legacy solver the improved SOL400 in Nastran is used. SOL400 includes the functionality

78

of SOL129 as well as more. SOL400 is an implicit nonlinear solver recommended as default by MSC Software. The nonlinear problems are classified into three categories: geometric, material and contact. The formulation and setup utilized in this thesis implies a material nonlinearity (i.e. the stiffness $k$). See [22], [5], [21] and [4] for more on Nastran.

**Relevant Element Formulations**

One key part of this thesis is navigating in the vast number of different elements and properties in NASTRAN which we may use in order to represent the nature of the problem.

| | |
|---|---|
| CVISC | Viscous damper element. 1D. Possible to define Extensional ($C1$) and Rotational ($C2$) Viscous Coefficient. |
| CBUSH | 1D Scalar bush element. Versatile spring-damper element. Various definitions of spring stiffness, both constant, frequency dependent and force-displacement relation directly. Possibility for spring-damper in 6 directions. |
| CBUSH2D | 1D-2D Linear/nonlinear bush element. |
| CGAP | Gap or friction element. Intended for nonlinear static analysis. Functions like a contact element and intended for contact analysis. Tweaking of contact spring parameters is required for convergence. Not suited for dynamic analysis with numerous opening and closing of gaps. |
| CELASi | CELAS1 or CELAS2. Scalar spring element. Need to define Spring Constant and DOF at node 1 and 2. |
| CDAMPi | CDAMP1 or CDAMP2. Scalar damper element. Need to define Damping Coefficient (force per unit velocity) and DOF at node 1 and 2. |
| CONM | CONM2, Concentrated Mass Element Connection. Defines a concentrated mass at a grid point. Defined by a mass value and a mass moment of inertia measure $I_{ij}$. Also possible to use the more general CONM1 element, where a 6x6 mass matrix serves as input. |

Table 6.2: Element formulations in Nastran.

## 6.1.2 Static Analysis

As we saw in sec 5.1.2 the experimental approach did not yield valid results. A linear static finite element analysis was run to attempt to remedy this.

The coupon CAD-files were altered with split lines in order to create surfaces which is to be used for applying loads and boundary conditions in MSC/Patran. The geometry was exported through parasolid `.xt` and then imported into MSC/Patran. A load of 500N in the first principal direction was applied as seen in fig 6.1 and a boundary condition of $u_1 = u_2 = u_3 = 0$ (fixed) was applied to the rim of the coupon[1]. In order to remedy for possible out-of-plane displacement, an $u_2 = 0$ condition was applied to the faces with a normal vector in the $y$-direction. The max displacement was read and through this, an estimated $k_e$ is given by Hooke's law:

$$k_e = F/u \qquad (6.4)$$
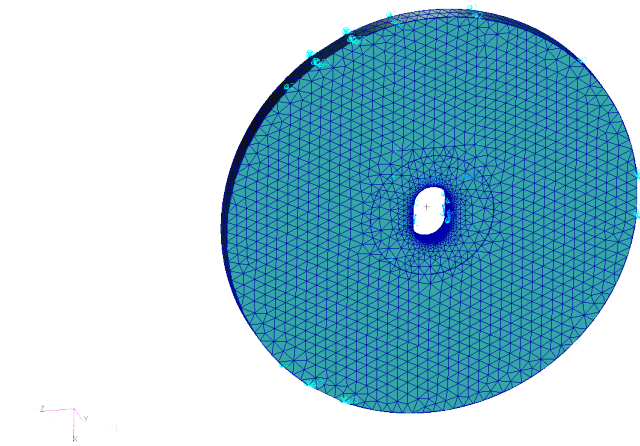


Figure 6.1: FE model of slot for linear static analysis

---

[1]This is not identical to the experimental setup. When it was realized that the experimental tensile test was flawed it was decided to use a more desired approach in FEM. If we were to do the test again we would like to apply the same boundary condition on the rim.

### 6.1.3 Dynamic Analysis I: Normal Modes Analysis

Initially, a normal modes analysis in NASTRAN using `SOL103` was conducted in order to classify the normal modes of the structure we might observe during the shaker tests. The analysis was done with geometry created in Patran for the radial joint. This creates triparametric geometry which makes it possible to mesh using Patrans IsoMesh-algorithm. Both a thin-shell formulation and a 3D solid formulation was used and compared. Both models had encastre[2] boundary conditions at the elements inside Ø16.7 mm of the center. This is where the bolt and bushing flange have contact with the coupon.

The modal analysis was limited to find only the first 10 modes and up to 3000 Hz (we are not interested in higher modes).

---

[2]$u_i = \theta_i = 0 \; i = 1, 2, 3$ No translation or rotation.

## 6.1.4 Dynamic Analysis II: Spring-Damper Model

**Objective**

The objective of this model is to propose a finite element formulation that serves as an initial solution on the problem. The initial goal of the finite element modeling was to correlate experimental results with a finite element model and in best case fine-tune parameters (within sensible bounds) such that one has a good correlation between simulation and experiments. However, as the experimental work yielded results much more chaotic and less clear the objective has shifted. After discussion, it is believed that attempting to replicate the phenomena we saw through the Duffing oscillator in Theory and through the numerical results in MATLAB, is more interesting. If we can display the period doubling and drop in natural frequency we saw when adding clearance to the system, we have come some way. Thus, the finite element approach for dynamic analysis is an iteration on the formulation that was used in the project thesis.

**Model**

The model is based on the model from the project thesis. We see the need to reduce the computational effort in order to run the problem on a standard office computer. The coupons are represented by a `CONM2` element with prescribed mass and inertia. Intertia is given by a 3x3 matrix. The mass has been scaled to 1kg, and the inertia for the coupon is scaled correspondingly. The resulting $\mathbf{I}$ is [3]:

$$\mathbf{I} = \begin{bmatrix} I_{xx} & I_{xy} & I_{xz} \\ I_{yx} & I_{yy} & I_{yz} \\ I_{zx} & I_{zy} & I_{zz} \end{bmatrix} = \begin{bmatrix} 633 & & \\ & 633 & \\ & & 1256 \end{bmatrix} \text{ kg mm}^2 \tag{6.5}$$

One node represents the ground, and one node represents the coupon. The two nodes are connected through a bar element. The CONM2 property is linked to a point element. In total there are two nodes and two elements in the model.
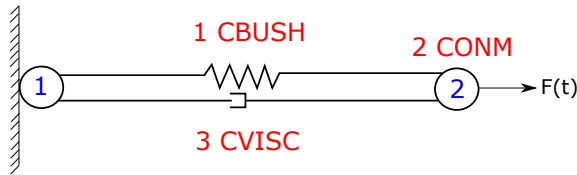


Figure 6.2: Nastran model. Elements in red and nodes in blue.

The CBUSH element spring stiffness $F_s$ is defined through

$$F_s = \kappa \left( x/a \right)^n \tag{6.6}$$

where $n = 3$.

**Constraints**

The node for ground is constrained to no translation ($u_i = 0$ for $i = 1, 2, 3$). The node for coupon is constrained to no translation in $u_3$ as the problem is considered to be in $\mathbb{R}^2$.

---

[3]The values of $\mathbf{I}$ is calculated in SolidWorks from the coupon geometry and mass properties.

**Solution method**
SOL400 is used. The following values are set in Step parameters - Load increment parameters.

| Property | Value |
| --- | --- |
| Increment type | Adaptive |
| Trial time step size | 0.005 |
| Time step scale factor | 1.1 |
| Min step size | 5E-05 |
| Max step size | 0.05 |
| Max # of steps | 29999 |
| Total time | 30.0 |
| # of steps of output | 15000 |

Table 6.3: Load increment parameters SOL400.

The solution convergence is quantified and monitored through the .sts file generated by Nastran in real-time. The .f06 file is routinely checked for any error messages.

**Mesh**
The model is 2D and uses bar and point elements. As we have modeled the coupon as a lumped mass CONM2 element, we are left with a very small mesh consisting of only two nodes and two elements.

**Input signal**
We use a sine sweep signal generated using `chirp` in MATLAB, see Appendix C. The signal sweeps linearly from 0-30 Hz over 30s. We sample the signal at $f_s = 1000$ Hz for input to Nastran. As the chirp signal only sweeps up to 30 Hz and we plan to sample output at much lower than $f_s/2$ we should not encounter aliasing in any link of the process..

**Output request**
We request displacement, velocity and acceleration for the point mass at 15000 instances. This yields a $f_s = 30/15000 = 500$ Hz.

## 6.2 Results

This section presents the key results from the numerical simulation work. The section presents the static and dynamic results previously discussed.

### 6.2.1 Static Analysis: Characterizing Stiffness

6 linear static finite element analysis' with different coupons and different load cases were conducted in NASTRAN. The simulation is set up according to sec 6.1.2. The results are

| Coupon and load case | Material | F (N) | $u$ (mm) | $k_e$ (N/mm) | $f_n$ (Hz) |
|---|---|---|---|---|---|
| Slot 1st principal | POM C | 500 | 3.22E-02 | 1.553E+04 | 2679 |
| Slot 2nd principal | POM C | 500 | 2.91E-02 | 1.718E+04 | 2818 |
| Radial 1st principal | POM C | 500 | 2.59E-02 | 1.931E+04 | 2987 |
| Slot 1st principal | S355 | 500 | 4.67E-04 | 1.071E+06 | 9509 |
| Slot 2nd principal | S355 | 500 | 4.43E-04 | 1.129E+06 | 9763 |
| Radial 1st principal | S355 | 500 | 4.26E-04 | 1.174E+06 | 9956 |

Table 6.4: Numerical results from linear static analysis in NASTRAN.

The natural frequency $f_n$ is calculated as

$$f_n = \frac{1}{2\pi}\sqrt{\frac{k_e}{m}}$$

where $k_e$ is in [N/m].
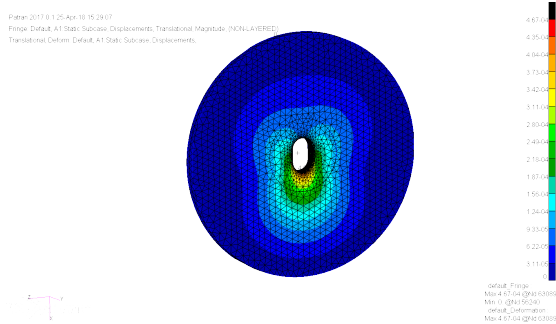


Figure 6.3: Deformation plot.
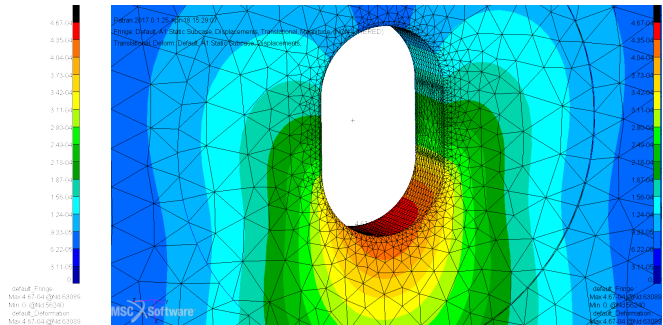


Figure 6.4: Detail of contact area

If the hypothesis of a "joint natural frequency" is true, this may be estimated from table 6.4. In the vicinity of 2700-3000 Hz for POM C and almost 10,000 Hz for S355 makes the frequency area of interest extremely high and rarely observed in reality. It is also way above the natural frequency of the coupon structure as we shall soon see.

We wish to elaborate and problematize the concept of finding a joint stiffness. This both in regards to experimental and finite element methods. From the experimental

point of view, we are dealing with *very* small deformations. Imagine, we are oscillating the bushing inside the joint but not really exerting a force on the joint contact area. The contact event is of impact in nature. Thus, to measure the stiffness we need to measure small deformations. This requires a test jig and test equipment which are designed to operate at such small magnitudes. Neither did this in our case. Small clearances in nuts, bolts and other contact areas in this thesis' jig make the total deformation measure the sum of several contact deformations and it is with the current jig impossible to separate them apart. Also, a more accurate measurement device than the tensile machine in itself is required. Perhaps an extensometer would be an improvement. Otherwise, very high resolute cameras may be able to capture the small deformation (imagine a setup like DIC [4]). In general, the complete test setup has to be designed with small deformations in mind - from the FE analysis we estimate an order of magnitude of 1E-04 mm for steel.

From the finite element point of view there are certain improvements that should be done. First and foremost a proper contact analysis must be done. Here it is important that both the joint and the bushing are deformable. The question of where to measure the total deformation from arises. Also, the analysis will be both mesh and material dependent. The reason a contact analysis is not conducted in this thesis is that it is not considered to be in the scope as this work revolves more around the oscillatory properties. However, a true description of the problem will likely involve a proper evaluation of the stiffness both experimentally and in FE.

Overall, the idea of characterizing the joint stiffness on basis on the methods given in this thesis was initially thought to be "good enough". However, the author realized that this was not the case as the analysis' were conducted. Time was a limiting factor, and the method and results are presented "as is" - that being with great disclaim when it comes to the usability of the results. They are meant as merely a guideline.

---

[4]DIC - digital image correlation: an optical technique where imaging and tracking of material points are used to quantify deformation or strain

## 6.2.2 Dynamic Analysis I: Normal Modes

**Natural frequencies and modes with $a = 0$**

The numerical model was built by using a standard thin-shell [5] A total of 1600 CQUAD4 elements with a constant width of 2.6 mm represents the coupon. The inner elements are fixed in $u_1, u_2, u_3$ translation. `SOL 103` Normal Modes Analysis in NASTRAN yields $\omega_{n1} = 314\,\text{Hz} = \omega_{n2}$ (mode shapes are identical, eigenvectors directed in different planes), $\omega_{n3} = 364$ Hz, $\omega_{n4} = 410$ Hz.
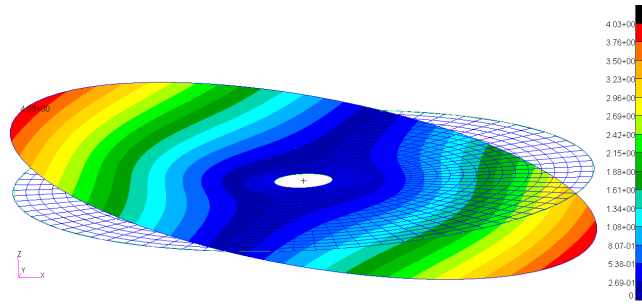


Figure 6.5: Mode 1 &2, 314 Hz. Mode 2 at same frequency but with eigenvector in YZ-plane instead of XZ as shown here.



Figure 6.6: Mode 3, 364 Hz.



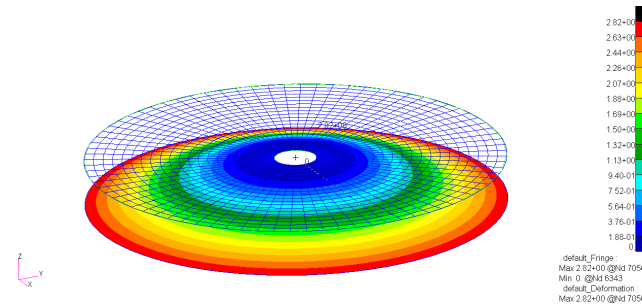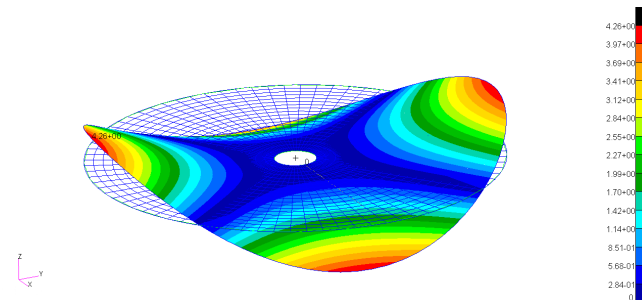Figure 6.7: Mode 4, 410 Hz.

We observe from the experimental results in fig 5.20 that the first natural frequency is located at 316 Hz. This corresponds well with the numerical $w_{n1}$. Thus we conclude that peaks occurring in the vicinity of 314 and 364 Hz are the coupons natural frequency *and not the joint frequency.*

---

[5]Thickness-to-span ratio of 1/20 which makes it borderline formulation.
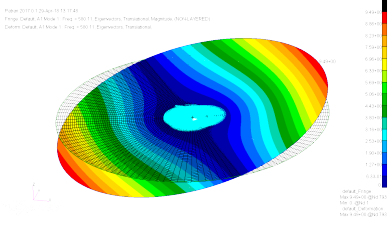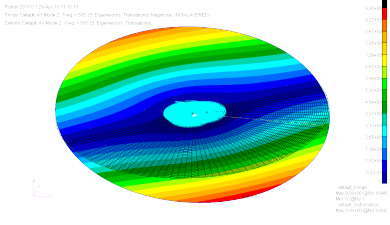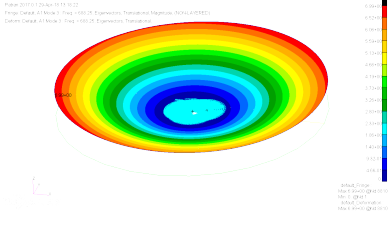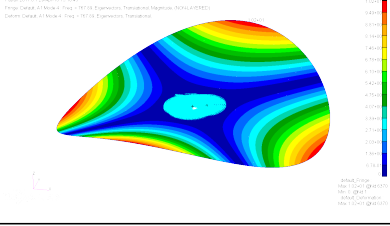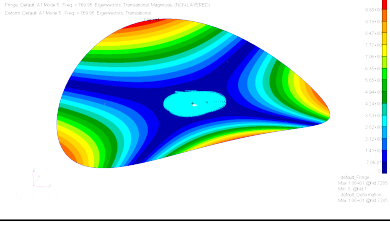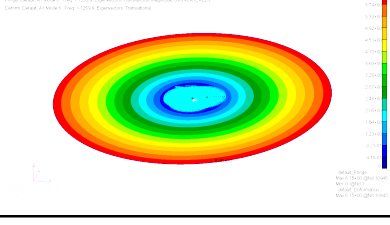
| Mode no. | Eigenvalue Shell | Material | Joint type | Mode shape |
|---|---|---|---|---|
| 1 | 314 | POM C | Radial |  |
| 2 | 314 | POM C | Radial |  |
| 3 | 364 | POM C | Radial |  |
| 4 | 410 | POM C | Radial |  |
| 5 | 412 | POM C | Radial |  |
| 6 (Torsion) | 851 | POM C | Radial |  |

Table 6.5: 6 first modes from normal modes analysis of radial coupon of POM C $t = 2.6$ mm from NASTRAN. Shell elements depicted.

We report the value of S355 for comparison (although not used when the switch to POM C was made).
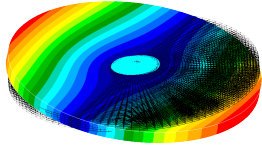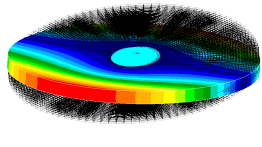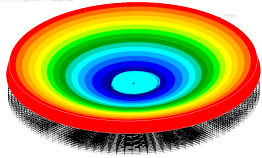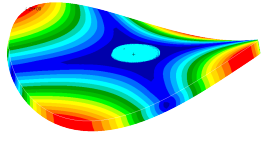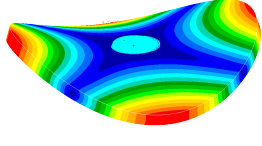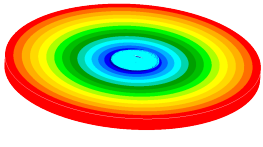
| Mode no. | Eigenvalue Solid/Shell | Material | Joint type | Mode shape |
|---|---|---|---|---|
| 1 | 2030.7/2024.9 | S355 | Radial |  |
| 2 | 2030.7/2024.9 | S355 | Radial |  |
| 3 | 2329.9/2332.5 | S355 | Radial |  |
| 4 | 2898.7/2908.1 | S355 | Radial |  |
| 5 | 2897.7/2908.1 | S355 | Radial |  |
| 6 (Torsion) | 4456.7/4793.2 | S355 | Radial |  |

Table 6.6: 6 first modes from normal modes analysis of radial coupon in steel S355 ($t = 5$ mm ) from NASTRAN. Solid elements depicted.

### 6.2.3 Dynamic Analysis II: Spring-Damper Model

**Vary gap distance** $a$

We vary the gap distance $a$ in the spring stiffness formulation $F_s$. The input signal is the sine sweep presented above, but with an amplitude of 5 N. $a = [0.1\ 0.25\ 0.5\ 1.0]$.

| Parameter | Value |
|:---------:|:-----:|
| $\kappa$ | 10 |
| $\zeta$ | 0.01 |
| $c$ | 0.06324 |
| $m$ | 1 |

Table 6.7: Fixed parameters for gap simulations.
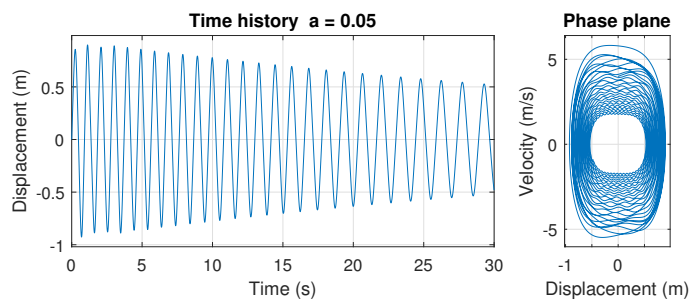


Figure 6.8: Time history and phase plane plots of $a = 0.5$.
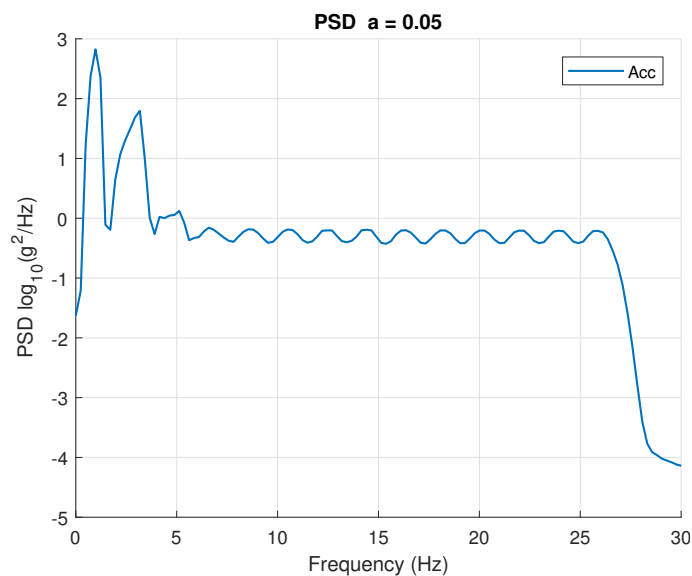


Figure 6.9: Power spectrum density $a = 0.5$.
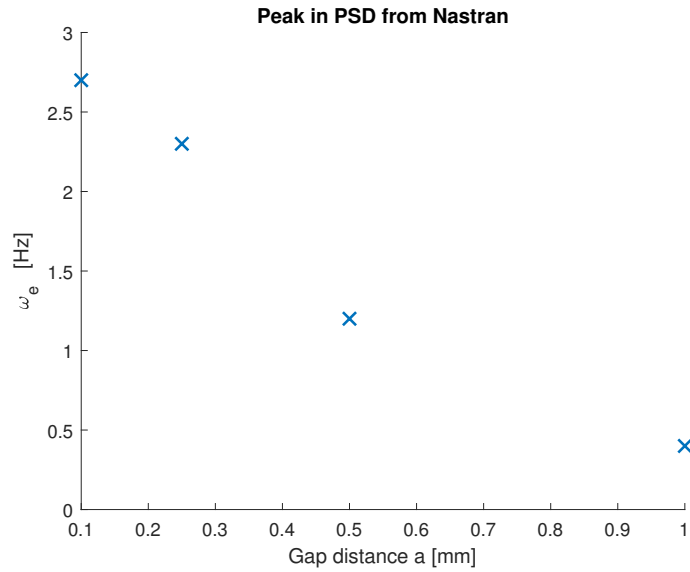
Figure 6.10: Peak in PSD

The results above are similar to the results from the project thesis. The most prominent difference between this formulation and the formulation in the project thesis is 1) the usage of SOL400 instead of the legacy SOL129 and 2) the use of the cubic Duffing spring stiffness. Otherwise the workflow is comparable as seen in fig 6.11.
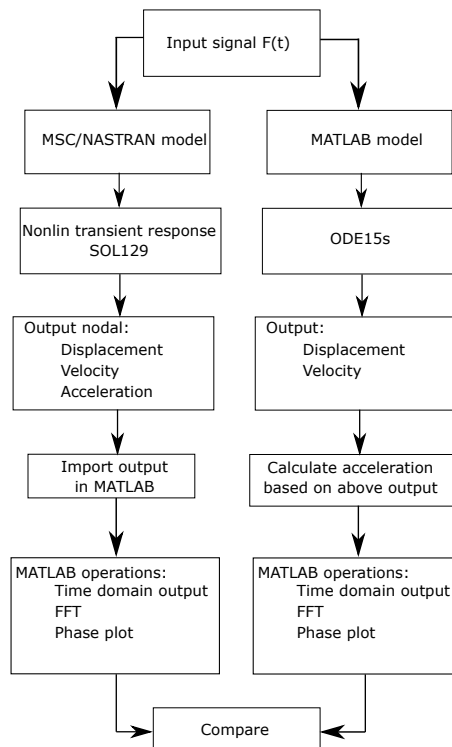


Figure 6.11: Flowchart of the Nastran/Matlab workflow

We take the liberty to discuss the most important results from the project thesis as they are very much linked to the current formulation.
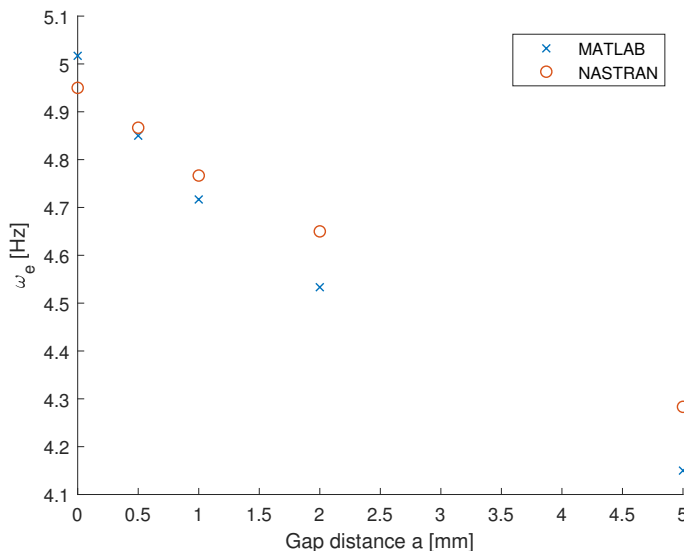
Figure 6.12: Results from varying gap distance $a$.

$\omega_e$ decreases with increasing gap distance $a$, similar to fig 6.10.
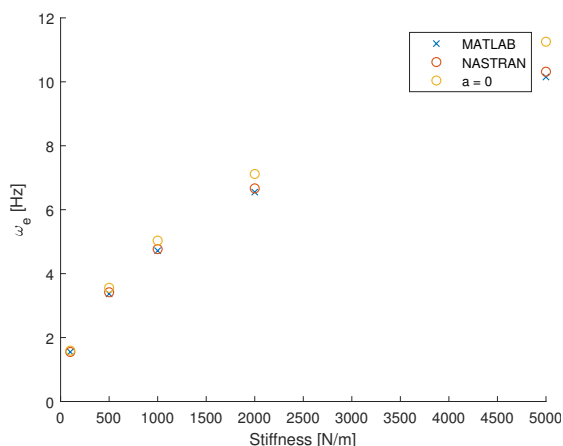


Figure 6.13: Results from varying stiff-ness $k$
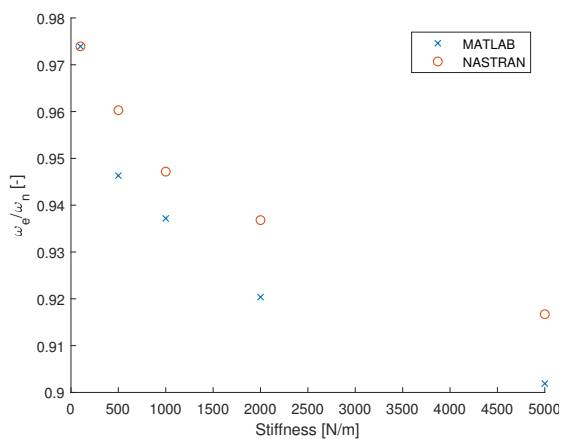


Figure 6.14: Results from varying stiff-ness $k$ considering the relative frequency

Figure 6.13 shows that increasing $k$ increases the effective natural frequency. This result is however not that interesting as the natural frequency *should* increase with $k$. If we plot the relative difference $\omega_e/\omega$ we will however see the behavior relative to $\omega$. This is illustrated in fig 6.14 and shows that increasing $k$ will give a relatively lower $\omega_e$.

The main conclusion in the project thesis was that the nonlinearities introduced in the EOMs through a discrete $k$ give rise to an overall decrease in the effective natural frequency. It was also concluded that this is supporting the behavior the Department of Prototyping at FFI observed with the shaker test of RIMFAX, as it too lowered its natural frequency when nonlinear gaps were introduced. The work done here is consistent with that.

## 6.3 Discussion

**Values for Stiffness and Damping**

The stiffness values used in this FE analysis are nowhere near being correct as the tensile test experiment is not valid. Ideally, a proper tensile test experiment should yield approximate results to be used in FEA later. In order to continue the thesis progress, more or less arbitrary values have been set and the general effect of stiffness has been investigated as a parameter study. This is the same as for the differential equation analysis conducted in MATLAB presented earlier. Ideally, the parameters used in FEA should only need tuning in order to provide correlation.

In order to improve the values for stiffness and damping, see the discussion in chap. 5.3.1 and chap. 6.2.1.

**Relevance to the Experiments**

An inherent challenge in the solution of the thesis problem is that the experimental and numerical work is highly intertwined. When the experimental work does not provide reliable estimates on input (such as stiffness, damping) for the analysis, it is difficult to claim a clear connection between simulated results in Nastran and experiments the other way around afterward. Unreliable input values yield unreliable output.

The author considers the numerical and finite element approaches to be an *indication*, rather than a truth. There are indications that reappear in all approaches, but the direct link between experiments and analysis is not present. Nor was intended to be, when the experimental results were investigated.

**Expanding to Higher Dimensions**

For a complete understanding of the problem, an expansion to higher dimension (2D, 3D models) is believed to be necessary. However, the author believes that one should fully grasp the lower order dimension before tackling the undoubtedly more complex 3D problems. One should maybe reduce the number of DOFs in the real world experiments as much as possible and try to correlate those two cases (1-2 DOF experimental and FEA) first. If expanding to higher dimensions where the problem becomes mesh dependent, a mesh convergence study is a natural task to include.

**The Next Steps**

In regards to the finite element modeling the author suggests the following steps in order to further the work:

- Ideally, one should not solve the problem in the time domain. The author has tried to find methods of solving directly in the frequency domain but was unsuccessful. This does not imply that there is none. If there is developed methods to handle this, it should greatly reduce the computational effort and make it possible to efficiently tackle more complex problems. The 2 node, 2 element model we have discussed in this thesis have a solution time of 600 s on an average desktop computer [6]. It may be outside the scope of a Master's

---

[6]16 GB RAM, 8 core processor, SSD

thesis to develop the numerical scheme and finite element solver to do this. The author believes that finding the work of others (and maybe build on it) is the way to go for a Master's thesis.

- In regards to the current developed model, more iterations would be useful. A broader characterization of parameters as well as input signals (free oscillation, harmonic, sine, random) could perhaps give new insight.

- Although most of the post-processing in this thesis has been automated through `for` and `while` loops in Matlab, it would be effective to automate the generation of Nastran input files (.bdf-files) for looping through a range of iterations. As the problem at hand is sensitive to numerous parameters (e.g. $a$, $k$, $\zeta$) as well as amplitude dependent, there is need for a greater number of simulations to better map the system's behavior.

# Chapter 7

# Discussion

This chapter summarizes the discussions made throughout the thesis. It attempts to give a more clear description of what has been observed, why and how it may be relevant or irrelevant to pursue further.

## 7.1   Experimental Results and Method

The following bullet points will summarize the findings and shed light on the most important difficulties encountered throughout experimental work of this project.

- Overall, it is difficult to be conclusive about the shaker test results. A drop in the peak response is seen through Power spectrum density and frequency response function when clearance is introduced. This is seen in all out of plane shaker tests.

- The main reason for the inconclusiveness is assumed to be an excessive number of degrees of freedom in the experiment. Creating an experimental setup with fewer degrees of freedom will hopefully remedy this. Then it will be more clear what kind of behavior one is actually observing. In general, the experimental setup for the shaker tests has too many unknown variables.

- The influence of peak in PSD was investigated through several parameters (excitation form, g-load, gap distance, joint type) but no clear trend is found.

- Using steel is difficult as the material hardness creates a ringing sound on impact. This creates excessive noise for the output signals. Also, using a material with a high Young's modulus increases the natural frequency - making it more difficult to both run experiments, post-process and match with simulation. All of this was corrected by using a material with lower Young's modulus, thinner geometry and lowering the clearance.

- It is challenging to have full double-impact[1] as the displacement is inversely proportional to the frequency. This significantly limits the frequency range

---

[1]Double impact - where the coupon is excited in such a manner that the excitation displacement exceeds the clearance distance. It makes it possible for the coupon to contact both limits of the clearance. When the excitation displacement is lower than the clearance distance, the coupon is observed to not impact both limits of the clearance.

where double impact is possible. This relates to the above, emphasizing the importance of low natural frequency.

- The tensile jig experiment is severely flawed in that it does not measure one single contact stiffness, but several stiffness' for the whole system - as well as some assumed slippage in the clamps. It is also not suitable for measurement accuracy needed for joint contact stiffness.

For a detailed discussion, the reader is referred to the relevant chapters and sections. Materials, test jig (DOFS), post-processing, tensile jig, frequency / g-range.

## 7.2 Numerical Results and Method

The following bullet points will summarize the findings and shed light on the most important difficulties encountered throughout numerical and finite element work of this project.

The MATLAB and FEA in Nastran show correlation in the following parameter variations:

- Increasing the gap distance $a$ lowers the effective natural frequency $\omega_e$, see fig 6.10 and fig 6.12.

- Increasing the stiffness $k$ lowers the relative $\omega_e$, see fig 6.13.

- Increasing damping ratio $\zeta$, lowers $\omega_e$, see fig 4.3.

Further we may point out the following related to the numerical work in Matlab:

- Through the solution of the Duffing equation we find that exciting at one frequency generates subharmonic solutions, as predicted by the literature.

- We also saw that the system is amplitude dependent, also in accordance with predictions.

- The system in Matlab is sensitive to the variation of parameters.

For the finite element approach:

- The `CBUSH` is an efficient element formulations, capable of nonlinear stiffness definitions.

- Even a model with very few DOFs such as the one in this project demand a long compute time (600 s). This does not seem viable for practical use on large models.

- The finite element approach should be mapped further when it comes to variation of parameters.

# Chapter 8

# Conclusion and Further Work

## 8.1    Conclusion

Gaps and clearances and other forms of nonlinear stiffness formulations of mechanical joints are found in many aspects in the real world. From poorly torqued bolts and irregular riveting to thermal expansion and contraction in joint elements, general wear and tear - among others. How to account for these effects in design and construction through analysis, experiments and simulation may in some applications be of great use. This thesis has developed the theoretical framework for the case of an impact oscillator. The model is used to look at how the vibration properties change when clearance is introduced - through experiments and simulation.

The numerical model investigates the second-order nonlinear differential equation, Duffing equation - classically used to model softening or hardening springs. Solving the Duffing equation in the time domain and transforming the acceleration to the frequency domain through a Fast Fourier transform shows that the peak in power spectrum density shifts towards the left when clearance is introduced - indicating a lower eigenvalue compared to a zero-clearance linear system. The solution also shows phenomena such as period doubling, where a 1 DOF system excited at 1 frequency yields a response consisting of several frequencies.

The experimental work has conducted shaker tests on joints similar to those on the RIMFAX antenna. Two different joint types have been tested with 3 different clearance distances in two different directions. Several different load amplitudes have been run, together with different ways of input signal (harmonic, sine sweep and random). In total, 92 tests have been reported through 3 one-axis accelerometers. Numerous shaker tests served as initials runs for calibration and gauging. Both steel S355 and the polymer plastic POM C has been used. The experimental results have been post-processed by the same means as the numerical work - through FFT and investigation of power spectrum density and frequency response functions. Also, the coherence spectrum has been used. The results overall show that introducing clearance to the system lowers the effective natural frequency by 30 %.
The in-plane vibration shows no peak in PSD. Also, the experimental test does have a fair degree of uncertainty associated as the number of degrees of freedom is more than necessary.

A finite element model has been proposed. The model shows good correlation with the numerical simulations. The FE-model is not attempted correlated with the experimental data as the input values for stiffness obtained through tensile tests are invalid. The model does represent the problem and is able to be expanded to several dimension through the CBUSH-card in the FEA-solver NASTRAN. The FE-model is fairly time-consuming as one 2 node, 2 element 30.0 s simulation with 15,000 output steps on a standard desktop computer have a run time of 600 s. Also, the finite element analysis shows that introducing clearance lowers the natural frequency.

The thesis has discussed several aspects revolving around the weaknesses and possible remedies for further work. Both the numerical, experimental and finite element approach shows a clear reduction of natural frequency from gaps. The methods used in this thesis *indicates* that there is a causality between nonlinear stiffness and natural frequency. Some work is however left in order to effectively apply the methods to real-life problems.

## 8.2 Recommended Further Work

From the author's point of view there are several possible improvements for further work on this topic of research:

- Focus exclusively on one of the following areas: experimental, numerical (theoretical modeling and Matlab simulations) or finite element analysis. Each of these areas may be greatly improved in terms of accuracy.

- For the experimental work: create a setup where the DOFs are as few as possible. Limit the motion to one direction. Use materials and geometry which lowers the first eigenvalue even further. The contact stiffness-task should investigate high accuracy measurement techniques such as DIC.

- For the numerical work: explore the theory even further. Vary more parameters and look into introducing friction models.

- For the FEA: try to implement the CBUSH-formulations in 3D-models. Find computationally cost-effective ways of conducting the analysis.

- Thermal effects on natural frequency. The original reason this thesis came about is due to thermal strain in joints. It would be very interesting conducting shaker experiments on joints with very small clearances using a thermal chamber. In the Environmental Testing Laboratories at FFI there is such equipment, fully able to run thermal cycles while on a shaker table. Running various thermal cycles while doing random over a prolonged period of time is a proposal of such an experiment. If one is able to have accurate control on the thermal strains in the coupon one could easily test a range of clearances using only one test specimen.

It is in the author's belief that the topic of research in this thesis has a vast range of interesting, unsolved problems with practical applications. Additionally, the problems require a broad multidisciplinary perspective in order to be fully understood and solved. All of this makes the potential learning and knowledge gain substantial, in the author's opinion.

# Bibliography

[1] Wikipedia, Duffing equation. `https://en.wikipedia.org/wiki/File:Duffing_frequency_response.svg`. Accessed: 2018-04-19.

[2] Wikipedia, Fast Fourier transform. `https://en.wikipedia.org/wiki/Fast_Fourier_transform`. Accessed: 2018-04-07.

[3] Wikipedia, Fast Fourier transform. `https://commons.wikimedia.org/wiki/File:FFT-Time-Frequency-View.png`. Accessed: 2018-04-14.

[4] MSC Nastran Quick Reference Guide MSC Nastran 2017.1. Quick reference guide, November 2017.

[5] MSC Nastran 2018. Dynamic analysis user's guide, November 2017.

[6] C. J. Begley and L.N. Virgin. Impact response and the influence of friction. *Journal of Sound and Vibration*, 211(5):801–818, 1997.

[7] G. W. Blankenship and A. Kahraman. Steady state forced response of a mechanical oscillator with combined parametric excitation and clearance type nonlinearity. *Journal of Sound and Vibration*, 185(5):743–765, 1994.

[8] S. Bograd, P. Reuss, A. Schmidt, L. Gaul, and M. Mayer. Modeling the dynamics of mechanical joints. *Mechanical Systems and Signal Processing*, 25(8):2801–2826, 2011.

[9] Bernard Brogliato. *Nonsmooth Mechanics*. Springer, INRIA Rhône-Alpes Saint-Ismier, France, 3 edition, 2016.

[10] H.G. Davies. Random vibration of a beam impacting stops. *Journal of Sound and Vibration*, 68(4):479–487, 1979.

[11] J. P. den Hartog. *Mechanical Vibrations*. McGraw-Hill, New York, 1 edition, 1934.

[12] Mathworks Documentation. Choose an ode solver. `https://se.mathworks.com/help/matlab/math/choose-an-ode-solver.html`. Accessed: 2018-04-07.

[13] S. Dubowsky and F. Freudenstein. Dynamic analysis of mechanical system with clearances part 1: Formation of dynamic model. *Journal of Engineering for Industry*, 279:305–309, 1971.

[14] S. Dubowsky and F. Freudenstein. Dynamic analysis of mechanical system with clearances part 2: Dynamic response. *Journal of Engineering for Industry*, 279:310–316, 1971.

[15] L Gaul and R Nitsche. The role of friction in mechanical joints. *Applied Mechanics Review*, 54(2):93–106, 2001.

[16] Anders Hauglid. Loose Joints Subjected to Mechanical Vibrations. *Norwegian University of Science and Technology*, 2017.

[17] E. Hinton. *NAFEMS Introduction to Nonlinear Finite Element Analysis.* NAFEMS, 1 edition, 1992.

[18] Raouf A. Ibrahim. *Vibro-Impact Dynamics*, volume 43 of *Lecture Notes in Applied and Computational Mechanics.* Springer, Detroit, USA, 1 edition, 2009.

[19] D. W. Jordan and P. Smith. *Nonlinear Ordinary Differential Equations.* Oxford University Press, Oxford, United Kingdom, 4 edition, 2007.

[20] Cornelius Lanczos. *The Variational Principles of Mechanics.* Dover Books on Physics. Dover Publications, 4 edition, 1986.

[21] MSC Nastran. SOL400 Demonstration problems, 2018.

[22] MSC Nastran. SOL400 User's guide, 2018.

[23] Norwegian University of Science and Technology. Lecture Notes in Nonlinear Finite Element Analysis TKT4197, 2017.

[24] Singiresu S. Rao. *Mechanical Vibrations.* Pearson Prentice Hall, New Jersey, 5 edition, 2004.

[25] S. W. Shaw and P. J. Holmes. A periodically forced piecewise linear oscillator. *Journal of Sound and Vibration*, 90(1):129–155, 1983.

[26] Siemens PLM Software. Handbook of Nonlinear Analysis, 2001.

[27] Jyoti Kumar Sinha. *Vibration Analysis, Instruments and Signal Processing.* CRC Presss, 1 edition, 2015.

[28] William D. Thomson and Marie Dillon Dahleh. *Theory of Vibration with Applications.* Prentice Hall, New Jersey, 4 edition, 1998.

# Appendices

# Appendix A

# NASTRAN Code

## Dynamic Analysis II: Spring-Damper Model

```
$ MSC.Nastran input file created on June      16, 2018 at 13:06:22 by
$ Patran 2017.0.2
SOL 400
CEND
$ Direct Text Input for Global Case Control
ECHO = NONE
SUBCASE 1
 STEP 1
$  Direct Text Input for this Step
   ANALYSIS = NLTRAN
   NLSTEP = 1
   SPC = 2
   IC = 1
   DLOAD = 2
   DISPLACEMENT(PRINT,PUNCH,SORT1,REAL)=ALL
   VELOCITY(PRINT,PUNCH,SORT1,REAL)=ALL
   ACCELERATION(PRINT,PUNCH,SORT1,REAL)=ALL
BEGIN BULK
$ Direct Text Input for Bulk Data
PARAM    POST    1
PARAM   PRTMAXIM YES
PARAM    LGDISP  1
NLSTEP   1       30.
         ADAPT                                         15000   29999
NLSTRAT  1       IKUPD   29999
$ Elements and Element Properties for region : M
CONM2    2       2               1.
         633.07          633.07                  1265.02
$ Elements and Element Properties for region : Bush-Spring
PBUSHT   1       KN      1
PBUSH    1       K       .01
$ Pset: "Bush-Spring" will be imported as: "pbush.1"
CBUSH    1       1       1       2
$ Elements and Element Properties for region : Damper_elem
PVISC    2       .06324
$ Pset: "Damper_elem" will be imported as: "pvisc.2"
CVISC    3       2       1       2
$ Nodes of the Entire Model
GRID     1               0.      0.      0.
GRID     2               1.      0.      0.
$ Loads for Load Case : Default
SPCADD   2       1
$ Initial Velocities of Load Set : Init_vel
TIC      1       2       1               4.
TLOAD1   4       3                       2
DLOAD    2       1.      1.      4
$ Displacement Constraints of Load Set : Base_fixed
SPC1     1       123     1
$ Nodal Forces of Load Set : Forcing_term
FORCE    3       2       0       1.      1.      0.      0.
$ Referenced Dynamic Load Tables
$ Dynamic Load Table : Duffing_K
```

```
TABLED1  1
[Table of Duffing_spring input (600 data points)]
$ Dynamic Load Table : Force
TABLED1  2
[Table of Force input (30,000 data points)]
$ Referenced Coordinate Frames
ENDDATA 1a313e46
```

# Post-processing .pch files

```matlab
% This script takes in the results.mat file generated in punch_import.m and
% post-process (PSD, FRF). Averaging techniques is used.

clc
close all
clear variables

iter = '10';
% mat_path = ('E:\Master\Nastran NTNU\Dynamic Analysis\SOL400\Iter_a\a_0_05');
loadpath = sprintf('E:\\Master\\Nastran NTNU\\Dynamic Analysis\\SOL400\\Iter_a\\a_0_%s\\results_a_0_%s.mat', iter, iter);
load(loadpath);

load('E:\\Master\\Nastran NTNU\\Dynamic Analysis\\SOL400\\Iter_a\\sinesweep_input_5A.mat');    %Load input vector for FRF
in = interp1(tspan',y1,time);
%% Global parameters
tend = time(end);                   %
N = length(time);
Fs = N/tend;
fs = Fs;
% freq = 0:Fs/length(time):Fs/2;   % Frequency range based on Nyquist
f0 = 0;                            % Start frequency known from meta-file
fend = 30;                         % End freq known from meta-file
freq = linspace(0,fs/2,N/2+1);     % Frequency range based on meta-file


%% Welch' Method for Averaging
window = 1024*2;           % Window length
noverlap = window/2;       % Number of overlapped samples
nfft = [];                 % Number of DTF points
% see help pwelch for more

pxx = zeros(1,window/2+1);              % Placeholder Welch PSD vector
fi = zeros(1,window/2+1);               % Placeholder Welch frequency vector
[pxx, f] = pwelch(acc, window,noverlap,nfft,Fs);
[pyy, fy] = pwelch(in,window,noverlap,nfft,Fs); % PSD of input
fi = linspace(0,fs/2,length(pxx));

printpath = 'C:\Users\Anders\Dropbox\NTNU\Vaar 18\Master\LaTeX\Chapters\Finite_Element_approach\Finite_Element_Results\vary_a
printpath_png = 'C:\Users\Anders\Dropbox\NTNU\Vaar 18\Master\LaTeX\Chapters\Finite_Element_approach\Finite_Element_Results\va

%% Welch plot
figure; hold on;
    plot(fi,log10(pxx),'LineWidth',1.125,'DisplayName','Acc')
grid on
title(sprintf('PSD  a = 0.%s',iter))
xlabel('Frequency (Hz)')
ylabel('PSD log_1_0(g^2/Hz)')
legend('show')
xlim([f0 fend])
hold off
printname_a_PSD = sprintf('%s\\PSD_a_0_%s',printpath,iter);
print(printname_a_PSD,'-depsc')
printname_a_PSD = sprintf('%s\\PSD_a_0_%s',printpath_png,iter);
print(printname_a_PSD,'-dpng')

figure; hold on;
plot(fy,pxx./pyy,'LineWidth',1.125,'DisplayName','Acc')
grid on
title(sprintf('FRF  a = 0.%s',iter))
xlabel('Frequency (Hz)')
ylabel('In/Out')
legend('show')
xlim([f0 fend])
```

```
hold off

%% Time history and phase plane plots
figure; hold on;
% subplot(1,3,[1,2])
subplot('Position',[0.1, 0.45, 0.6, 0.4])
plot(time,disp)
xlabel('Time (s)')
ylabel('Displacement (m)')
title(sprintf('Time history  a = 0.%s',iter))
ylim([1.1*min(disp) 1.1*max(disp)])
grid on

% subplot(1,3,3)
subplot('Position',[0.8, 0.45, 0.15, 0.4])
plot(disp,vel)
xlabel('Displacement (m)')
ylabel('Velocity (m/s)')
title('Phase plane')
ylim([1.1*min(vel) 1.1*max(vel)])
xlim([1.1*min(disp) 1.1*max(disp)])
grid on
hold off;
printname_a_timehist = sprintf('%s\\timehist_a_0_%s',printpath,iter);
print(printname_a_timehist,'-depsc')
printname_a_timehist = sprintf('%s\\timehist_a_0_%s',printpath_png,iter);
print(printname_a_timehist,'-dpng')
```

# Appendix B

# MATLAB Code for Numerical Method

This includes the Duffing equation solver scripts and post-processing.

### Duffing func

```
function f = duffing_func(t, x)
global m c a krelax kappa n A w

%DUFFING FUNCTION Mass-spring damper free oscillation
% Aproximated by a power-law

f = zeros(2,1);
f(1,1) = x(2);
f(2,1) = (1/m)*(A*sin(w*t) - krelax*x(1) - kappa*(x(1)/a)^(n) - c*x(2));

end
```

### Duffing solver script

```
clear all
close all
clc
%% Author Anders Hauglid
% Duffing oscillator. Excites the mass with a force F(t) = A cos(w*t).
%% Solver conditions and init conditions

global m c crelax a keff krelax tend x0 kappa n A w
tend = 20;                      % [s]
tspan = linspace(0, tend, 1000*tend);
a = 0.001;                      % Gap size [m]
x0 = [a; 0.1];                  % x0(1) = init_disp    x0(2) = init_vel [m m/s]

m = 1;                          % Mass [kg]
krelax = 1E-05;                 % Relaxation spring stiffness [N/m]
n = 15;                         % Nonlinearity factor in Power-law (must be odd)
kappa = 10;                     % Spring stiffness in Power-law
keff = kappa/a;                 % Spring stiffness [N/m]

A = 25;                         % Force amplitude [N]
w = 20;                         % Circular forcing freq [rad/s]
f_forcing = w/(2*pi);           % Forcing freq [Hz]

wn = sqrt(keff/m);              % Assumed natural frequency [rad/s]
fn = wn/(2*pi);                 % [Hz]

c_crit = 2*m*(sqrt(kappa/m)); % Assumed critical damping [Ns/m]
zeta = 0.01;                    % Damping ratio [--]
c = c_crit*zeta;                % Damping value used in funcs [Ns/m]
```

```
crelax = 1E-05;                         % Relaxtion damping coefficient [Ns/m]

t_crit = 2/wn;                          % Critical time step [s]

%% Solving

[t1, x1] = ode15s(@(t,x) duffing_func_free(t, x), tspan, x0);
% Change out tspan with [0:2*pi:tend*fs] to sample for every period

%% Plot
figure; hold on;
plot(t1,x1(:,1),'DisplayName','Response')
ylim([-1.5*a 1.5*a])
grid on
legend('show')
title(sprintf('A = %d \\omega = %d \\kappa = %d \\zeta = %0.3f', A, w, kappa, zeta))
hold off;

%% Plot Duffing Force
xspan = linspace(-1.5*a,1.5*a,500);                     % Span of x-values
Duff_F = xspan.*krelax + (kappa/a^n)*(xspan).^n; % Spring force

figure; hold on;
plot(xspan,Duff_F,'LineWidth',1.5)
plot([-1.5*a, 1.5*a],[A, A],'--r',[-1.5*a, 1.5*a],[-A, -A],'--r','LineWidth',1.5)
grid on
xlabel('Displacement (m)')
ylabel('Spring force (N)')
title(sprintf('Spring force with \\kappa = %d and n = %d', kappa, n))
hold off;

%% Exporting data
disp = x1(:,1);
vel = x1(:,2);
time = t1;
acc = diff(vel)./diff(time);
acc = [acc; 0];            % Append 0 to get size of acc = disp, vel, time;
y1 = A*sin(w.*tspan);

%% True export
savename = sprintf('C:\\Users\\ahh.NTU.000\\Dropbox\\NTNU\\Vaar 18\\Master\\MATLAB\\Duffing\\Results\\vary_n\\n_%d.ma
save(savename,'disp','vel','acc','time','y1','fn','kappa','keff','a','zeta','f_forcing','tend');
```

## Post-processing Duffing

```
clear all
close all
%% POST-PROCESSING
% This script post-process all the data from the ODE-solution and
% MSC/NASTRAN solution.
% 1) Import .mat-files consisting of disp, vel and acc
% 2) Plot time history and phase plane directly from .mat
% 3) Do FFT-analysis producing PSD and FRF plots
% 4)

%% Importing
% MATLAB iteration
% load('C:\Users\Anders\Dropbox\NTNU\Vaar 18\Master\MATLAB\Power-law approximation\Results\results_mass__excit.mat')

% MATLAB sandbox
load('C:\Users\ahh.NTU.000\Dropbox\NTNU\Vaar 18\Master\MATLAB\Duffing\Results\sandbox_results.mat')

%% NASTRAN iteration
% load('E:\Patran\1D-iteration\vary_zeta\results\z_0_01.mat')
% load('E:\Patran\1D-iteration\template\sinesweep_input.mat')
% fn = 1/(2*pi)*sqrt(1000);

%%
int_data = acc;                % What data set interest us? disp, vel, acc?

%% FFT (PSD)
tend = tend;                   % Imported from solver
N = length(time);
```

```
                    Fs = N/tend;
                    xdft1 = fft(int_data);
                    xdft1 = xdft1(1:N/2+1);

                    ydft = fft(y1);
                    ydft = ydft(1:N/2+1);
                    psdy = (1/(Fs*N)) * abs(ydft).^2;
                    psdy(2:end-1) = 2*psdy(2:end-1);

                    psdx1 = (1/(Fs*N)) * abs(xdft1).^2;
                    psdx1(2:end-1) = 2*psdx1(2:end-1);

                    freq = 0:Fs/length(int_data):Fs/2;

                    %% FFT plots (PSD anf FRF)
                    [pks_psd, n_e_psd] = findpeaks(10*log10(psdx1),'MinPeakDistance',0.999*length(psdx1));  % For which value of freq-vector does
                    [pks_frf, n_e_frf] = findpeaks(psdx1./psdy','MinPeakDistance',0.999*length(psdx1));

                    fe_psd = freq(n_e_psd);       % Natural freq from PSD-plot
                    fe_frf = freq(n_e_frf);            % Natural freq from FRF-plot

                    % PSD
                    figure; hold on;
                    subplot(1,2,1)
                    plot(freq,10*log10(psdx1),[fn,fn],[-500,100] ,'DisplayName','Acc')
                    grid on
                    title('Periodogram Using FFT')
                    xlabel('Frequency (Hz)')
                    ylabel('Power/Frequency (m^2/Hz) [/Hz]')
                    % legend('show')
                    xlim([0 10*fe_psd])
                    ylim([min(10*log10(psdx1))+20 max(10*log10(psdx1))+20])

                    % Frequency response function (FRF)
                    subplot(1,2,2)
                    plot(freq,psdx1./psdy',[fn,fn],[0,5000]) % PSD of output/ PSD of input
                    grid on
                    title('Frequency response function (FRF)')
                    xlabel('Frequency [Hz]')
                    ylabel('Output / input')
                    ylim([0 2*psdx1(n_e_psd)/psdy(n_e_psd)]) % Scaling plot
                    xlim([0 10*fe_frf])
                    hold off;

                    % print('C:\Users\Anders\Dropbox\NTNU\Host 17\UNIK4910 Vibrasjonsanalyse\matlab\free gaps\plots\vary_k\k_5000_FRF_PSD','-deps
                    % print('E:\Patran\1D-iteration\plots\vary_zeta\z_0_01_FRF_PSD_patran','-depsc')

                    %% Time history and phase plane plots
                    figure; hold on;
                    % subplot(1,3,[1,2])
                    subplot('Position',[0.1, 0.45, 0.6, 0.4])
                    plot(time,disp)
                    xlabel('Time (s)')
                    ylabel('Displacement (m)')
                    title('Time history')
                    ylim([1.1*min(disp) 1.1*max(disp)])
                    grid on

                    % subplot(1,3,3)
                    subplot('Position',[0.8, 0.45, 0.15, 0.4])
                    plot(disp,vel)
                    xlabel('Displacement (m)')
                    ylabel('Velocity (m/s)')
                    title('Phase plane')
                    ylim([1.1*min(vel) 1.1*max(vel)])
                    xlim([1.1*min(disp) 1.1*max(disp)])
                    grid on
                    hold off;

                    % print('C:\Users\Anders\Dropbox\NTNU\Host 17\UNIK4910 Vibrasjonsanalyse\matlab\free gaps\plots\vary_k\k_5000_time_hist_pp',
                    % print('E:\Patran\1D-iteration\plots\vary_zeta\z_0_01_time_hist_pp_patran','-depsc')

                    % save('C:\Users\Anders\Dropbox\NTNU\Host 17\UNIK4910 Vibrasjonsanalyse\matlab\free gaps\results\post_processed\vary_k\k_5000
```

```
% save('E:\Patran\1D-iteration\results\post_processed\vary_zeta\z_0_01.mat','fn','fe_psd','fe_frf','freq','psdx1','ps
```

## Sine sweep generator

```
clear all
close all

tend = 100;                          % End time [s]
fs = 1000;                           % Sampling frequency [Hz]
fn = fs/2;                           % Nyquist frequency [Hz]
tspan = linspace(0, tend, tend*fs);
f0 = 5;                              % Start frequency [Hz]
t1 = tend/2;                         % Time at which f1 occurs [s]
f1 = 100;                            % End frequency [Hz]


y = chirp(tspan, f0, t1, f1, 'linear');

figure; hold on;
plot(tspan, y)
grid on
xlabel('Time (s)')
ylabel('Input amplitude')
hold off;

no_DFT = 256;                % Number of DFT points
no_samp = 250;               % Number of samples of overlap
l_hamm = 256;                % Hamming windows length

figure; hold on;
spectrogram(y,no_DFT, no_samp, l_hamm, fs, 'yaxis')
hold off
% print('C:\Users\Anders\Dropbox\NTNU\Host 17\UNIK4910 Vibrasjonsanalyse\matlab\free gaps\plots\force_input\sinesweep

y1 = y;                      % Displacement vector
y2 = diff(y1)./diff(tspan);  % Velocity vector
y2 = [y2 0];                 % Append 0 to get size of y2 = y1;

tspan = tspan';
y1 = y1';
y2 = y2';
yexport = [tspan y1 y2];
export_data_disp = [tspan y1];
export_data_vel = [tspan y2];

%% Saving input
save('sinesweep_input.mat', 'yexport')
% save('E:\Patran\1D-iteration\template\sinesweep_input.mat', 'tspan','y1','y2')
%
%
% csvwrite('E:\Patran\1D\01 Common files\sinesweep_dispinput.csv', export_data_disp);
% csvwrite('E:\Patran\1D\01 Common files\sinesweep_velinput.csv', export_data_vel);
% csvwrite('E:\Patran\1D-iteration\template\sinesweep_force.csv', export_data_disp);
```

# Appendix C

# MATLAB Code for Post-Processing Experiments

### Tensile test script

```
clear all
close all
clc

%% TENSILE TEST SCRIPT
% This script imports .mat-files, process them and export plots for the
% tensile tests done
coup = 'Slot';
mat = 'S355';
dir = '1st';
filename = sprintf('C:\\Users\\ahh.NTU.000\\Dropbox\\NTNU\\Vaar 18\\Master\\Experiments\\Lab\\Tensile_lab\\Mat_files\\%s_%s_c
load(filename);

figure; hold on;
for i = 1:length(spec)
    plot(spec{i}(:,1),spec{i}(:,2),'LineWidth',1.5,'DisplayName',sprintf('Run %d',i))
    legend('-DynamicLegend')
end
xlabel('Displacement (mm)')
ylabel('Force (N)')
ylim([0 1.2*spec{end}(end,2)])
grid on
legend('Location','southeast')
legend('show')
title(sprintf('%s A020 %s %s dir.',coup,mat,dir))
hold off;
printname1 = sprintf('C:\\Users\\ahh.NTU.000\\Dropbox\\NTNU\\Vaar 18\\Master\\LaTeX\\Chapters\\Experimental_results\\plots\\t
print(printname1,'-depsc')

%% Estimating k based on the 2 last runs
disp_sample = zeros();
f_sample = zeros();
for i = length(spec)-2:length(spec)
    disp_sample(i) = spec{i}(200,1);
    f_sample(i) = spec{i}(200,2);
end

disp_mean = mean(disp_sample);
f_sample_mean = mean(f_sample);
k_est = f_sample_mean/disp_mean;
wn_est = sqrt((k_est*10^3)/(0.307));

sprintf('%s %s dir %s. The estimated k is %0.1f N/mm',coup, dir, mat, k_est)
sprintf('The estimated k is %0.2d N/m',k_est*10^(3))


figure; hold on;
for i = length(spec)-2:length(spec)
    plot(spec{i}(:,1),spec{i}(:,2),'LineWidth',1.5,'DisplayName',sprintf('Run %d',i))
```

```matlab
    legend('-DynamicLegend')
end
xlabel('Displacement (mm)')
ylabel('Force (N)')
ylim([0 1.2*spec{end}(end,2)])
grid on
legend('Location','southeast')
legend('show')
title(sprintf('%s A020 %s %s dir. k = %0.0f (N/mm)',coup,mat,dir,k_est))
hold off;
printname2 = sprintf('C:\\Users\\ahh.NTU.000\\Dropbox\\NTNU\\Vaar 18\\Master\\LaTeX\\Chapters\\Experimental_results\\
print(printname2,'-depsc')
```

# Importing .tdms acceleration data

```matlab
clear all
close all
clc

%% MASTER FILE FOR IMPORT OF .TDMS%%

% Created by Anders for own use.
% Objective: chose file, import, plot time series, PSD.
% Sampling freq set to 5.6 kHz. Calculated to be 5688.89 Hz. We use this.
fs = 5688.89;                                    % [Hz]

% testnumber =[54 61 68 75 82 89];
testnumber = [89];

%% Choose file to be imported
for count = 1:length(testnumber)
    t = testnumber(count);
    path = '\Users\ahh.NTU.000\Desktop\Master\Lab\Raw data\Thin POM C';
    filename = sprintf('%s\\Test_%d\\Acceleration.tdms',path,t);

%% Import
my_struct = TDMS_readTDMSFile(filename);% Import the whole struct

tot_acc = [];                                    % Empty 10x10 placeholder
for i = 3:7
    tot_acc(i,:) = my_struct.data{1,i};          % Channel 3-7
end

l_tot = length(tot_acc(1,:));                    % Total length of the acc data series
tend = l_tot/fs;                                 % End time [s]
tspan = linspace(0, tend, tend*fs);              % Time vector from t = 0 [s] to t = end [s]
fspan = logspace(log10(30),log10(3000),l_tot);

% Ch 3 = Control accelerometer 1
% Ch 4 = Control accelerometer 2
% Ch 5 = Input 1
% Ch 6 = Input 2
% Ch 7 = Input 3

%% Manually clip data (in case of spike / noise in beginning)
% If data has spikes, use this. May need some greasing to work.

c_a = 4.186*1e05; % After noise, before start
c_b = l_tot;                    % After test end, before definite end
c_length = c_b - c_a;        % Cut-out length
tot_acc_c = zeros(7,c_b-c_a);
tot_acc_c(3:7,:) = tot_acc(3:7,c_a:c_b-1);
tot_acc = tot_acc_c;
l_tot = length(tot_acc(3,:));
tend = c_length/fs;

%% Locate where test started and stopped
threshold = 0.45; % Threshold value for acceleration [m/s2]
ch = 4;                          % Use this channel for check
j = 1;
while tot_acc(ch,j) < threshold
    j = j + 1;
end
```

```
start_val = j;

k = l_tot;
while tot_acc(ch,k) < threshold
    k = k - 1;
end
stop_val = k;


tend = (stop_val+1)/fs;
tstart = start_val/fs;
l = stop_val-start_val-1;
time = linspace(0,(tend-tstart),(tend-tstart)*fs);  % (tend-tstart) is correct length of run


a = start_val;
b = stop_val;                       % Typically also -1

%% Making vectors even
vector_l = b-a+1;                   % b-a+1 is length of a:b
if vector_l > length(time)          % vector_l > length of time
    time = [time, time(end)];       % Add 1 to time
elseif vector_l < length(time)
    b = b + 1;                      % Add 1 to b (vector_l 1 larger)
end

figure; hold on;
for i = 3:4
    plot(tot_acc(i,:),'DisplayName',sprintf('Ch(not acc) = %d',i))
    legend('-DynamicLegend');
    legend('show')
end
% plot(tot_acc(ch,:),'DisplayName',sprintf('Check ch = %d',ch))
plot([start_val,start_val],[-1,1],'LineWidth',2.0)
plot([stop_val,stop_val],[-1,1],'LineWidth',2.0)
grid on
ylabel('Acceleration g (m/s^2)')
xlabel('Elapsed timestamp')
title(sprintf('Location of stop and start time Test = %d used Ch = %d',t,ch))
hold off

%% Plot data

figure; hold on;
for i = 5:7
    plot(time,tot_acc(i,a:b),'DisplayName',sprintf('Accelerometer %d',i-2));
    ylabel('Acceleration g (m/s^2)')
    xlabel('Elapsed time (s)')
    legend('-DynamicLegend');
    legend('show')
    title(sprintf('Time series of saved data Test = %d',t))
end
hold off

%% Exporting true measured data.
% Ch 1-5, from time of approx run start to run end
data_accel = [];
for j = 1:5
    data_accel(j,:) = tot_acc(j+2,start_val:stop_val);
end

%% Converting to post_processing.m
acc = data_accel(3,:);              % Output accel
y1 = data_accel(1,:);               % Input accel

savepath = 'C:\Users\ahh.NTU.000\Desktop\Master\Lab\Mat files\Thin POM C';
savename = sprintf('%s\\Test_%d.mat',savepath,t);

save(savename,'data_accel','time','fs')


end
```

# Post-processing .tdms

```
clc
close all
clear variables
%% POST-PROCESSING TDMS
% This script post-process data from TDMS files processed in master_tdms.m
% 1) Import .mat-files consisting of acc
% 2) Plot time history and phase plane directly from .mat
% 3) Do FFT producing PSD (and FRF plots)

set(0,'defaulttextinterpreter','tex')                    % Standard font in figures


%% Importing
% number = [1 23 30 46 55 62];     % 0.51g out of plane
% number = [2 24 31 47 56 63];     % 1g out of plane
% number = [3 25 32 48 57 64];     % 2g out of plane
% number = [4 26 33 49 58 65];     % 5g out of plane
% number = [5 27 34 50 59 66];     % 10g out of plane
% number = [7 28 35 51 60 67];     % 15g out of plane
number = [54 61 68];        % Random




for count = 1:length(number)
    mat_path = ('E:\Master\Experiments FFI\Mat files shaker\Thin POM C');
%   mat_path = ('C:\Users\ahh.NTU.000\Desktop\Master\Lab\Mat files\Thin POM C');
    loadpath = sprintf('%s\\Test_%d.mat',mat_path,number(count));
    load(loadpath);

%% Making vectors even numbered
% This makes N/2 = an integer
even = mod(length(time),2); % = 0 if even, = 1 if odd
if even ~= 0                                             % If not even
    time = [time, time(end)];                            % Append the last value of time to itslef (duplicate)
    data_accel = [data_accel, data_accel(:,end)];% Append the last value of data_accel to itself (duplicate)
end

%% Global parameters
tend = time(end);                   %
N = length(time);
Fs = N/tend;
% freq = 0:Fs/length(time):Fs/2;    % Frequency range based on Nyquist
f0 = 5;                             % Start frequency known from meta-file
fend = 1000;                        % End freq known from meta-file
freq = linspace(0,fs/2,N/2+1);      % Frequency range based on meta-file
%% Looping through data set "data_accel" for  accelerometers
% xdfti = zeros(5,round(N/2)+1);    % Empty placeholder. Possible +1
% psdxi = zeros(5,round(N/2)+1);  % Possible +1
%
% for i = 1:5                                   % i = 1 and 2 are control accelerometers
%     int_data = data_accel(i,:);       % What data set interest us?
%     % FFT (PSD)
%     xdft = fft(int_data);
%     xdft = xdft(1:N/2+1);
%     psdx = (1/(Fs*N)) * abs(xdft).^2;
%     psdx(2:end-1) = 2*psdx(2:end-1);
%
%     xdfti(i,:) = xdft;
%     psdxi(i,:) = psdx;
% end

%% Welch' Method for Averaging
window = 512*2;                 % Window length
noverlap = window/2;        % Number of overlapped samples
nfft = [];                      % Number of DTF points
% see help pwelch for more

pxxi = zeros(5,window/2+1);             % Placeholder Welch PSD vector
fi = zeros(5,window/2+1);               % Placeholder Welch frequency vector
for i = 1:5
    [pxx, f] = pwelch(data_accel(i,:),window,noverlap,nfft,Fs);
    pxxi(i,:) = pxx;
```

```
    fi(i,:) = linspace(0,fs/2,length(pxx));
end


% Coherence Spectrum
Cxyi = zeros(5,window/2+1);                          % Placeholder for Welch'd Coherence vector
fxyi = zeros(5,window/2+1);                          % Placeholder for Welch'd Coherence frequency vector
input = (data_accel(1,:)+data_accel(2,:))/2;  % Input is average of control acc 1 and 2.
for i = 3:5
    [Cxy, fxy] = mscohere(data_accel(i,:),input,hamming(window),noverlap,window,Fs);
    Cxyi(i,:) = Cxy;
    fxyi(i,:) = fxy;
end


% print_path = 'C:\Users\ahh.NTU.000\Desktop\Master\Lab\PNG';
print_path = 'C:\Users\Anders\Dropbox\NTNU\Vaar 18\Master\LaTeX\Chapters\Experimental_approach\Experimental_results\plots\sha
filename = sprintf('%s\\Test_%d',print_path, number(count));

%% FFT plots (PSD anf FRF)

% % PSD
% figure; hold on;
% for i = 3:5
%     plot(freq,log10(psdxi(i,:)),'LineWidth',1.125,'DisplayName',sprintf('Ch %d',i))
%     legend('-DynamicLegend')
% end
% grid on
% title('Periodogram')
% xlabel('Frequency (Hz)')
% ylabel('PSD log_1_0(g^2/Hz)')
% legend('show')
% xlim([f0 fend])
% hold off
% printname_PSD = sprintf('%s_PSD_nowelch',filename);
% % print(printname_PSD,'-depsc')
%
%
% % Frequency response function (FRF)
% psdy = (psdxi(4,:) + psdxi(5,:))./2;            % Average PSD of input signal
% figure; hold on;
% for i = 3:5
%     plot(freq,psdxi(i,:)./psdy,'LineWidth',1.125,'DisplayName',sprintf('Ch %d',i))  % PSD of output/ PSD of input
%     legend('-DynamicLegend')
% end
% grid on
% title('Frequency response function (FRF)')
% xlabel('Frequency (Hz)')
% ylabel('S_x_x  / S_y_y')
% xlim([f0 fend])
% hold off;
% printname_FRF = sprintf('%s_FRF_nowelch',filename);
% % print(printname_FRF,'-depsc')

%% Welch plot
figure; hold on;
for i = 3:5
    plot(fi(i,:),log10(pxxi(i,:)),'LineWidth',1.125,'DisplayName',sprintf('Ch %d',i))
    legend('-DynamicLegend')
end
grid on
title(sprintf('PSD Test #%d',number(count)))
xlabel('Frequency (Hz)')
ylabel('PSD log_1_0(g^2/Hz)')
legend('show')
xlim([f0 fend])
hold off
printname_PSD = sprintf('%s_PSD',filename);
print(printname_PSD,'-depsc')

pxxy = (pxxi(1,:) + pxxi(2,:))./2;                  % Average PSD of input signal
figure; hold on;
for i = 3:5
    plot(fi(i,:),pxxi(i,:)./pxxy,'LineWidth',1.125,'DisplayName',sprintf('Ch %d',i))  % PSD of output/ PSD of input
    legend('-DynamicLegend')
```

```
end
grid on
title(sprintf('FRF Test #%d',number(count)))
xlabel('Frequency (Hz)')
ylabel('S_x_x  /  S_y_y')
xlim([f0 fend])
hold off;
printname_FRF = sprintf('%s_FRF',filename);
print(printname_FRF,'-depsc')


figure; hold on;
for i = 3:5
    plot(fxyi(i,:),Cxyi(i,:),'LineWidth',1.125,'DisplayName',sprintf('Ch %d',i))
    legend('-DynamicLegend')
end
grid on
title(sprintf('Coherence Spectrum Test #%d',number(count)))
xlabel('Frequency (Hz)')
ylabel('')
xlim([f0 fend])
hold off;
printname_coher = sprintf('%s_coher',filename);
print(printname_coher,'-depsc')


% Subplot (FRF, PSD and choherence in one)
figure; hold on;
subplot(1,2,1)
for i = 3:5
    plot(fi(i,:),log10(pxxi(i,:)),'LineWidth',1.125,'DisplayName',sprintf('Ch %d',i))
    hold on;
%     legend('-DynamicLegend')
end
grid on
title(sprintf('PSD Test #%d',number(count)))
ylabel('PSD log_1_0(g^2/Hz)')
% legend('show')
xlim([f0 fend])

subplot(1,2,2)
for i = 3:5
    plot(fi(i,:),pxxi(i,:)./pxxy,'LineWidth',1.125,'DisplayName',sprintf('Ch %d',i))  % PSD of output/ PSD of input
    hold on;
    legend('-DynamicLegend')
end
grid on
title(sprintf('FRF Test #%d',number(count)))
ylabel('S_x_x  /  S_y_y')
xlim([f0 fend])

% subplot(1,3,3)
% for i = 3:5
%     plot(fxyi(i,:),Cxyi(i,:),'LineWidth',1.125,'DisplayName',sprintf('Ch %d',i))
%     hold on;
%     legend('-DynamicLegend')
% end
% grid on
% title(sprintf('Coherence Spectrum Test #%d',number(count)))
% ylabel('')
% xlim([f0 fend])
hold off
printname_2in1 = sprintf('%s_2in1',filename);
print(printname_2in1,'-depsc')

%% Exporting data to matfile

% freq = fi(1,:);                % Welch frequency vector, there is enough with one column
% PSD = pxxi(3:5,:);            % Welch PSD vector for ch 1-5
% FRF = pxxi(3:5,:)./pxxy;      % Average of PSD input signal

% Storing the data in a processed_struct
proc_struct(number(count)).freq = fi(1,:);
proc_struct(number(count)).PSD = pxxi(3:5,:);
proc_struct(number(count)).FRF = pxxi(3:5,:)./pxxy;
```

```
proc_struct(number(count)).f0 = f0;
proc_struct(number(count)).fend = fend;

savepath = 'E:\Master\Experiments FFI\Mat files shaker\Thin POM C Processed';
savename = sprintf('%s\\Test_%d_processed.mat',savepath,number(count));

save(savename,'proc_struct')


end
```

## Finding peaks

```
clc
close all
clear variables

%% PEAK PSD
% This script finds the peak in several PSD-plots and plot the values
% againts each other

%% Importing pre-processed .mat files froom post_processing_tdms
% number = [1 23 30 46 55 62 ...
%              2 24 31 47 56 63 ...     % 1g out of plane
%              3 25 32 48 57 64 ...     % 2g out of plane
%              4 26 33 49 58 65 ...     % 5g out of plane
%              5 27 34 50 59 66 ...     % 10g out of plane
%              7 28 35 51 60 67];     % 15g out of plane
number = [8 29 36 54 61 68];         % Random


for count = 1:length(number)
    mat_path = ('E:\Master\Experiments FFI\Mat files shaker\Thin POM C Processed');
    loadpath = sprintf('%s\\Test_%d_processed.mat',mat_path,number(count));
    load(loadpath);

    freq = proc_struct(number(count)).freq;
    PSD = proc_struct(number(count)).PSD;
    FRF = proc_struct(number(count)).FRF;
    f0 = proc_struct(number(count)).f0;
    fend = proc_struct(number(count)).fend;

    % Shortening the data
    % We wish to look at data below 1000 or 500 Hz. freq(end) = 5689/ = 2844 Hz and
    % so freq
    freql = round(length(freq)/2);        % Should limit to  569 Hz
    % Finding the peak
    psd_data = log10(PSD(2,1:freql));
    frf_data = FRF(1,1:freql);
    [pks_psd, n_e_psd] = findpeaks(psd_data,'MinPeakDistance',0.49*length(psd_data));  % For which value of freq-vector does
    [pks_frf, n_e_frf] = findpeaks(frf_data,'MinPeakDistance',0.4*length(frf_data),'MinPeakHeight',5);

    fe_psd = freq(n_e_psd);        % Natural freq from PSD-plot
    fe_frf = freq(n_e_frf) ;       % Natural freq from FRF-plot

    toDelete = fe_psd < 25;        % Only pass freqs over 20 Hz
    fe_psd(toDelete) = [];

figure; hold on;
plot(freq,log10(PSD(:,:)))
plot(freq(n_e_psd(1)),pks_psd(1),'o') % We're only interested in the first mode
xlim([f0 fend])
title(sprintf('PSD Test #%d, peak = %0.1f',number(count),freq(n_e_psd(1))))
grid on
hold off

figure; hold on;
plot(freq,FRF(:,:))
plot(freq(n_e_frf(1)),pks_frf(1),'o') % We're only interested in the first mode
xlim([f0 fend])
title(sprintf('FRF Test #%d, peak = %0.1f',number(count),freq(n_e_frf(1))))
grid on
hold off
```

_____

```
peak_struct(number(count)).fe_PSD = fe_psd;
peak_struct(number(count)).fe_FRF = fe_frf;
peak_struct(number(count)).test_no = number(count);

end
peak_struct_random = peak_struct;
save('peak_struct_random.mat','peak_struct_random')
% save('peak_struct.mat','peak_struct');
```

## Notch filter

```
%% Post processing with Notch filtering
% This script samples out a portion of the time series data of the harmonic
% input files (#90-98) and use a Notch filter to filter out the driving
% frequency

clc
close all
clear variables

%% Importing
number = [93 95];
for count = 1:length(number)
    mat_path = ('E:\Master\Experiments FFI\Mat files shaker\Thin POM C');
    loadpath = sprintf('%s\\Test_%d.mat',mat_path,number(count));
    load(loadpath);

%% Making vectors even numbered
% This makes N/2 = an integer
even = mod(length(time),2);                        % = 0 if even, = 1 if odd
if even ~= 0                                       % If not even
    time = [time, time(end)];                      % Append the last value of time to itslef (duplicate)
    data_accel = [data_accel, data_accel(:,end)];  % Append the last value of data_accel to itself (duplicate)
end

%% Global parameters
tend = time(end);                %
N = length(time);
Fs = N/tend;
% freq = 0:Fs/length(time):Fs/2;     % Frequency range based on Nyquist
f0 = 5;                            % Start frequency known from meta-file
fend = 500;                       % End freq known from meta-file
freq = linspace(0,fs/2,N/2+1);    % Frequency range based on meta-file


%% Welch' Method for Averaging
window = 512*4;         % Window length
noverlap = window/2;    % Number of overlapped samples
nfft = [];              % Number of DTF points
% see help pwelch for more

%% FILTER DESIGN
filter_freq = 50;

filter_freqlow = filter_freq-1;
filter_freqhigh = filter_freq+1;

d = designfilt('bandstopiir','FilterOrder',2, ...
               'HalfPowerFrequency1',filter_freqlow,'HalfPowerFrequency2',filter_freqhigh, ...
               'DesignMethod','butter','SampleRate',Fs);

% Filtering
data_accel_filt = [];
for i = 3:5
    data_accel_filt(i,:)= filtfilt(d,data_accel(i,:));
end


% print_path = 'C:\Users\Anders\Dropbox\NTNU\Vaar 18\Master\LaTeX\Chapters\Experimental_approach\Experimental_results
print_path = 'C:\Users\Anders\Dropbox\NTNU\Vaar 18\Master\Experiments\Lab\PNG';
filename = sprintf('%s\\Test_%d_Notch',print_path, number(count));
```

```
%% Compare Unfiltered / filtered
figure; hold on;
plot(time,data_accel(3,:),'DisplayName','Unfiltered')
plot(time,data_accel_filt(3,:),'DisplayName','Filtered')
grid on
legend('show')
title(sprintf('Time series segment Test #%d @ %d Hz', number(count), filter_freq))
xlabel('Time (s)')
ylabel('Acceleration (m/s^2)')
xlim([round(tend/2) round(tend/2) + 2*(1/filter_freq)])
hold off
printname_timeser = sprintf('%s_timeser',filename);
print(printname_timeser,'-dpng')


%% Welch Averaging

pxxi = zeros(5,window/2+1);              % Placeholder Welch PSD vector
fi = zeros(5,window/2+1);                % Placeholder Welch frequency vector
for i = 1:2
    [pxx, f] = pwelch(data_accel(i,:),window,noverlap,nfft,Fs);
    pxxi(i,:) = pxx;
    fi(i,:) = linspace(0,fs/2,length(pxx));
end


for i = 3:5
    [pxx, f] = pwelch(data_accel_filt(i,:),window,noverlap,nfft,Fs);
    pxxi(i,:) = pxx;
    fi(i,:) = linspace(0,fs/2,length(pxx));
end

% Coherence Spectrum
Cxyi = zeros(5,window/2+1);                  % Placeholder for Welch'd Coherence vector
fxyi = zeros(5,window/2+1);                  % Placeholder for Welch'd Coherence frequency vector
input = (data_accel(1,:)+data_accel(2,:))/2;   % Input is average of control acc 1 and 2.
for i = 3:5
    [Cxy, fxy] = mscohere(data_accel_filt(i,:),input,hamming(window),noverlap,window,Fs);
    Cxyi(i,:) = Cxy;
    fxyi(i,:) = fxy;
end


%% Plot Welch
figure; hold on;
for i = 3:5
    plot(fi(i,:),log10(pxxi(i,:)),'LineWidth',1.125,'DisplayName',sprintf('Ch %d',i))
    legend('-DynamicLegend')
end
grid on
title(sprintf('PSD Test #%d, Notch filter @ %d Hz',number(count), filter_freq))
xlabel('Frequency (Hz)')
ylabel('PSD log_1_0(g^2/Hz)')
legend('show')
xlim([f0 fend])
hold off
printname_PSD = sprintf('%s_PSD',filename);
print(printname_PSD,'-dpng')

pxxy = (pxxi(1,:) + pxxi(2,:))./2;            % Average PSD of input signal
figure; hold on;
for i = 3:5
    plot(fi(i,:),pxxi(i,:)./pxxy,'LineWidth',1.125,'DisplayName',sprintf('Ch %d',i))  % PSD of output/ PSD of input
    legend('-DynamicLegend')
end
grid on
title(sprintf('FRF Test #%d, Notch filter @ %d Hz',number(count), filter_freq))
xlabel('Frequency (Hz)')
ylabel('S_x_x  /  S_y_y')
xlim([f0 fend])
hold off;
printname_FRF = sprintf('%s_FRF',filename);
print(printname_FRF,'-dpng')
```

119

```
end
```

# Appendix D

# Measured Dimensions of Manufactured Parts

## POM C

| Name | Base $d$ (mm) | Meas. $d$ | Diff. | $t$ (mm) |
|---|---|---|---|---|
| a_0_00 | 9.80 | 9.85 | 0.05 | 2.54 |
| a_0_05 | 9.85 | 9.85 | 0.00 | 2.49 |
| a_0_10 | 9.90 | 9.90 | 0.00 | 2.50 |
| Bushing | 9.80 | 9.80 | 0.00 | 2.69 |

Table D.1: POM C: Measurements for the manufactured radial coupons.

| Name | Base $l$ (mm) | Meas. $l$ | Diff. | $b$ | $t$ (mm) |
|---|---|---|---|---|---|
| a_0_00 | 13.820 | 13.82 | 0.00 | 8.830 | 2.50 |
| a_0_05 | 13.870 | 13.87 | 0.00 | 8.840 | 2.51 |
| a_0_10 | 13.920 | 13.90 | -0.02 | 8.820 | 2.50 |
| Bushing | 13.820 | 13.82 | 0.00 | 8.820 | 2.69 |

Table D.2: POM C Measurements for the manufactured slot coupons.

# S355

| Name | Base $d$ (mm) | Meas. $d$ (mm) | Diff. | $t$ (mm) |
|------|---------------|----------------|-------|----------|
| a_0_00 | 9.800 | 9.830 | -0.03 | 4.700 |
| a_0_05 | 9.850 | 9.840 | 0.01 | 4.700 |
| a_0_10 | 9.900 | 9.880 | 0.02 | 4.695 |
| a_0_15 | 9.950 | 9.940 | 0.01 | 4.700 |
| a_0_20 | 10.000 | 9.980 | 0.02 | 4.700 |
| a_0_40 | 10.200 | 10.180 | 0.02 | 4.710 |

Table D.3: S355: Measurements for the manufactured radial coupons.

| Name | Base $d$ (mm) | Meas. $d$ (mm) | Diff. | $t$ (mm) |
|------|---------------|----------------|-------|----------|
| 1 | 9.800 | 9.790 | 0.01 | 4.980 |
| 2 | 9.800 | 9.780 | 0.02 | 4.990 |
| 3 | 9.800 | 9.780 | 0.02 | 4.980 |
| 4 | 9.800 | 9.790 | 0.01 | 4.990 |
| 5 | 9.800 | 9.790 | 0.01 | 4.990 |

Table D.4: S355 Measurements for the manufactured cylindrical bushing.

| Name | Base $l$ (mm) | Meas. $l$ | Diff. | $b$ | $t$ (mm) |
|------|---------------|-----------|-------|-----|----------|
| a_0_00 | 13.820 | 13.840 | -0.02 | 8.830 | 4.690 |
| a_0_05 | 13.870 | 13.880 | -0.01 | 8.830 | 4.690 |
| a_0_10 | 13.920 | 13.940 | -0.02 | 8.830 | 4.690 |
| a_0_15 | 13.970 | 13.990 | -0.02 | 8.830 | 4.680 |
| a_0_20 | 14.020 | 14.040 | -0.02 | 8.830 | 4.700 |
| a_0_40 | 14.220 | 14.230 | -0.01 | 8.830 | 4.670 |

Table D.5: S355 Measurements for the manufactured slot coupons.

| Name | Base $l$ (mm) | Meas. $l$ | Diff. | $b$ | $t$ (mm) |
|------|---------------|-----------|-------|-----|----------|
| 1 | 13.820 | 13.810 | 0.010 | 8.830 | 5.000 |
| 2 | 13.820 | 13.840 | -0.020 | 8.830 | 5.000 |
| 3 | 13.820 | 13.830 | -0.010 | 8.830 | 5.000 |
| 4 | 13.820 | 13.825 | -0.005 | 8.830 | 5.000 |
| 5 | 13.820 | 13.830 | -0.010 | 8.830 | 5.000 |

Table D.6: S355 Measurements for the manufactured slot bushings.

# Appendix E

# Production Drawings

CAD-fil finnes på:
\Ansatte-S-Ptv\Prosjekter\Klaringstest vibrasjon RIMFAX Masteroppgave\Parts

$\sqrt{3.2}$

200

200

55

200

70

200

4 x ⌀ 5 ▽ 15
M6 - 6H ▽ 12

⌀176

22,50°

8 x ⌀ 9 THRU ALL
⌀ 18,01 ▽ 50,30

1. For part measure write down dimension on part drawing.

F=G. Freses ned like mye på begge sider.

G
F

0,45 X 45°

2,50 ±0,05

B

Tillates grov pga
svelling /
deformasjon
i materiale etter
bearbeiding

2,60

SECTION A-A

DETAIL B
SCALE 4 : 1

A

ø30

C

3 x 120°

3 x 49,75

R50

A

13,92 +0,05 / 0

8,82 +0,02 / 0

DETAIL C
SCALE 2 : 1

| NS-ISO 2768-1 | | | | | | | | | | | Tillatte vinkelavvik for lengdeområder i mm av det korteste vinkelben | | | | | |
|---|---|---|---|---|---|---|---|---|---|---|---|---|---|---|---|---|
| | Tillatte avvik for basisområde | | | | | | | | | | 0-10 | 10-50 | 50-120 | 120-400 | 400 | over 400 |
| Nøyaktighetsgrad | 0,5-3 | 3-6 | 6-30 | 30-120 | 120-400 | 400-1000 | 1000-2000 | 2000-4000 | | | ±1° | ±0°30' | ±0°20' | ±0°10' | | ±0°5' |
| m middels | ±0,1 | ±0,1 | ±0,2 | ±0,3 | ±0,5 | ±0,8 | ±1,2 | ±2 | | | | | | | | |

CAD-fil finnes på Ansatte-S-Ptv\Prosjekter\Klaringstest vibrasjon RIMFAX Masteroppgave\Parts\POM C\Slot

1. For part measure write down dimension on part drawing.

F=G. Freses ned like mye på begge sider.

G

F

0,45 X 45°

2,50 ±0,05

B

SECTION A-A

DETAIL B
SCALE 4 : 1

Tillates grov pga
svelling /
deformasjon
i materiale etter
bearbeiding

2,60

A

A

⌀ 10 −0,05 −0,15 � 2,05

⌀ 30

3 x 120°

3 x ⌀ 4,75

R50

CAD-fil finnes på Ansatte-S-Ptv\Prosjekter\Klaringstest vibrasjon RIMFAX Masteroppgave\Parts\POM C\Radial

| Rev. | Revisjonsbeskrivelse |
|---|---|

| Dato | Materiale |
|---|---|
| 05.02.2018 | POM C |
| Konstruert av | Ant. |
| AHH | 1 |

FFI
PROTOTYPVERKSTEDET

Målestokk 1:1

Projeksjon

Coupon radial a_0_10 POM C

Henvisning
SolidWorks

Prosjektnr 143702

Navn Sheet1

Ark nr. 1

Tot. ant. ark 1

Format A3

# Appendix F

# Shaker Test Log

This appendix show what parameters each test was exposed to. Notice that some tests were discarded due to operation error and thus the total number of tests (92) does not match the numerical value of the last test in this table (98).

| ID | Coupon and clearance | Orientation | g | Freq | Comment |
|---|---|---|---|---|---|
| Test1 | Radial a_0_00 | Out of plane | 0.5 | 5-500 | |
| Test2 | Radial a_0_00 | Out of plane | 1.0 | 15-500 | |
| Test3 | Radial a_0_00 | Out of plane | 2.0 | 15-500 | |
| Test4 | Radial a_0_00 | Out of plane | 5.0 | 25-500 | |
| Test5 | Radial a_0_00 | Out of plane | 10.0 | 50-500 | |
| ~~Test6~~ | ~~Radial a_0_00~~ | ~~Out of plane~~ | ~~15.0~~ | ~~50-500~~ | Test discarded |
| Test7 | Radial a_0_00 | Out of plane | 15.0 | 50-500 | |
| Test8 | Radial a_0_00 | Out of plane | 0.0002 | 5-1000 | Random vib |
| Test9 | Radial a_0_00 | In plane | 0.5 | 5-500 | |
| Test10 | Radial a_0_00 | In plane | 1.0 | 15-500 | |
| Test11 | Radial a_0_00 | In plane | 2.0 | 15-500 | |
| Test12 | Radial a_0_00 | In plane | 5.0 | 25-500 | |
| Test13 | Radial a_0_00 | In plane | 10.0 | 50-500 | |
| Test14 | Radial a_0_00 | In plane | 15.0 | 50-500 | |
| Test15 | Radial a_0_00 | In plane | 0.0002 | 5-1000 | Random vib |
| Test16 | Radial a_0_05 | In plane | 0.5 | 5-500 | |
| Test17 | Radial a_0_05 | In plane | 1.0 | 15-500 | |
| Test18 | Radial a_0_05 | In plane | 2.0 | 15-500 | |
| Test19 | Radial a_0_05 | In plane | 5.0 | 25-500 | |
| Test20 | Radial a_0_05 | In plane | 10.0 | 50-500 | |
| Test21 | Radial a_0_05 | In plane | 15.0 | 50-500 | |
| Test22 | Radial a_0_05 | In plane | 0.0002 | 5-1000 | Random vib |
| Test23 | Radial a_0_05 | Out of plane | 0.5 | 5-500 | |
| Test24 | Radial a_0_05 | Out of plane | 1.0 | 15-500 | |
| Test25 | Radial a_0_05 | Out of plane | 2.0 | 15-500 | |
| Test26 | Radial a_0_05 | Out of plane | 5.0 | 25-500 | |
| Test27 | Radial a_0_05 | Out of plane | 10.0 | 50-500 | |
| Test28 | Radial a_0_05 | Out of plane | 15.0 | 50-500 | |

| Test29 | Radial a_0_05 | Out of plane | 0.0002 | 5-1000 | Random vib |
|---|---|---|---|---|---|
| Test30 | Radial a_0_10 | Out of plane | 0.5 | 5-500 | |
| Test31 | Radial a_0_10 | Out of plane | 1.0 | 15-500 | |
| Test32 | Radial a_0_10 | Out of plane | 2.0 | 15-500 | |
| Test33 | Radial a_0_10 | Out of plane | 5.0 | 25-500 | |
| Test34 | Radial a_0_10 | Out of plane | 10.0 | 50-500 | |
| Test35 | Radial a_0_10 | Out of plane | 15.0 | 50-500 | |
| Test36 | Radial a_0_10 | Out of plane | 0.0002 | 5-1000 | Random vib |
| Test37 | Radial a_0_10 | In plane | 0.5 | 5-500 | |
| Test38 | Radial a_0_10 | In plane | 1.0 | 15-500 | |
| Test39 | Radial a_0_10 | In plane | 2.0 | 15-500 | |
| Test40 | Radial a_0_10 | In plane | 5.0 | 25-500 | |
| Test41 | Radial a_0_10 | In plane | 10.0 | 50-500 | |
| Test42 | Radial a_0_10 | In plane | 15.0 | 50-500 | |
| Test43 | Radial a_0_10 | In plane | 0.0002 | 5-1000 | Random vib |
| Test44 | Radial a_0_00 | Out of plane | 0.0002 | 5-1000 | Fixed w/ washer |
| Test45 | Radial a_0_00 | Out of plane | 0.5 | 5-500 | Fixed w/washer |
| Test46 | Slot a_0_00 | Out of plane | 0.5 | 5-500 | |
| Test47 | Slot a_0_00 | Out of plane | 1.0 | 15-500 | |
| Test48 | Slot a_0_00 | Out of plane | 2.0 | 15-500 | |
| Test49 | Slot a_0_00 | Out of plane | 5.0 | 25-500 | |
| Test50 | Slot a_0_00 | Out of plane | 10.0 | 50-500 | |
| Test51 | Slot a_0_00 | Out of plane | 15.0 | 50-500 | |
| Test52 | | | | | Test discarded |
| Test53 | | | | | Test discarded |
| Test54 | Slot a_0_00 | Out of plane | 0.0002 | 5-1000 | Random vib |
| Test55 | Slot a_0_05 | Out of plane | 0.5 | 5-500 | |
| Test56 | Slot a_0_05 | Out of plane | 1.0 | 15-500 | |
| Test57 | Slot a_0_05 | Out of plane | 2.0 | 15-500 | |
| Test58 | Slot a_0_05 | Out of plane | 5.0 | 25-500 | |
| Test59 | Slot a_0_05 | Out of plane | 10.0 | 50-500 | |
| Test60 | Slot a_0_05 | Out of plane | 15.0 | 50-500 | |
| Test61 | Slot a_0_05 | Out of plane | 0.0002 | 5-1000 | Random vib |
| Test62 | Slot a_0_10 | Out of plane | 0.5 | 5-500 | |
| Test63 | Slot a_0_10 | Out of plane | 1.0 | 15-500 | |
| Test64 | Slot a_0_10 | Out of plane | 2.0 | 15-500 | |
| Test65 | Slot a_0_10 | Out of plane | 5.0 | 25-500 | |
| Test66 | Slot a_0_10 | Out of plane | 10.0 | 50-500 | |
| Test67 | Slot a_0_10 | Out of plane | 15.0 | 50-500 | |
| Test68 | Slot a_0_10 | Out of plane | 0.0002 | 5-1000 | Random vib |
| Test69 | Slot a_0_00 | In plane | 0.5 | 5-500 | |
| Test70 | Slot a_0_00 | In plane | 1.0 | 15-500 | |
| Test71 | Slot a_0_00 | In plane | 2.0 | 15-500 | |
| Test72 | Slot a_0_00 | In plane | 5.0 | 25-500 | |
| Test73 | Slot a_0_00 | In plane | 10.0 | 50-500 | |

| | | | | | |
|---|---|---|---|---|---|
| Test74 | Slot a_0_00 | In plane | 15.0 | 50-500 | |
| Test75 | Slot a_0_00 | In plane | 0.0002 | 5-1000 | Random vib |
| Test76 | Slot a_0_05 | In plane | 0.5 | 5-500 | |
| Test77 | Slot a_0_05 | In plane | 1.0 | 15-500 | |
| Test78 | Slot a_0_05 | In plane | 2.0 | 15-500 | |
| Test79 | Slot a_0_05 | In plane | 5.0 | 25-500 | |
| Test80 | Slot a_0_05 | In plane | 10.0 | 50-500 | |
| Test81 | Slot a_0_05 | In plane | 15.0 | 50-500 | |
| Test82 | Slot a_0_05 | In plane | 0.0002 | 5-1000 | Random vib |
| Test83 | Slot a_0_10 | In plane | 0.5 | 5-500 | |
| Test84 | Slot a_0_10 | In plane | 1.0 | 15-500 | |
| Test85 | Slot a_0_10 | In plane | 2.0 | 15-500 | |
| Test86 | Slot a_0_10 | In plane | 5.0 | 25-500 | |
| Test87 | Slot a_0_10 | In plane | 10.0 | 50-500 | |
| Test88 | Slot a_0_10 | In plane | 15.0 | 50-500 | |
| Test89 | Slot a_0_10 | In plane | 0.0002 | 5-1000 | Random vib |
| Test90 | Radial a_0_10 | Out of plane | 1 | 250 | |
| Test91 | Radial a_0_10 | Out of plane | 1 | 315 | 1st mode |
| Test92 | Radial a_0_10 | Out of plane | 1 | 366 | 2nd mode |
| Test93 | Radial a_0_10 | Out of plane | 1 | 50 | |
| Test94 | | | | | Test discarded |
| Test95 | Radial a_0_10 | Out of plane | 10 | 50 | |
| Test96 | Radial a_0_10 | Out of plane | 10 | 250 | |
| Test97 | Radial a_0_10 | Out of plane | 10 | 366 | |
| Test99 | Radial a_0_10 | Out of plane | 10 | 315 | |

Table F.1: Shaker Test Log

# Plots of all tests from table F.1

As many of the in-plane experiments display very much the same response, not all of the in-plane results are attached.
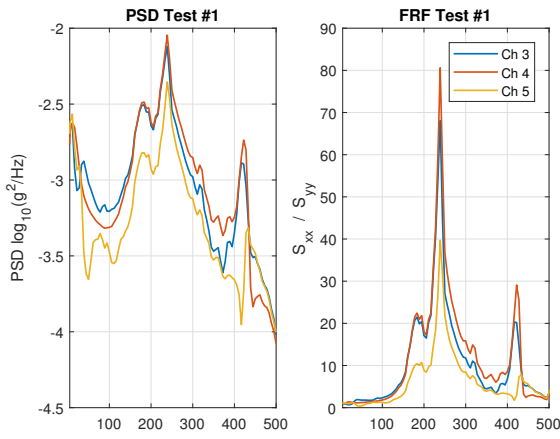
Figure F.1
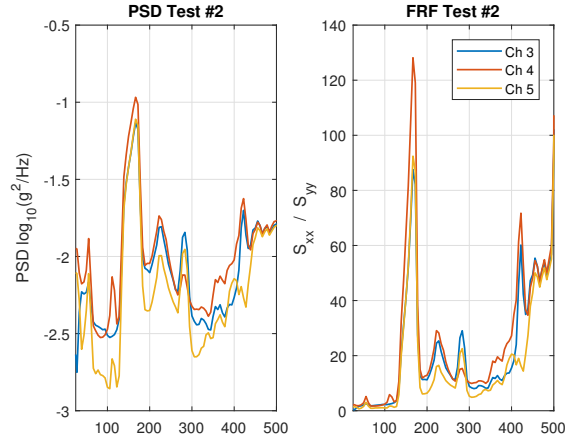
Figure F.2
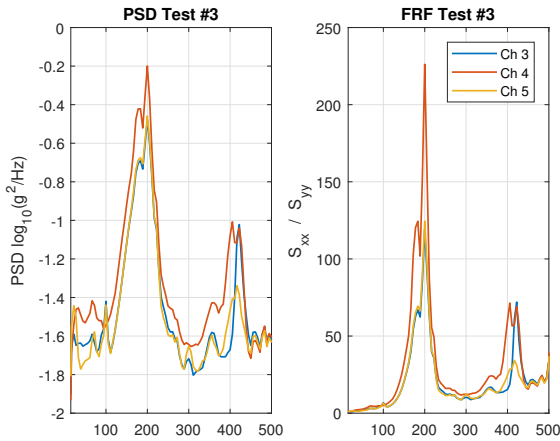


Figure F.3
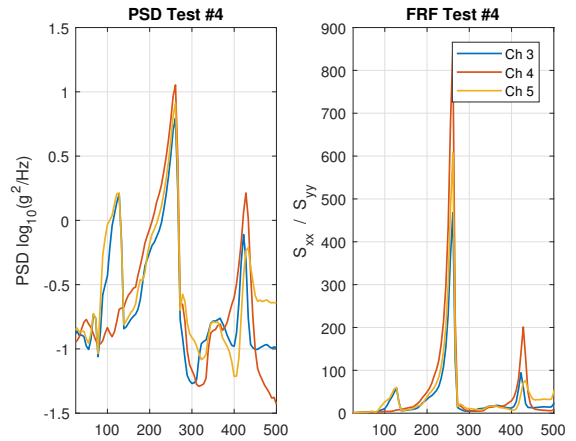
Figure F.4
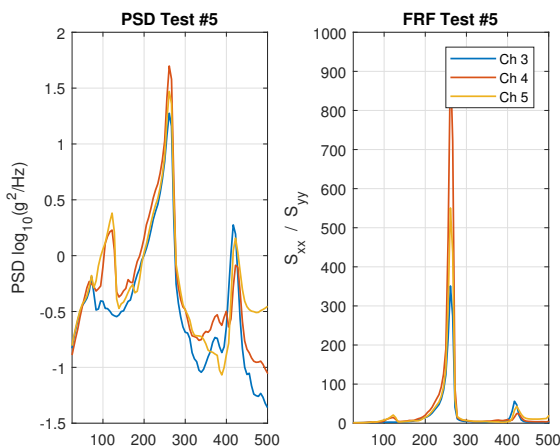


Figure F.5
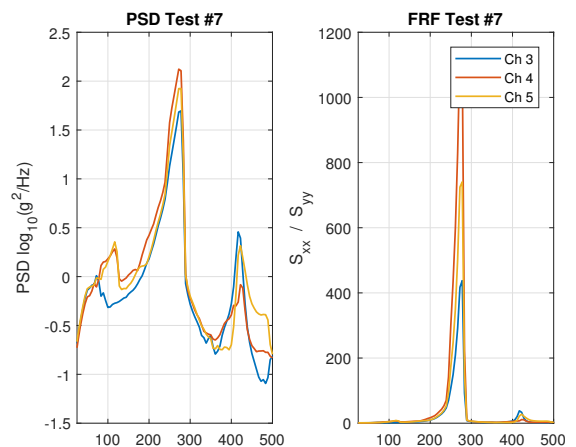
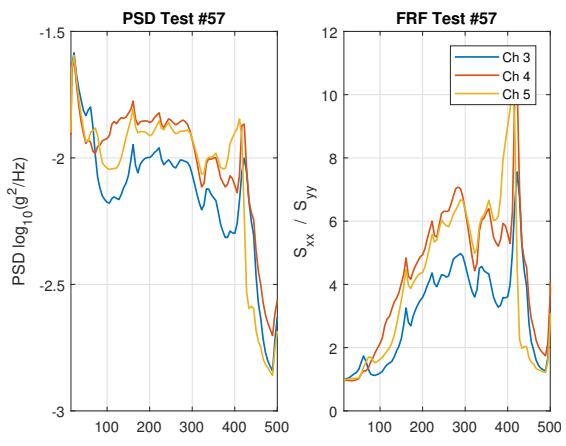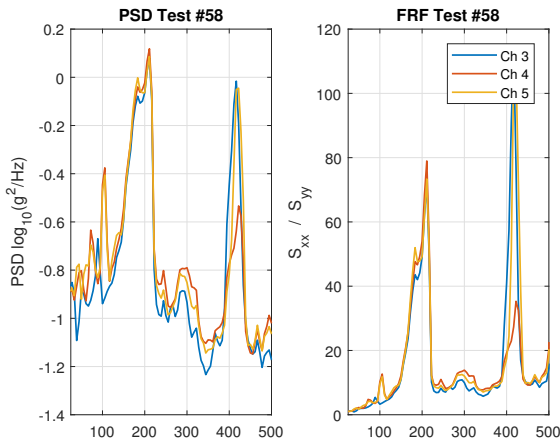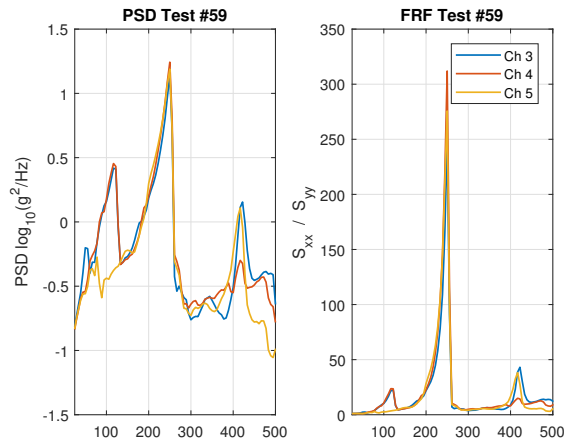Figure F.6
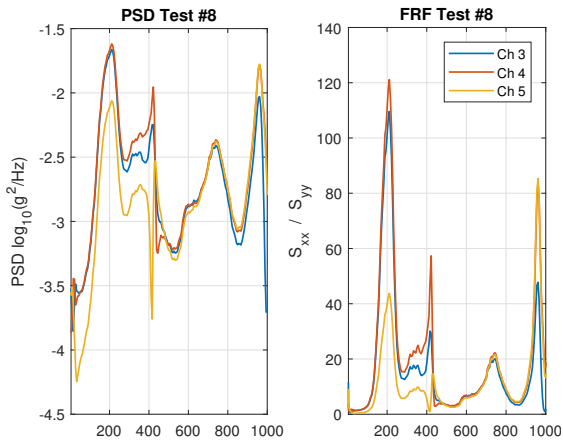
Figure F.7
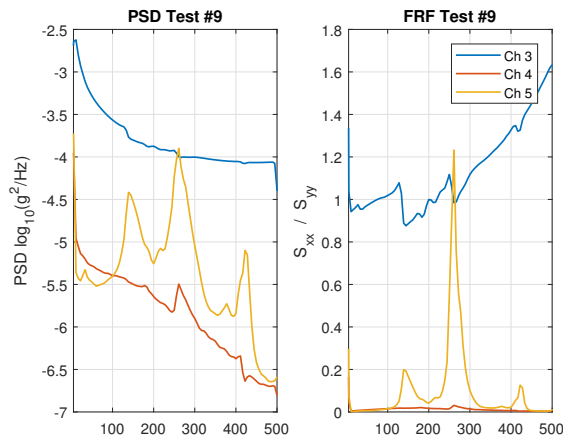


Figure F.8
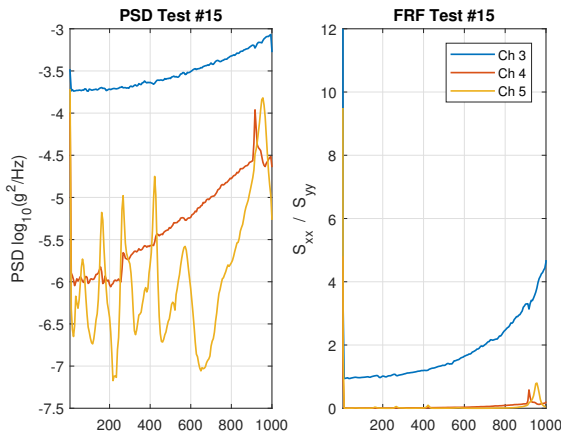


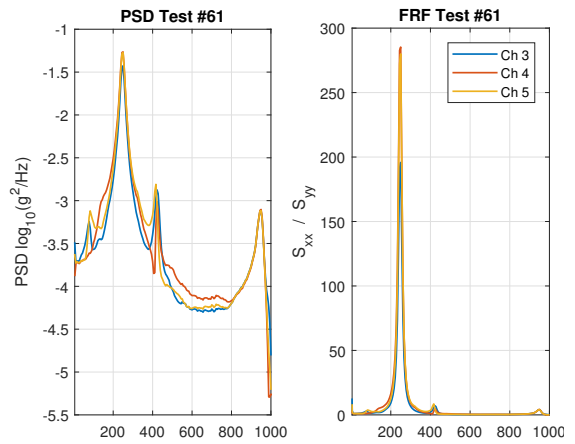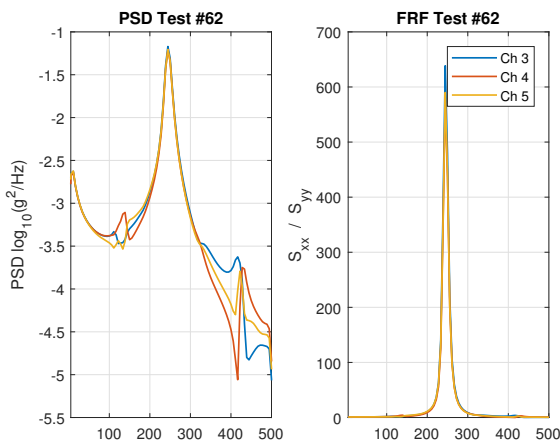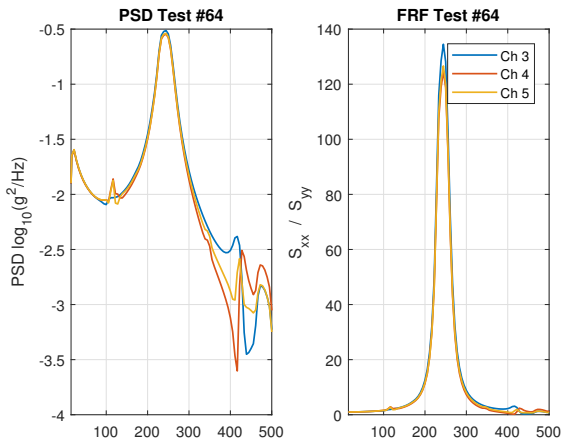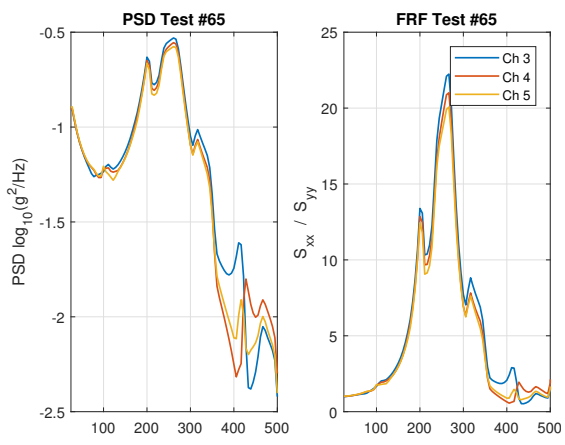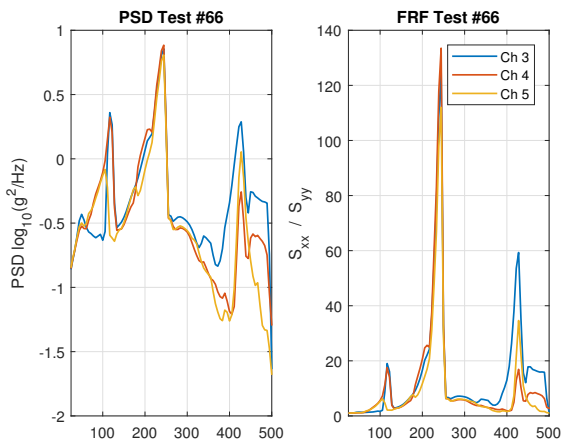Figure F.9
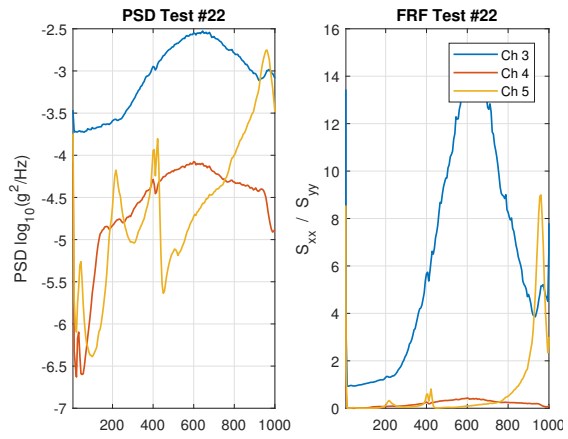


Figure F.10
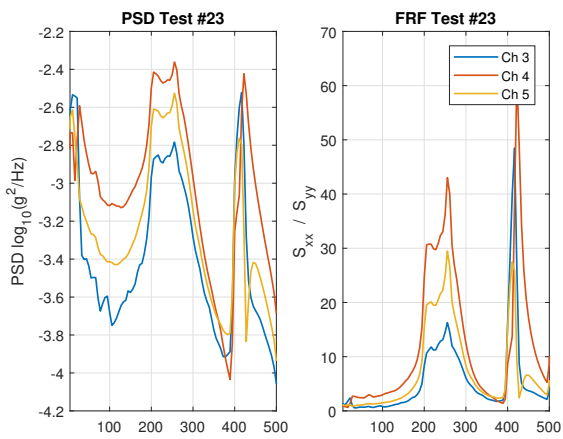


Figure F.11
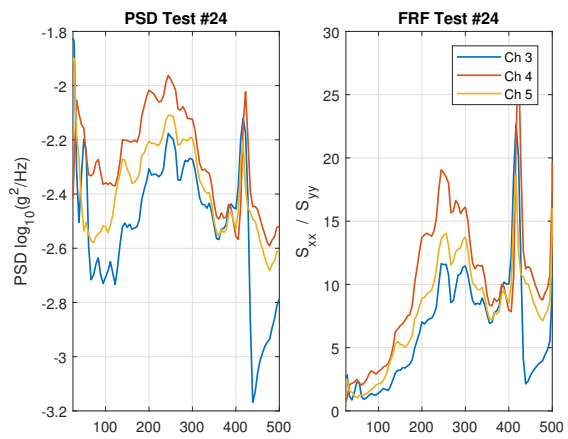


Figure F.12
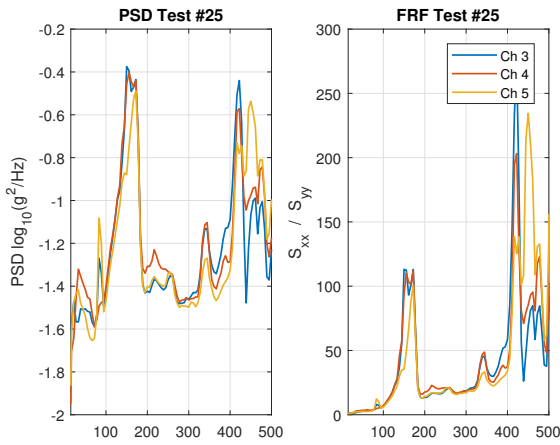
Figure F.13
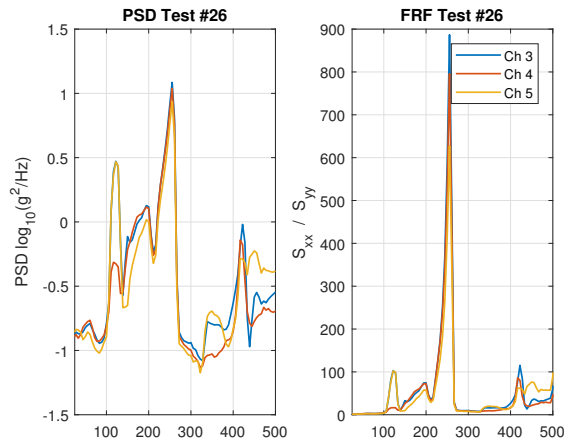

Figure F.14
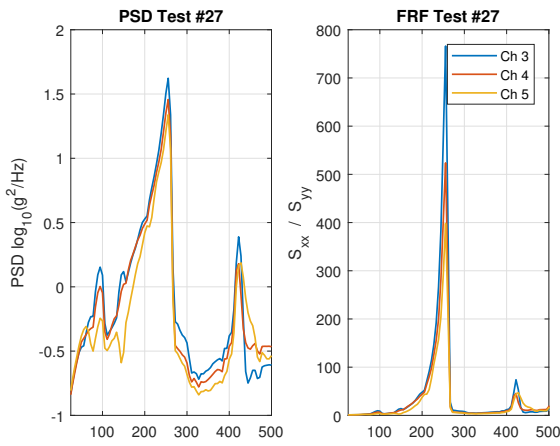

Figure F.15
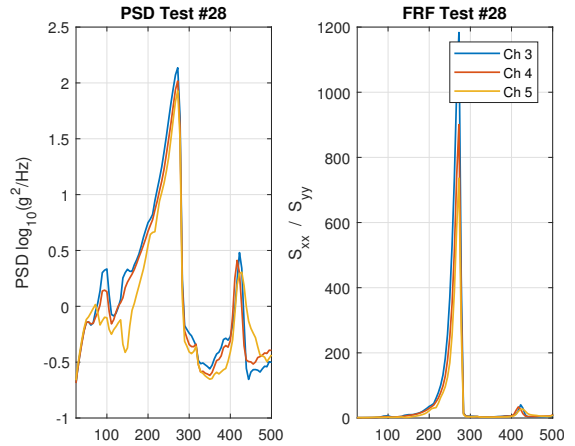

Figure F.16
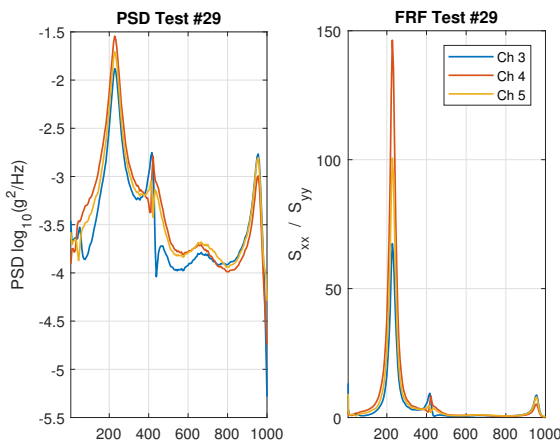

Figure F.17
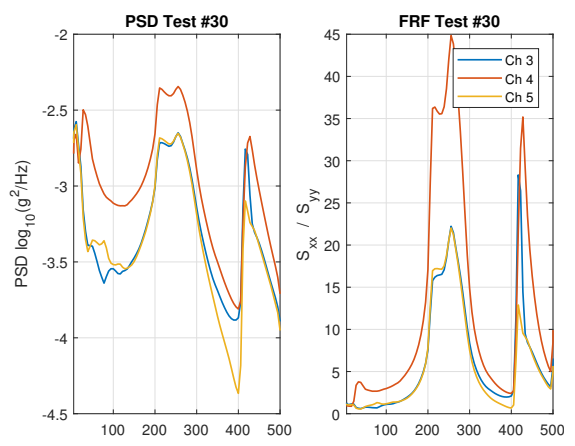

Figure F.18
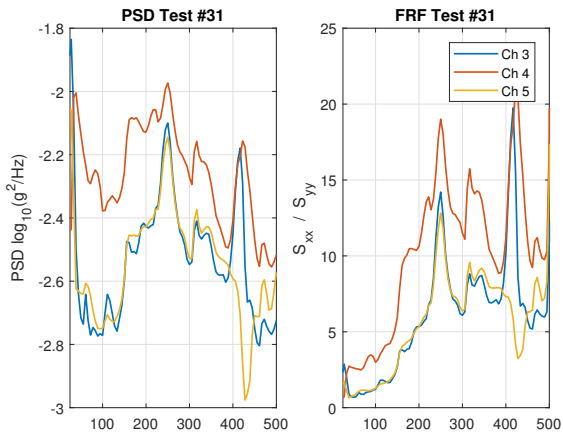
Figure F.19
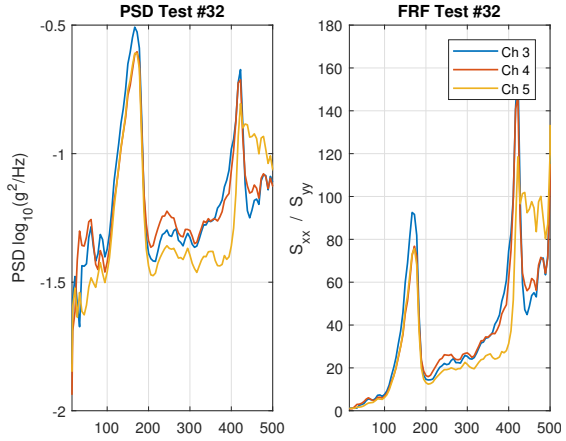


Figure F.20
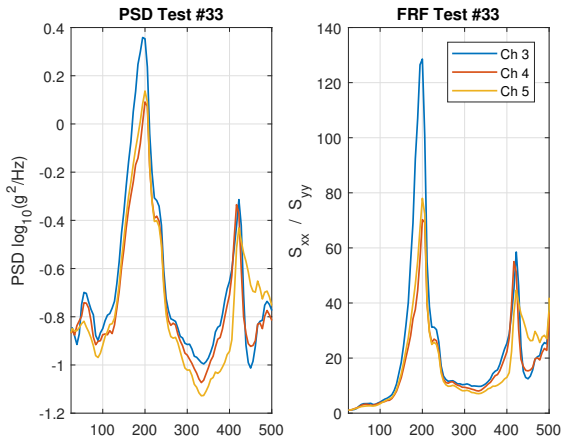


Figure F.21
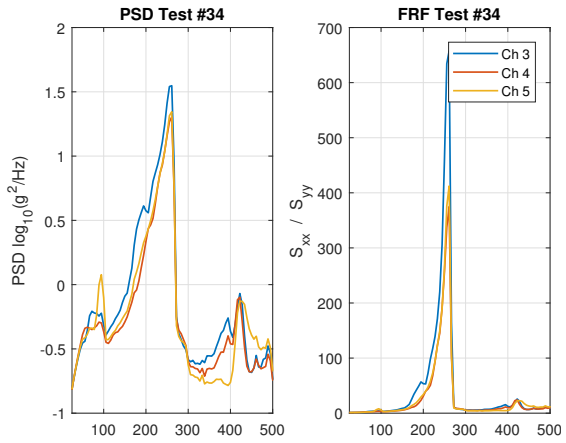


Figure F.22
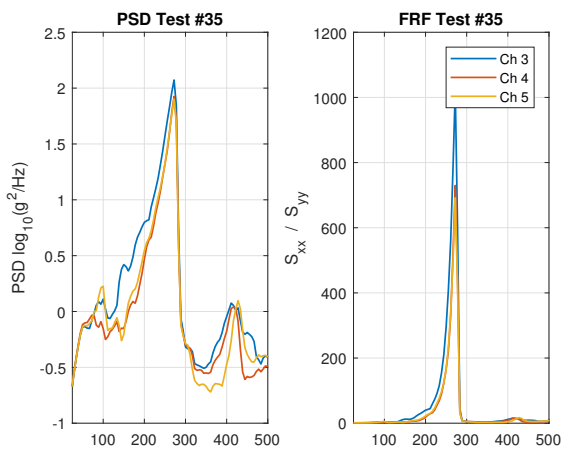


Figure F.23
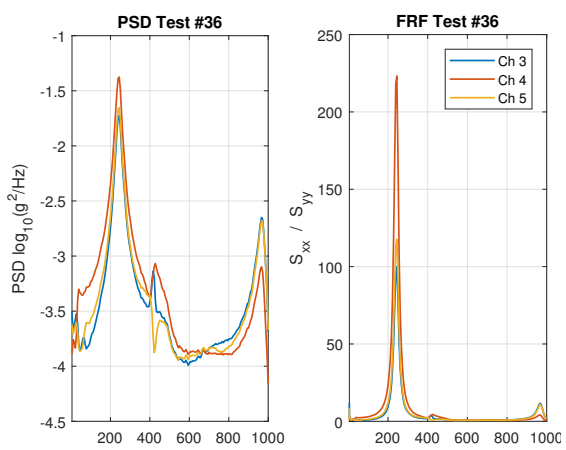


Figure F.24
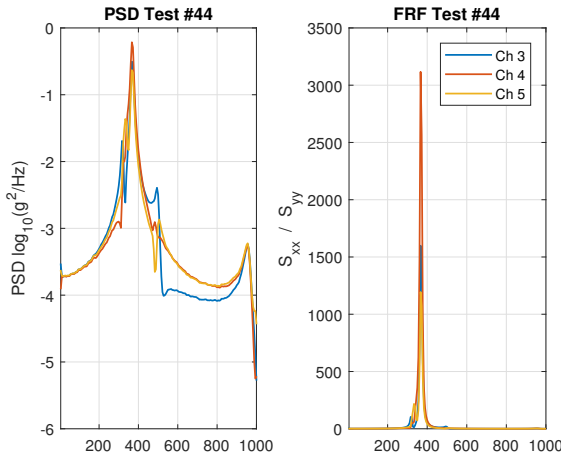
Figure F.25
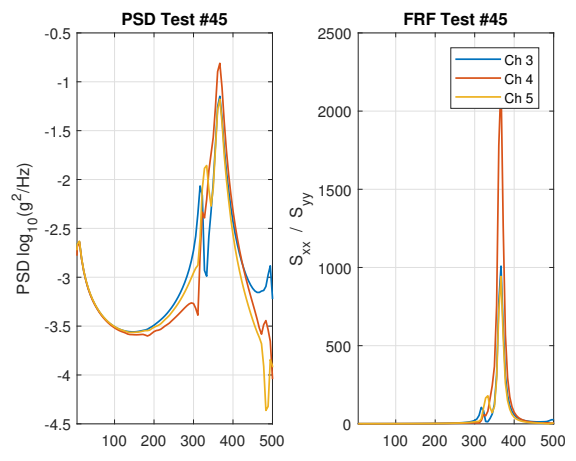


Figure F.26
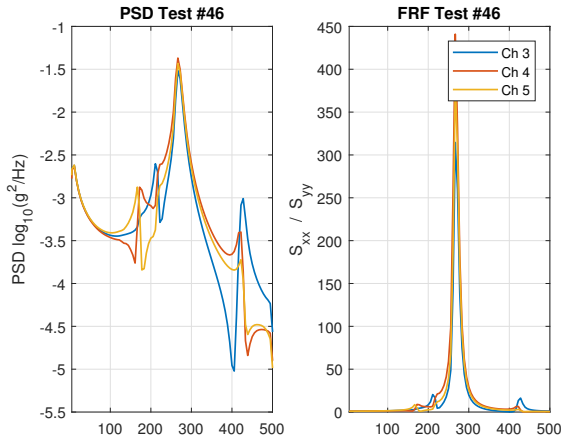


Figure F.27
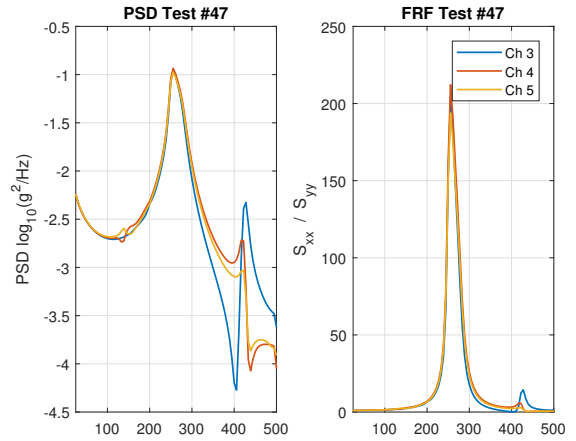


Figure F.28
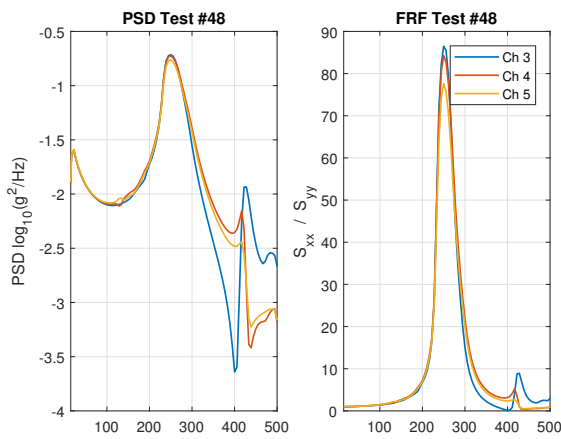


Figure F.29
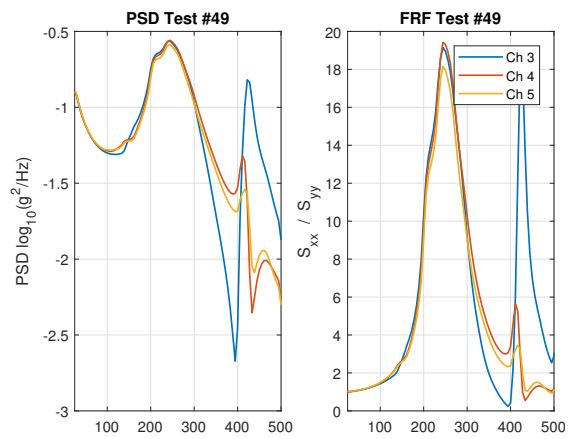


Figure F.30
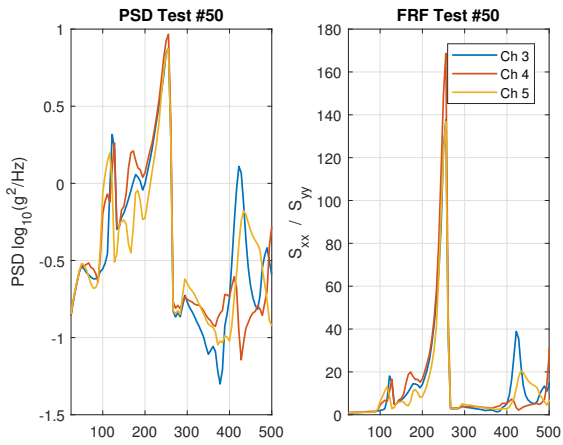
Figure F.31
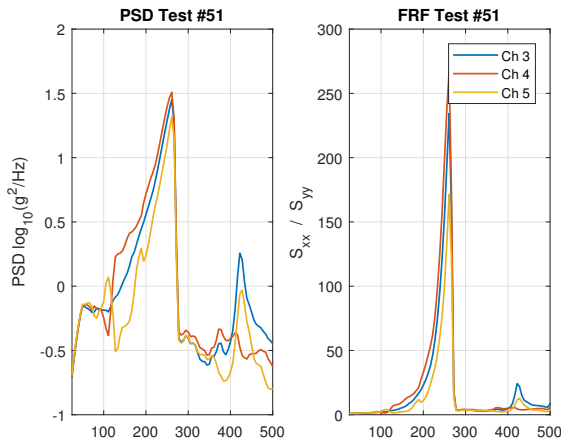
Figure F.32
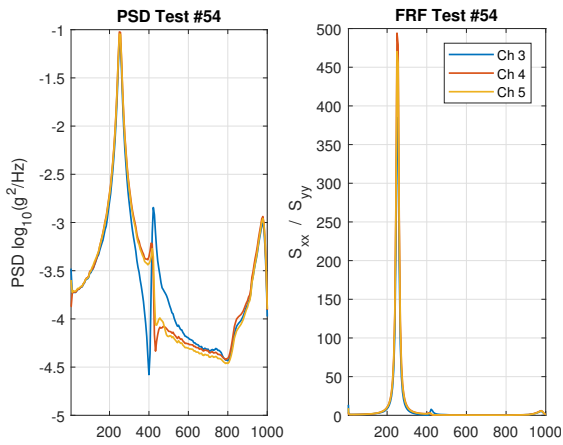


Figure F.33
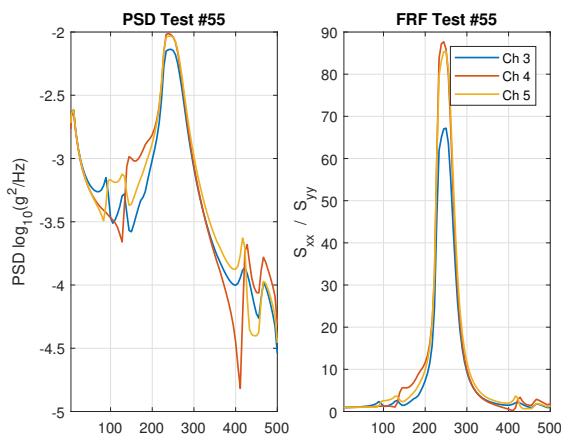
Figure F.34
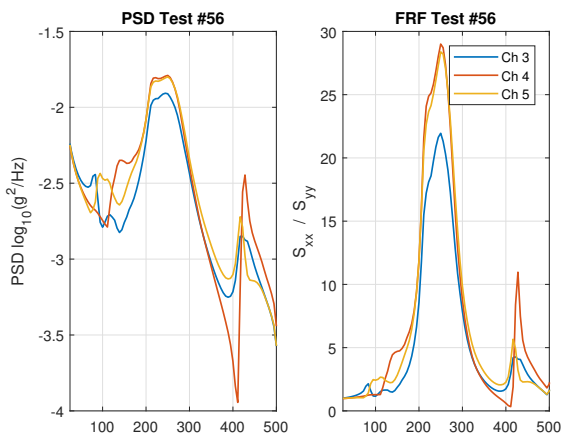


Figure F.35

Figure F.36

Figure F.37



Figure F.38
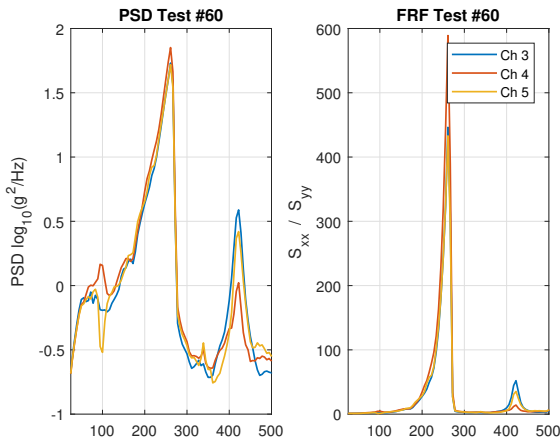


Figure F.39
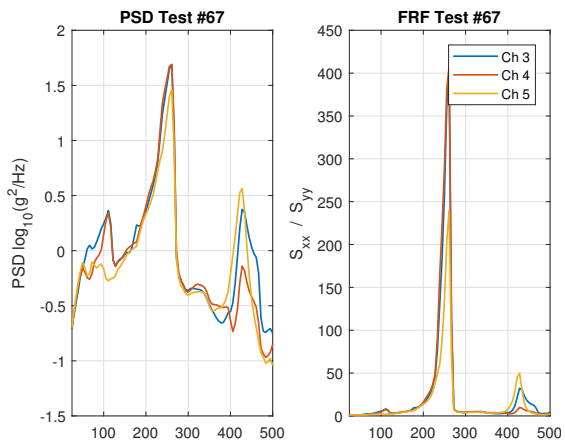


Figure F.40



Figure F.41
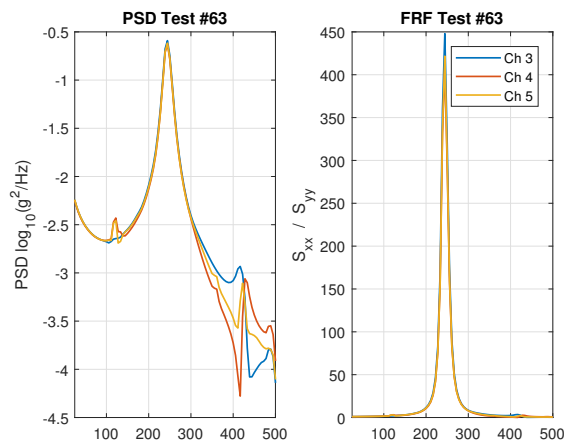


Figure F.42

Figure F.43



Figure F.44



Figure F.45



Figure F.46



Figure F.47



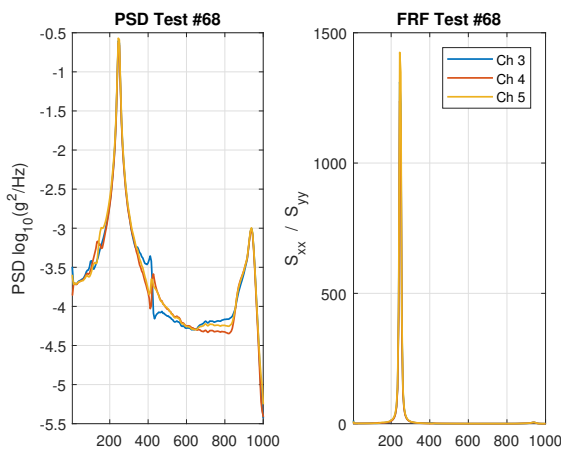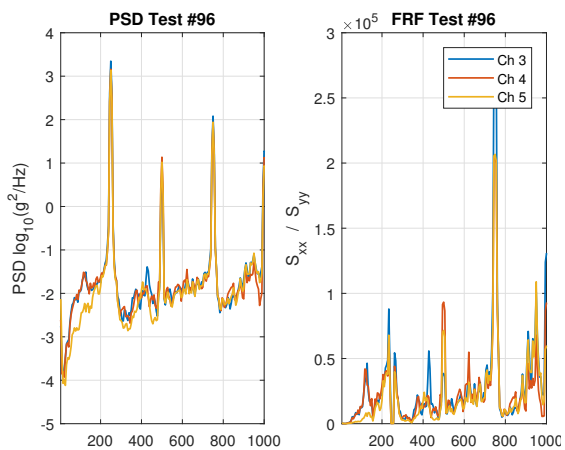Figure F.48